A Study of Photon Counting X-ray Radiography

Tsutsui, Hiroshi

(Degree)
博士（工学）

(Date of Degree)
1993-09-24

(Date of Publication)
2014-02-04

(Resource Type)
doctoral thesis

(Report Number)
乙1762

(JaLCDOI)
https://doi.org/10.11501/3078466

(URL)
https://hdl.handle.net/20.500.14094/D2001762

A Study of Photon Counting X-ray Radiography

（光子計数によるX線ラジオグラフィ）

1993年 8 月

Hiroshi Tsutsui

（筒井 博司）

Contents

SYMBOLS

CHAPTER 1

λ : the drift length of the carrier	(cm)
μ : the mobility	(cm/V)
τ : the mean free path	(cm)
E : the applied electric field	(V/cm)

CHAPTER 2

R : the electron range	(cm^{-1})
E : the energy of the secondery electron	(eV)
E0 : the incident X-ray energy	(eV)
Ek : the energy of the K-shell absorption edge	(eV)
x : the range of secondery electron	(cm)
ϱ : the dencity	(mg/cm^3)

CHAPTER 3

f0(E): incident X-ray spectrum	
f(E): absorbed X-ray spectrum	
μ (E): absorption coefficient	(cm^{-1})
g(E): output X-ray spectrum	
k : K-shell absorption energy	(eV)
d : thickness of the material	(cm)

CHAPTER 4

V0 : output voltage	(V)
R0 : detector resistance	(Ω)
Rf : negative feedback resistance	(Ω)
C0 : detector capacity	(F)
Ci : input floating capacity	(F)
A0 : amplifier gain	
fc : cut-off frequency	(Hz)
I0 : input (irradiated) X-ray intencity	
I : output (penetrated) X-ray intencity	
I/I0 : transmissivity	

CHAPTER 5

I0(E): irradiated X-ray photons

I(E): penetrated X-ray photon

μ (E): absorption coefficient (cm^{-1})

d : material thickness (cm)

CHAPTER 6

p(k): probability to produce a value k

λ : mean value

λ : variance

f(x): probability density function

N(λ , λ): normal distribution with the mean value λ

y : random number of the normal distribution N(λ , λ)

x*: random number of the normal distribution N(0,1)

X : contrast data (%)

d : phantom thickness (cm)

T : X-ray strength ratio

CHAPTER 1
Introduction

1-1. Introduction

Reported here is the research and development carried out to confirm the feasibility of a linear array X-ray imaging sensor having the capability for "X-ray radiography with energy spectrum information".

The measurement of the X-ray energy spectrum in addition to X-ray intensity distribution from an object exposed to X-rays is very effective in obtaining valuable information on the characteristics of the object. This provides us with the compositional material property using the X-ray transmission.

Up to now, various attempts have been made to obtain X-ray images directly by electronic means without using X-ray film. The xenon ion chambers [1]-[2] having multi electrodes, compact scintillators [3]-[5], and luminescent sheet have been investigated and applied to industrial and medical purposes. Recently, a new process called Digital Radiography have been developed using a digital image processing. However, no attempts to obtain energy information from the transmitted X-rays have been made so far.

CdTe compound semiconductor radiation detector, that is selected for this study, is one of the answer to obtain "X-ray radiography with energy spectrum information". In this study those are described: selection of the detector material, fabrication of the CdTe X-ray imaging sensor, methods to obtain X-ray images having energy information, image processing using the energy information, and kinds of images obtained by using X-ray imaging system.

1-2. Overview

Chapter 2 discusses the basic design for the application of the CdTe compound semiconductor radiation detector to the linear array X-ray imaging sensor and also discusses the preparation of the detector element and the characteristics of the response exposed to the single energy γ -rays(241Am). One unit of the CdTe crystal are composed of 32 elements and has a size of $1\times8\times0.3$ mm^3. The characteristics of the detector elements each having a pitch of 0.25 mm are measured and compared to the characteristics when using a single element having a sensing volume of $1\times1\times0.3$ mm^3. The comparison of the physical parameter of the ranges of Si and CdTe and the behavior of K-shell characteristic X-rays are discussed.

Chapter 3 presents the result of the X-ray energy spectrum measurement using one element of the 32 CdTe radiation detector elements exposed to the diagnostic X-ray source. The output spectrum is deformed because of the small size of the element. Errors caused by the escape of X-rays and by the energy dependency of the photoelectric absorption process are significant. The response function of the detector element to monochromatic 59.54 keV ^{241}Am gamma rays is measured and by fitting the results to a calibration curve, a small size CdTe detector is proved to be able to detect X-ray spectra reliably.

Chapter 4 presents the X-ray imaging sensor consisting of CdTe detector elements and the pulse counting circuit attached to each element. The circuit includes wide band amplifiers, discriminators and counters. Charge pulses are directly counted and separated into two energy regions. Digitized X-ray images containing energy information are obtained and two separated X-ray images of different energy can simultaneously be obtained.

Chapter 5 presents the characteristics of the newly designed 512

detector elements and 0.2 mm pitch X-ray imaging sensor and X-ray radiographic system. An analytical feasibility study is done using the energy subtraction method to separate the components in the object and to determine the material component of the object.

Chapter 6 describes about the contrast resolution of the X-ray radiography using a photon counting method. Using this method, it is cleared that the noise depends on only the fractuation of the X-ray photon flux while not significantly depend on the noise level of the amplifier. The contrast resolution is evaluated in two ways; one uses simulated digital images when considering the fractuation of the Poisson process of the X-ray photon generation, and the other is the measured digital images using this system and the contrast phantom..

Chapter 7 describes overall discussions and concluding remarks of this study.

CHAPTER 2

Fabrication and characteristics of a CdTe submillimeter detector

2-1.Introduction

The CdTe detector element of the linear array X-ray imaging sensor is selected and designed basically. For making a full use of characteristics of CdTe compound semiconductor material, and attaining an X-ray spatial resolution of 2 lp/mm, a linear array radiation detector with an element pitch of 0.25 mm was prepared and examined. Then the characteristics of the energy resolution of one detector element were measured and compared with those of an single element. In addition, the radiation shielding grid was developed and utilized to solve cross-talk problems.

2-2. Selection of CdTe compound semiconductor material

Up to now, various attempts have been made to obtain X-ray images directly by electronic means without using X-ray film. Recently, a new process called Digital Radiography have been developed using a digital image processing. However, no attempts to obtain energy information from the transmitted X-rays have been made so far.The reasons for this could be attributed to (1) the insufficient photo-electric absorption efficiency in the detector elements, (2) the longer secondary electron ranges than that of the element sizes, resulting in a high energy loss due to escaping secondary electrons and thus putting difficulties in determining the exact energy information, (3) the cross-talk between neighboring elements and (4) the luminescent or the scintillation light escaping from the element.

Thus, it has been nearly impossible to establish a concrete concept of arrayed detectors from which an exact energy spectra of the incident

photons can be determined, and no attempts, even in their primary stage, have been made so far.

On the other hand, the highest known energy resolution capability attainable by a cooled semiconductor radiation detector has been determined, and crystals operable at room temperature, typified by a high-purity silicon crystal, were recently reported although its characteristics were considered still inadequate [6]-[9].

However, a provision of the depression layer having an adequate thickness is nearly impossible with Si crystals at room temperature because of the comparatively low specific resistances of Si. With a limited Si thickness, the photo-electric absorption efficiency is too low and the energy loss from escaped secondary electrons is too high [10].

The above problems will be solved by employing a CdTe crystal which has higher absorption coefficients against X-rays and γ-rays because of its large atomic numbers (Cd:48,Te:52). Furthermore, owing to its high energy gap (Eg=1.47eV) and high specific resistance available at room temperature, stable CdTe detectors operating at room temperature have been developed [11],[12].

One of the inherent problems of CdTe is, however, that the holes created by radiation are trapped before they can reach an electrode because of their low mobility and short life time. The drift length λ of the carrier can be expressed by $\lambda = \mu \tau E$, where μ is the mobility, and τ is the mean free path of the carrier generated in the detector, and E is the applied electric field intensity. The value of λ therefore must be larger than the thickness of the detector element.

Since the product of $\mu \tau$ for the holes in CdTe is 10^{-4} cm^2/V, which is smaller by one order of magnitude than that for the electrons, this yields a condition of $\lambda = 1$ cm when the electric field of $E=10^4 V/cm$ is applied. Moreover, L must be less than 0.1 cm according to the Rule of

Thumb Condition, $L = 0.1\lambda$, required for the efficient electric charge collection at that electric field intensity. Thus, it is concluded that a CdTe crystal having a thickness of more than 1 mm is unrealistic, and only a substantially thinner crystal can be utilized as a pulse detector.

The most important point is that the detector, which operates at room temperature, can be attained only by employing a semiconductor crystal of reduced dimensions which is also essential for attaining a higher spatial resolution.

Although the problems already described still remain with submillimeter crystals designed for radiation energy analysis, the employment of CdTe crystal may solve these problems as long as the energy range of X-rays is limited to the range between 20 keV and 120 keV for industrial and diagnostic analysis. The reasons for this are attributed to (1) substantially high primary X-ray photon absorption, (2) efficient absorption of the secondary electron because of its high density and (3) the resultant small chances of cross-talk between elements.

The linear array X-ray imaging sensor using a CdTe compound semiconductor is designed basically by using the parameters already described. The X-ray radiographic system is developed to estimate the characteristics of the CdTe X-ray imaging sensor and to obtain all digital radiographic images. A feasibility study is made using a photon counting method and energy subtraction method. Basic characteristics on output response caused by X-ray photons, energy separation, energy resolution, specific resolution and contrast resolution are measured and evaluated. Also, the feasibility of application to all digital X-ray radiography will be discussed.

2-3.Preparation of CdTe linear array detector

In determining the dimension of the elements for the application to X-ray radiography, the parameters shown below are taken into consideration.

1) Array pitch of the elements. This is set at 0.25 mm in order to realize a spatial resolution of more than 2 lp/mm.

2) The sensitive thickness of the crystal. This is set at 0.3 mm, considering the X-ray absorption efficiency, drift length of holes, and cross-talk between neighboring channels.

The construction and the fabrication of the detector are described in the following. A Cl-doped CdTe single crystal with a specific resistance of 10^8 to 10^9 $\Omega \cdot$ cm supplied by RMD Co., is employed for the present experiment. The crystal is cut into 0.3-mm-thick wafers. Platinum-patterned electrodes are then deposited on them by electroless plating after mirror polishing, and these wafers were cut into the plates of 1(width)×8(length)×0.3(thickness) mm^3, as shown in Fig.2-1 (b), by means of a multiwire saw. A common electrode is deposited on one side of the surface, and the divided electrodes, each measuring 0.8×0.2 mm, are deposited on the other side.

The individual resistance of the element is measured by the I-V method using a Hewlett Packard Model 4140B PA meter, and is found to have the specific resistance of the order of 10^{10} Ω or 10^9 $\Omega \cdot$ cm when the element is placed in an electric field of 3.3 kV/cm, with which a best charge collection efficiency can be obtained.

In order to evaluate the changes in energy resolution and the effects of the peak of K-shell characteristic X-ray escape accompanied by miniaturized elements more exactly, a single detector with the size of $1 \times 1 \times 0.3$ mm^3 as shown in Figure 2-1 (a) is fabricated by employing the same process, and its output characteristics are compared with those of

the linear array detector.

2-4. Characteristics of the detector for γ -ray spectrum

The characteristics of a single element of the linear array detector shown in Figure 2-1 (b) is described in the following. Because of the effects of neighboring elements, problems which are not found in a single detector are encountered.

The system employed for the single element evaluation is shown in Figure 2-2 (a) in which a negative voltage is applied to the common electrode of CdTe detector, and the output pulse from an individual electrode is amplified by a current amplifier. A spectral analysis is performed using the main amplifier (Ortec Model-571), the linear-gate stretcher (Ortec Model-542), and the pulse height analyzer (Ortec Model-7100).

Figure 2-2 (b) shows the method for detecting the signals from a specified element. The measurement is conducted by grounding the elements of two neighboring elements giving equal input potential to both the amplifier and the neighboring elements, and the output of the specified element is connected to a current amplifier.

Evaluation of detector characteristics is carried out by measuring the output pulse waveform and the pulse height distribution with 59.54 keV γ -ray (^{241}Am) irradiation on the divided electrodes. Figure 2-3 shows a typical output pulse waveform obtained using the current amplifier.

A pulse width of 100 ns (FWHM) and pulse height of 250 mV are attained under an electric field of 3.3 kV/cm, and this pulse waveform is independent of the form of the detector. This means that the pulse waveforms are identical for linear array detector elements and a single detector which size is considerably larger than that of the linear array

detector elements.

Figure 2-4 shows the pulse height distribution obtained by the above mentioned two types of CdTe detector, where the curves are normalized by the peak values.

The spectrum obtained by a linear array detector element is nearly identical with that obtained by a single detector. However, the K-shell X-ray escape peak obtained by a linear array detector element is larger than that obtained by the single detector. This is attributed to 1) an increase in K-shell X-ray escape due to the reduced sensible volume, and 2) an overlap of pulse counts due to re-absorption of the K-shell X-ray escape photons from neighboring elements.

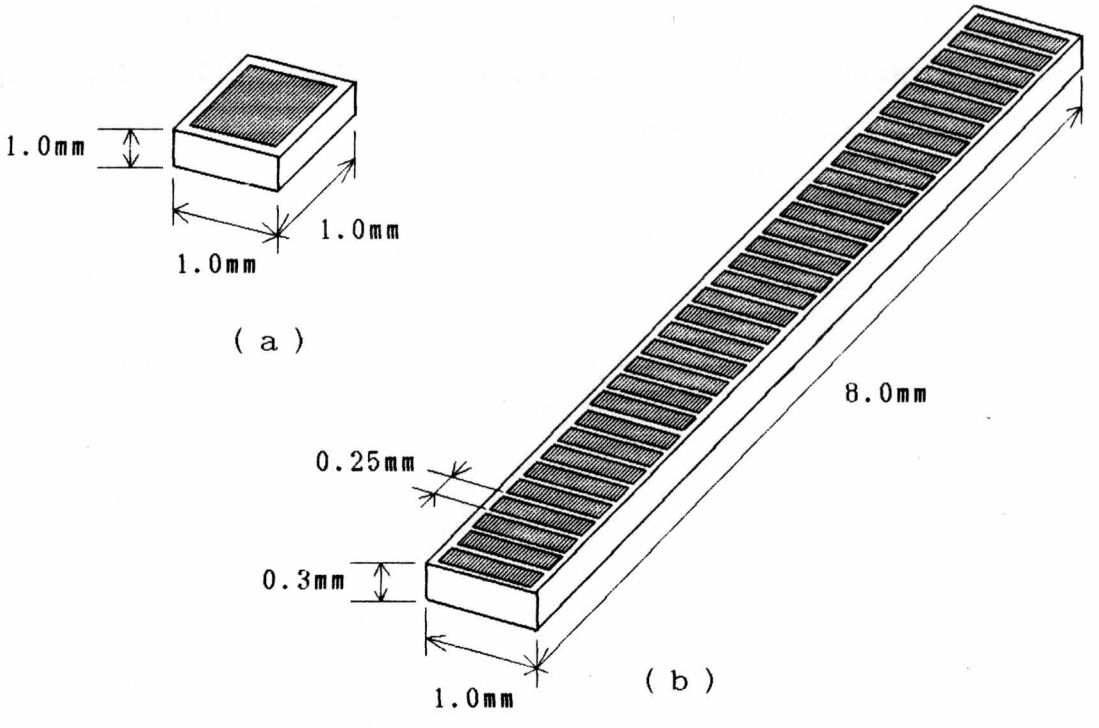

Fig.2-1. Dimensional drawing of sensors used in the experiment, (a):1×1×0.3 mm^3, (b):1×8×0.3 mm^3 and channel pitch: 0.25 mm.

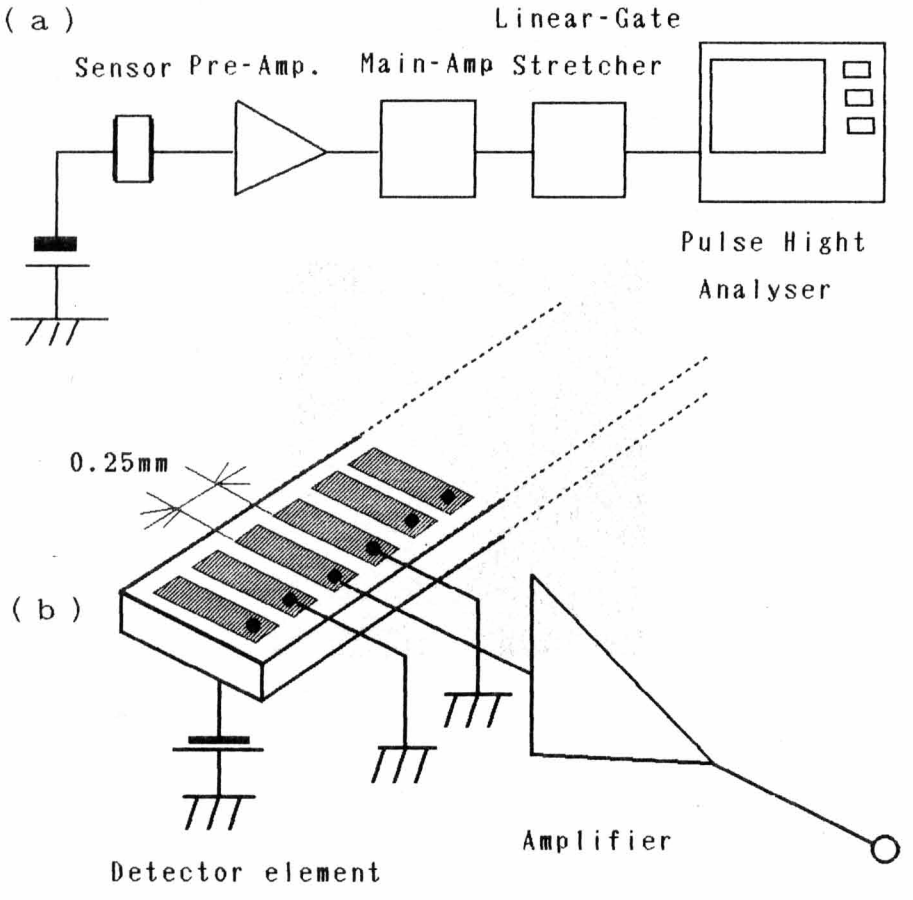

Fig.2-2 Experimental set up for spectroscopic measurement of single channel. Negative voltage is applied to the common electrode and two neighboring electrodes are grounded.

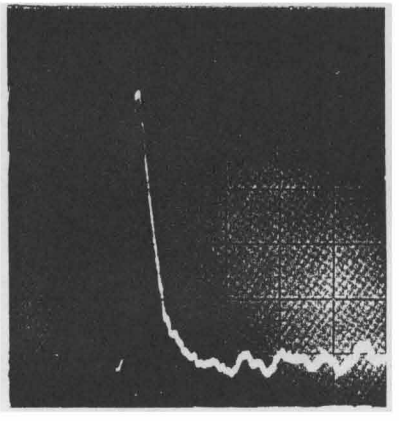

200 ns / div.

50 mV/ div.

Fig.2-3 Pulse form from a detector element.

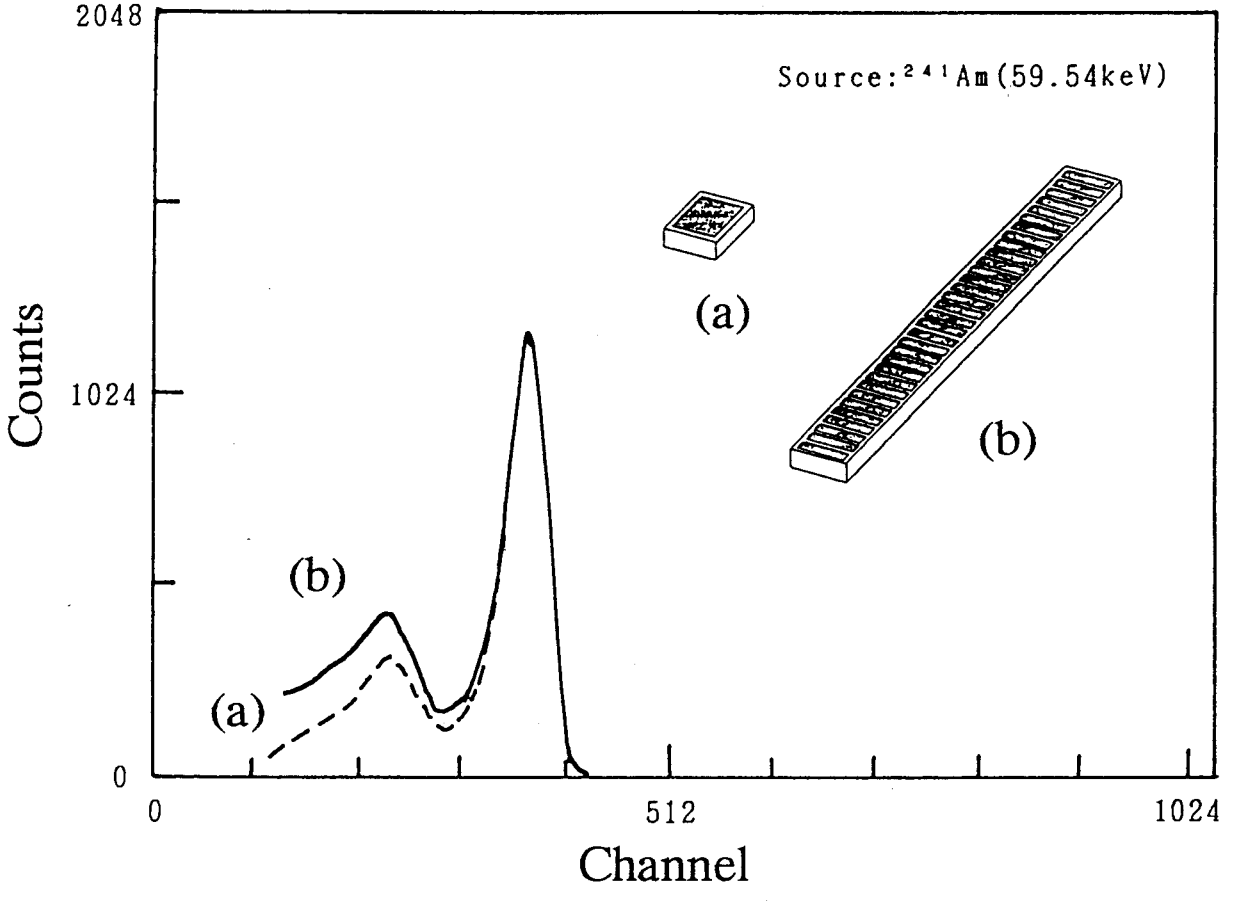

Fig.2-4 Pulse height distribution of 241Am γ -ray pulse height distribution detected by one of the linear array detector detector elements (solid line) and by a single detector (broken line).

2-5. Reduction of K-shell escape peak counts by providing radiation shielding grid

The ratio of K-shell X-ray escape peak counts to the total counts is larger for the detector of a smaller element size. The X-rays which escape to the neighboring elements are reabsorbed therein and produce cross talks which lowers not only the accuracy of the pulse-height spectrum but also the spatial resolution.

A proposed method to reduce this cross-talk is schematically shown in Figure 2-5 for the case of the linear array detector element wherein grids are provided as a radiation shield. These grids are provided on the incident side for the dual purpose; One is to prevent the irradiation on the boundary regions between neighboring elements, and the other purpose is to reabsorb the K-shell characteristic X-rays within the element itself to reduce the cross-talks with the neighboring directions.

Since the average energies of K-shell characteristic X-rays of Cd and Te are 23.17 and 27.47 keV, respectively, and the linear attenuation coefficients of CdTe at these energies are 85.4 cm^{-1} and 168.5 cm^{-1}, respectively, the cross-talks can be reduced to a half by providing a 50-μ m-thick dead zone.

Figure 2-6 shows the geometry of the radiation source and radiation shielding grid, and the dimensions of the element exposed to the radiation. It also shows the γ -ray irradiation width including a half-shadow on the incident plane of the element from a radiation source. Considering the shielding effect, a 0.5-mm-thick tungsten layer is employed as a shielding grid, which shows a transmissivity of less than 5 % for X- rays having the energy of less than 100 keV.

The grids whose aperture is 0.15 mm (=a) for each element are arrayed at 1.6 mm (=l_3) from the element incident plane or the individual element electrode. The γ -rays from ^{241}Am (59.54 keV) source

which is placed 500 mm (=l_1) from the element are used to determine the irradiation width X_2 including the half-shadow. The width of radiation transmitted through the radiation shielding grid is determined for a 7-mm diameter γ-ray source. From Figure 2-6, the irradiation width for the above condition is 0.18 mm, including the half-shadow. As a result, the effective shielded width is 0.07 mm for the elements arrayed at an electrode pitch of 0.25 mm.

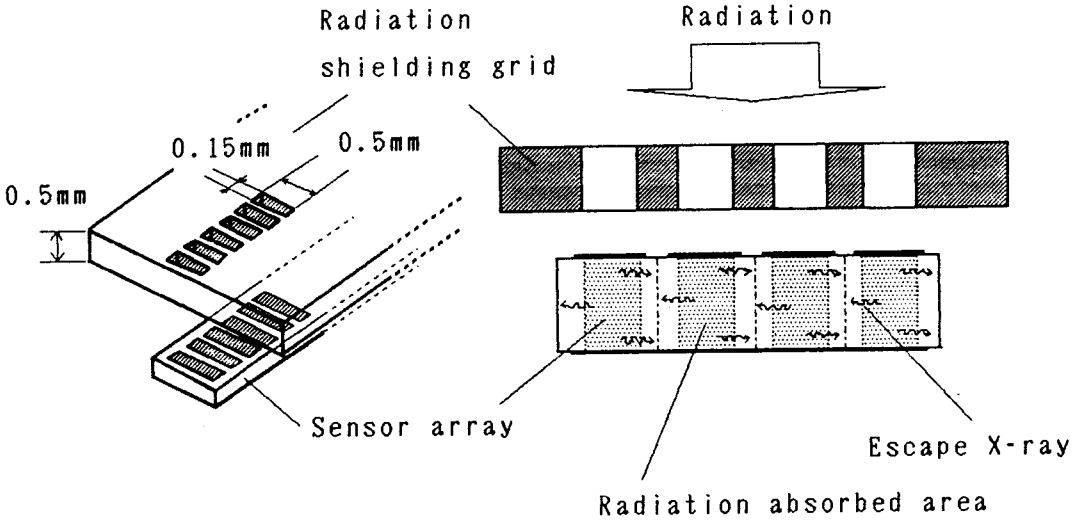

Fig.2-5 Schematics of detector elements and a radiation shielding grid.

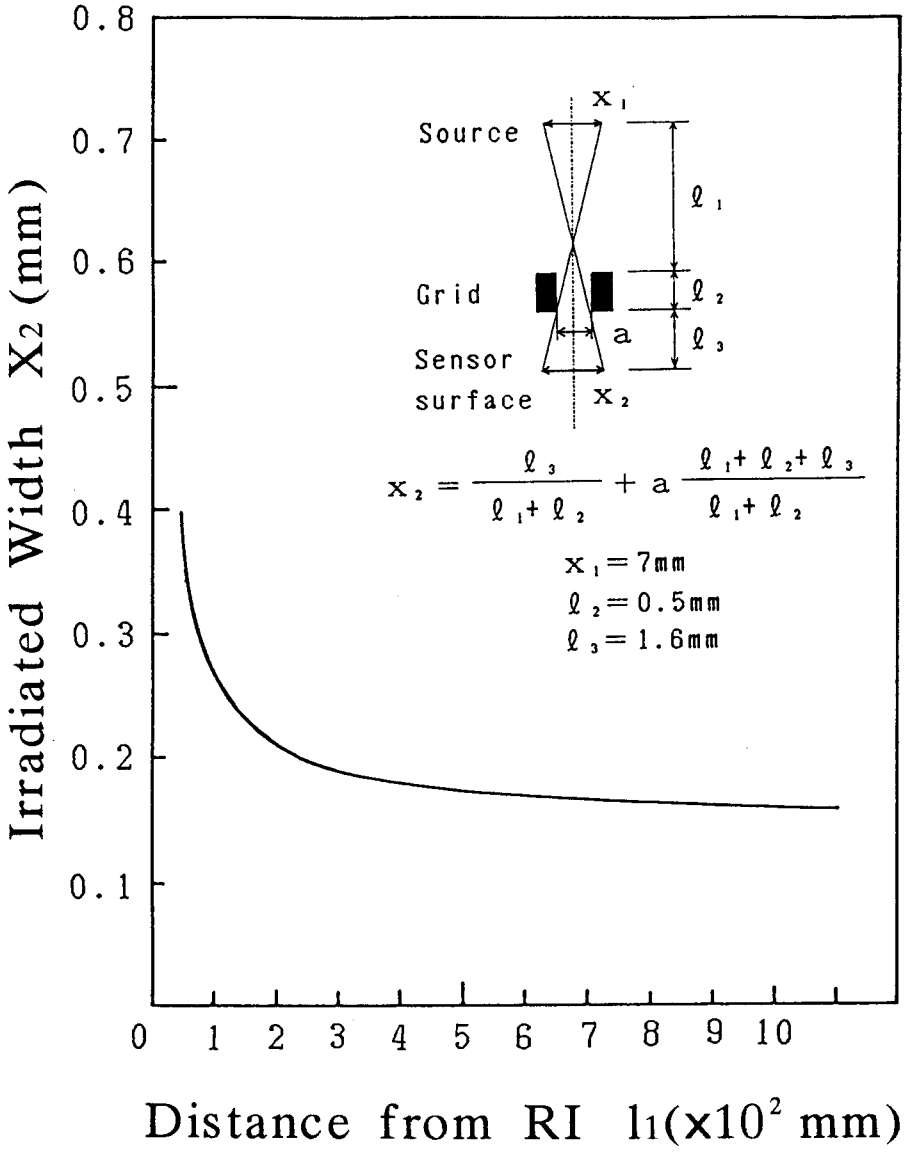

Fig.2-6 Geometry and calculation of the irradiated width to one detector element with a radiation shielding grid.

Figure 2-7 shows the effects of radiation shielding grid in terms of comparative changes of the pulse-height spectra. Figure 2-7(a) shows a spectrum using the radiation shielding grid, and (b), a spectrum without the grid. These spectra indicate substantial reductions of both X-ray escape peak counts and the crosstalk between neighboring elements caused by X-ray escape. A reduction of approximately 10 % is accomplished.

Figure 2-7 (c) shows a pulse-height spectrum obtained using a single detector with a sensitive volume of $1 \times 1 \times 0.3$ mm^3. This is nearly identical to (a) obtained by an element with a sensitive volume of $1 \times 0.25 \times 0.3$ mm^3 employing the radiation shielding grid.

As described before, the spectrum of low energy peaks for a single detector (c) contains only K-shell characteristic X-ray escape peaks of Cd and Te. The spectrum of low energy peaks for the linear array detector element contains two kinds of peaks: 1) K-shell characteristic X-ray peaks and 2) reabsorbed photopeaks of crosstalk X-rays. The main energies of the characteristic X-rays are 23.13 keV for Cd and 27.47 keV for Te, and the characteristic X-ray escape peaks are located at 32.07 keV and 36.37 keV, respectively. Considering the energy resolution of the detector, these peaks will be located at around 34 keV. In the same way, re-absorbed peaks of the crosstalk characteristic X-rays from neighboring elements will be located at around 25 keV. By providing the radiation shielding grid and limiting the irradiated area in each element, it was possible to reduce the low energy peaks from (b) to (a) by as much as 10 %. Especially in the spectrum (a), it was found that 1)the reduction of characteristic X-ray escape peaks of around 34 keV was remarkable and 2)there existed reabsorbed photo peaks of the crosstalk in the lower energy tail..

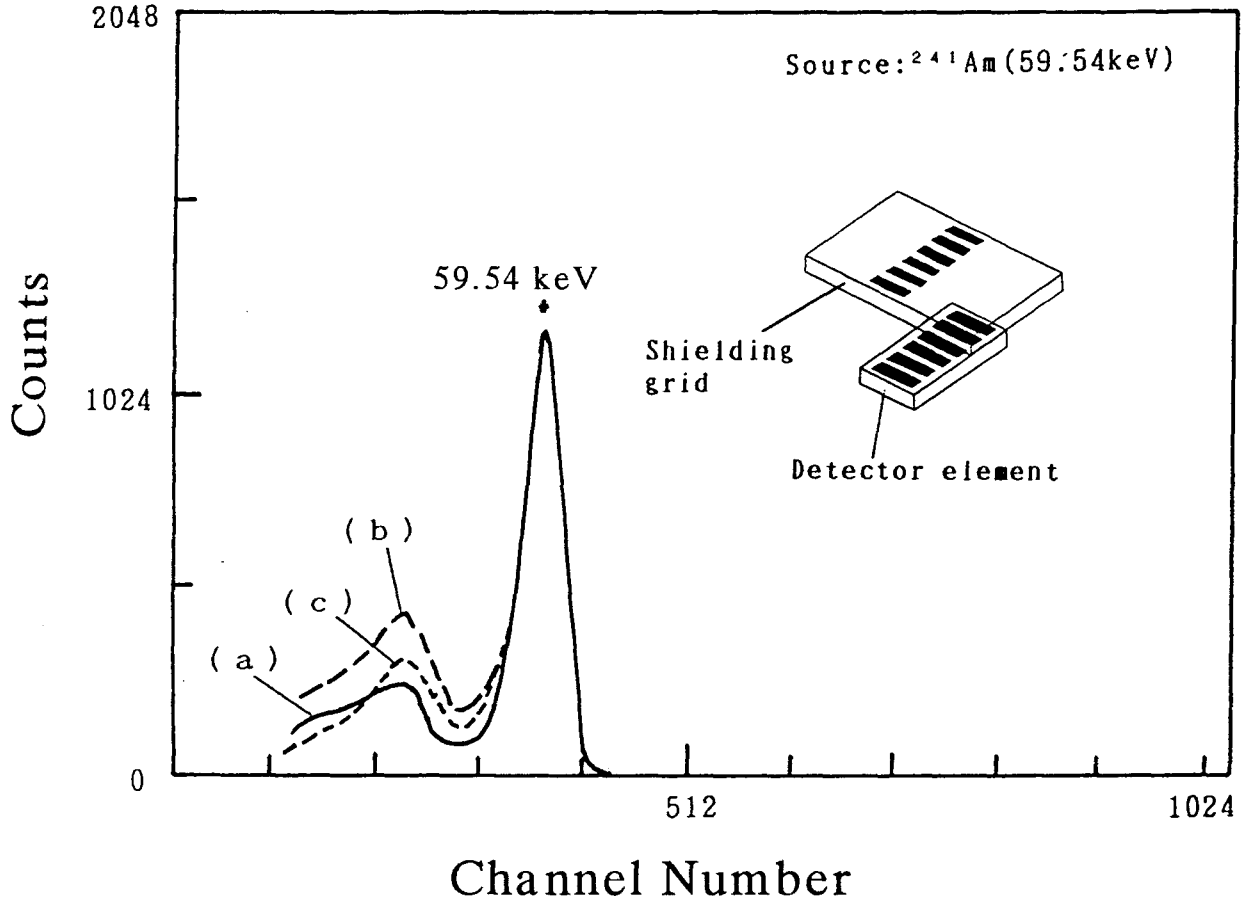

Fig.2-7 Spectra of ^{241}Am γ -ray detected by (a) one of the arrayed elements with a radiation shielding grid referring to (b) that without the radiation shielding grid and (c) that obtained by the simple detector $1 \times 1 \times 0.3\ mm^3$.

2-6. Discussion

The experimental results and discussions presented in the last paragraph demonstrated that the submillimeter CdTe detector submillimeter element ($0.25 \times 1 \times 0.3$ mm^3) formed on a crystal wafer has a spectral response to ^{241}Am γ-ray (59.54 keV). Further discussions to clarify the bases for this is given in the following.

The points to be discussed are: 1) the average traveling range of secondary electrons in a CdTe crystal, and 2) the escape of K-shell characteristic X-rays out of the element.

2-6-1 Range of secondary electron produced by the photo-electric effect.

Primary interaction of a CdTe crystal with X-rays of less than 100 keV is due to photo-electric absorption. The range of secondary electrons due to the K-shell photoelectric absorption of Si and CdTe is calculated for the energies of incident X-rays.

The Katz-Penfold's empirical formula is applicable for deriving the electron range in the material employed in this case.

$$R = 412 \times En \ (mg/cm^2) \qquad (0.01MeV < E < 3MeV) \qquad (1)$$
$$n = 1.265 - 0.09540 \times \ln E$$

The energy of the secondary electron E produced by photo-electric absorption can be expressed as

$$E = E_0 - E_k \quad (MeV) \qquad (2)$$

where E_0 is the incident X-ray energy and E_k is the K-shell absorption edge.

The range of secondary electron in the material, x (cm), can be expressed by

$$x = R / \varrho \ (cm) \qquad (3)$$

where ϱ is a density in (mg/cm^3).

The secondary electron range for the incident X-rays having an energy of up to 140 keV can be derived by applying Ek = 26.7 keV and 31.8 keV for Cd and Te, respectively, and $\varrho = 6.06 \times 10^3$ mg/cm^3 in eqs. (1),(2) and (3). The result is shown in Fig. 2-8, which shows that the range of the secondary electron caused by K-shell absorption of the incident X-rays with an energy of 100 keV is 12.2 μm for CdTe, while that for the silicon is 54.1 μm.

Therefore, CdTe is advantageous in terms of the smaller probability of a secondary electron escaping out of the crystal as compared with the Si. As a consequence, CdTe is suitable for fabricating linear array detectors because the crosstalk caused by the secondary electrons escaping out of the crystal is less than that of Si.

2-6-2 Absorption characteristics of K-shell X-ray in CdTe crystal

Figure 2-9 shows a plot of the absorption of characteristic X-ray against the thickness of CdTe crystal using the above-derived values. If the characteristic X-rays produced in an element are absorbed in the same element, the pulse observed gives a full height and does not give a minor photoelectric peak. The thickness necessary to absorb the photon is calculated. The energies of the K-shell characteristic X-rays are E(Cd)=23.17 keV and E(Te)=27.47 keV.

The thick solid line in the figure shows an average attenuation of both characteristic X-rays in CdTe crystal, and this shows that the thickness of CdTe which gives a decay of 50 % against K-shell characteristic X-rays is approximately 50 μm. The range determination of

the radiation shielding grid shown in Section 2-4 is made on this basis.

While the CdTe, though as thin as 50 μm, can give a good absorption characteristics for the X-rays, the Si crystal can not.

2-7. Conclusion

For the purpose of obtaining an X-ray detector array capable of energy resolution, a minimal element on a CdTe single-crystal wafer was prepared and the energy characteristics were obtained. The size of the effective element prepared was 1(length)×0.25(width)×0.3(thickness) mm^3 which provides a spatial resolution capability of 2 lp/mm along the array direction. A tungsten grid of 0.5 mm thick with an aperture of 0.5 (length)×0.15 (width) mm^2 was attached to reduce escape counts and crosstalk. Fortunately, the physical constants of 0.3-mm-thick CdTe are found to be optimum for the energy resolution of the diagnostic X-ray photons; the hole drift length is ideal for counter performance, and the X-ray photons and their photoelectrons can be sufficiently absorbed within this thickness. The resulting energy resolution for ^{241}Am γ-rays, which is the representative γ-ray of the diagnostic energy range, is 12 % (FWHM). This suggests a future possibility of X-ray imaging together with the supply of more accurate energy information by means of the linear array CdTe detector.

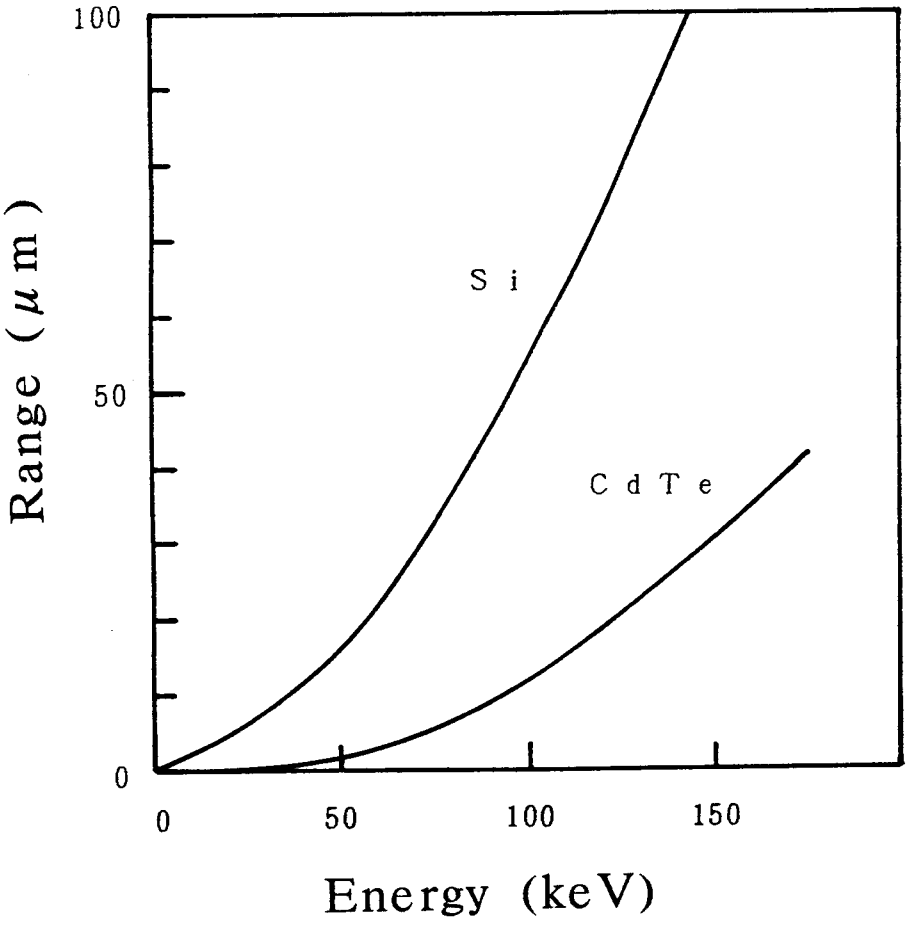

Fig.2-8 The range of secondary electron produced by K-shell photo-absorption to the incident photons.

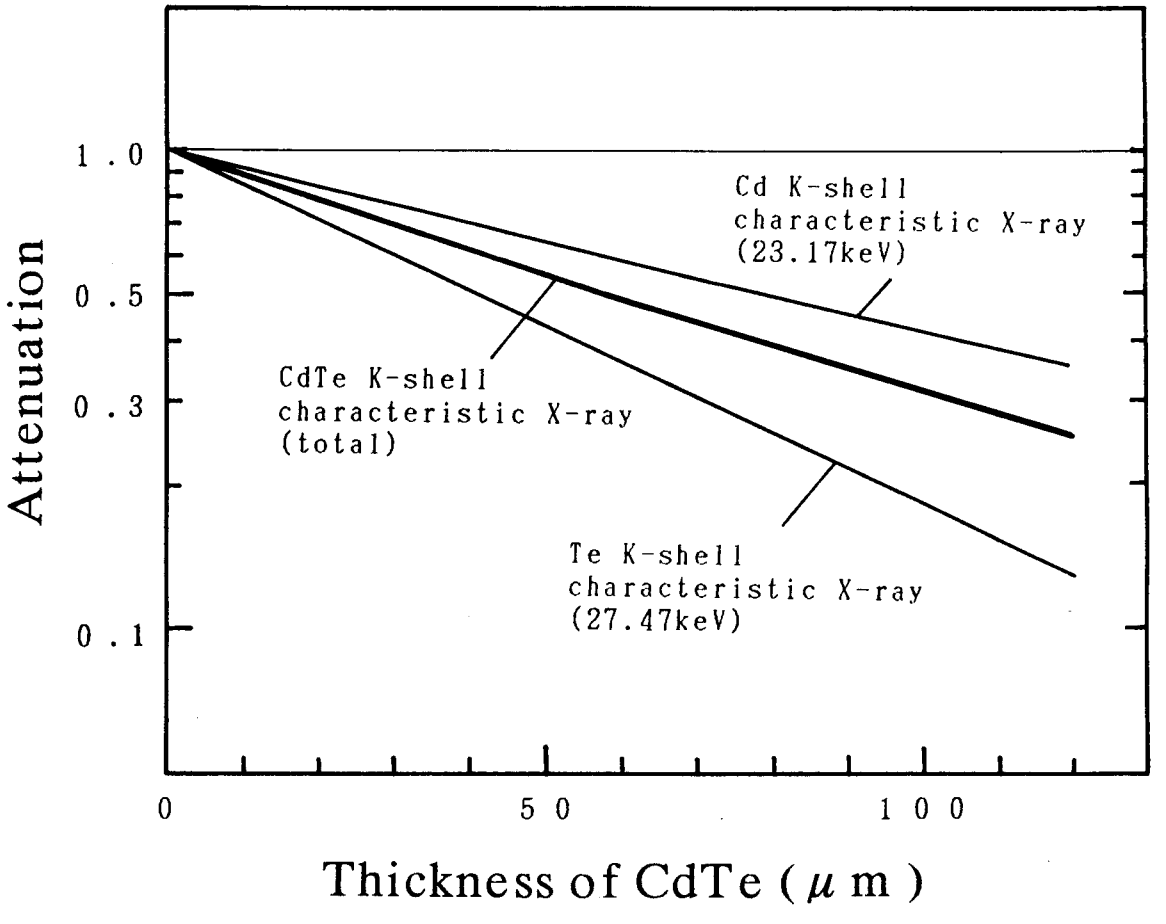

Fig.2-9 Absorption of characteristic X-rays against the thickness of CdTe crystal.

References

[1]D.J.Drost and A.Fenster: "Characteristics of A Linear Xenon Detector Array for Digital Radiography", SPIE Vol.273,Application of Optical Instrumentation in Medicine,1981.

[2]D.J.Drost and A.Fenster: "A xenon ionization detector for digital radiography", Med. Phys. Vol.9, No.2,March/April 1982.

[3]R.G.Fraser,E.Breatnach and G.T.Barnes: "Digital Radiography of the Chest- Clinical Experience with a Prototype Unit", Radiology, Vol.148, pp.1-5,1981

[4]R.A.Mattson,R.A.Sones,M.M.Tesic et al: "Design and Physical Characteristics of a Digital Chest Unit", SPIE Digital Radiography, Vol.314,1981.

[5]G.T.Barnes,R.A.Sones,M.M.Testic et al.: "Detector for Dual Energy Digital Radiography" Radiography, Vol.165,pp.595-601,1986.

[6]G.Ottaviani,C.Canali and A.Alberigi: "Charge Carrier Transport Properties of Semiconductor Materials Suitable for nuclear Radiation detector", IEEE Trans.Nucl.Sci.NS-22,1975,1980.

[7]P.A.Glasow, B.Conrad, K.Killing and W.Lichtenberg (Siemens A.G.) "Aspects of Semiconductor Current Node for X-ray Computed Tomography", IEEE Trans.Nucl. Sci. NS-28, 567, No.1 Feb. 1981

[8]P.A.Glasow, "Industrial Applications of Semiconductor Detectors", IEEE Trans. Nucl. Sci. NS-29, No.3, 1159, June 1982

[9]H. L. Malm, T. W. Raudorf, M. Martini and K. R. Zanio: "Gamma Ray Efficiency Comparisons for Si(Li), Ge, CdTe and HgI2 Detectors", IEEE Trans. Nucl. Sci. NS-20, No.1, 500,1973

[10]Y.Naruse, T. Sugita and T. Kobayashi: "Mulchi-channel Semiconductor Detectors for X-Ray Transmission Computed Tomography", IEEE Trans, Nucl. Sci. NS-27, No.1, 252, Feb. 1981.

[11]P. Siffert, A. Cornet and R. Stuck: "Cadmium Telluride Nuclear

Radiation Detectors", IEEE Trans. Nucl. Sci. NS-22, 211 feb. 1980.
[12]G. Ottaviani, C. Canali and A. Alberigi Quaranta.: "Charge Carrier Transport Properties of Semiconductor Materials Suitable for Nuclear Radiation Detector", IEEE Trans.Nucl. Sci. NS-27, 1975, 1980.

CHAPTER 3

Measurement of X-ray spectrum using a linear array CdTe detector

3-1. Introduction

X-ray imaging, using pixels capable of representing energy information, has possibilities for diagnosis of the human body and for inspection of intricate machinery. A linear array CdTe detector with an array of small size elements was prepared, and the characteristics of the detector element were examined using monochromatic gamma-rays from ^{241}Am. The detector was subjected to an analysis of the spectral response to X-rays from a diagnostic X-ray source.

Up to now, scintillation counters, semiconductor detectors and theoretical calculations have been used in a number of studies of the spectral measurement of X-rays. [1]-[7] For spectral analysis, large sized detectors, such as sodium-iodide scintillators, Xenon proportional counters, and Ge and Si semiconductors have been used; large Si detectors are known to give a good energy resolution; however, the measured spectral response must be compensated for the structure of the detector and the effect of scattering from the surrounding materials

Kaufman [8] and Ortendahl [9] used small size HPGe, CdTe, and HgI-based semiconductors to evaluate the feasibility of producing RI images. Detectors of millimeter aperture size showed both the possibility for practical use and limitations of these devices.

To our knowledge no work has been done with sub-millimeter detectors for X-ray radiography. Monochromatic gamma-rays at 59.54 keV from ^{241}Am are detectable using individual elements of $0.25 \times 0.3 \times 1.0$ mm^3 in a 32 element array giving an energy resolutions of 13.8 % FWHM. Unfortunately, the CdTe detector has a sub-peak extending to about 30 keV beyond the main photo-electric peak. Sub-peak

corresponds to the K-shell X-ray energies of Cd and Te. In our measurements the intensity ratio (the area under the two spectral curves) of the X-ray escape peak counts to the total counts was 43% A correction for the sub-peak resulted in a reduction of this error from 43 % to 30 %. In spite of this correction the energy response of the small size detector has deformed characteristics, with a small sub-peak below the photoelectric peak. The results of those measurement were discussed in chapter 2.

This chapter describes the spectral deformation of the small size detector exposed to X-rays having a continuous spectrum produced by an X-ray source. The deformation was due to several factors, the characteristic X-ray escape, the absorption and scattering by the element and the surrounding materials, and noise. In addition, a method for calibration of the deformed spectral characteristics is proposed, and some experimental results are presented.

3-2. Experimental procedure

The linear array detector used in this experiment was that of described in chapter 2-2. On the 32-electrode surface a radiation shield grid of tungsten sheet was mounted. The grid was mounted with a space of 1.6 mm above the detector element. One element of this array was chosen and examined. A current amplifier (ORTEC Model-571), a linear gate stretcher (ORTEC Model-542), and a multichannel analyzer (ORTEC Model-7100), were sequentially connected to the element. The electrode to the adjacent elements were grounded The X-ray source was a SIMAZU Model CIRCLE XP38D, and the array was placed at a point 100 cm apart from the focus.

As described in 3-1, an energy correction must be made for the sub-peak characteristics for X-rays. The element was subjected to gamma-rays

of ^{241}Am at 59.54 keV and the response function of the detector was recorded. The detector was set at a distance of 50 cm from the ^{241}Am source facing the 32- electrodes side to the source. The pulse obtained under these conditions had the FWHM of 30 ns, and the pulse height of 250 mV for an applied voltage of 3.3 keV/cm. Figure 3-1 shows an example of the result of spectral measurement: energy resolution of 13.8 % for 59.54 keV gamma-rays, with the escape count ratio of 30 %. This value was utilized in our analysis of X-ray spectral response for the CdTe linear array detector.

3-3.Correction strategy for flawed spectral response

The spectral response of this CdTe detector has deformed characteristics as shown in Figure 3-1, where the K-shell escape peak is seen.

The items causing the deformation include:

1) The energy dependence of the photoelectric absorption of the detector material.
2) The arrival of K-shell X-rays escaped from the adjacent elements due to the small-size of the element.
3) The escaped photoelectron and the resulting shrinking of the photo-peak owing to the small element size.
4) Noise counts due primarily to Compton-scattered electrons.

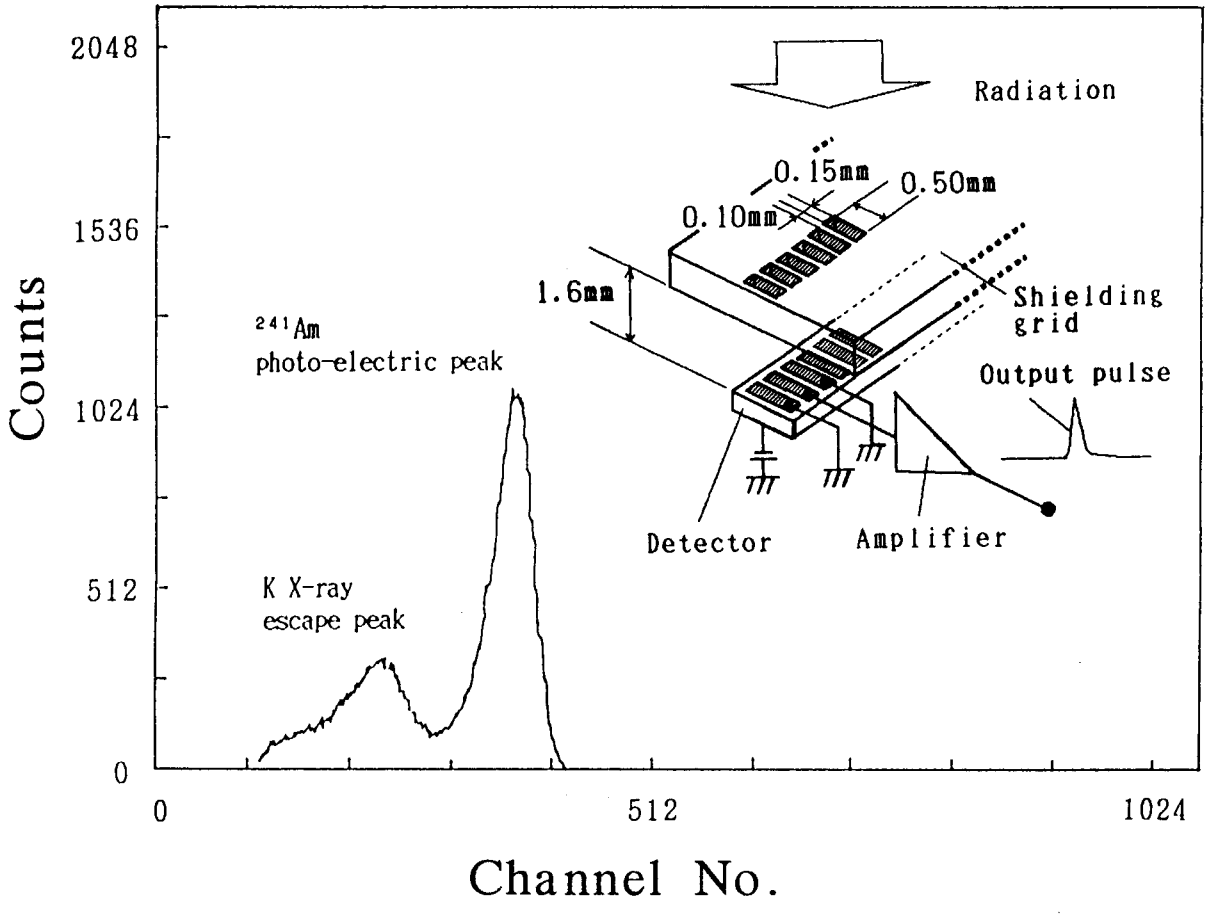

Fig.3-1 Schematics of the experimental detector set-up and the output spectrum for ^{241}Am gamma-rays (59.54 keV). The 32 elements are arrayed on a CdTe wafer; each element size is 0.25 $\times$0.3$\times$1 mm^3

Figure 3-2(A) shows the energy dependence of the fraction of the number of absorbed photons (photoelectric process) to the number of incident photons for a 0.3 mm-thick element, calculated using the table of absorption coefficients. The K-shell absorption edges due to Cd and Te are seen to be around 30 keV. The element thickness is so small that a decrease in the number of photons absorbed can be observed for energies over 40 keV. Figure 3-2(B) similarly shows the energy dependence of the scattered or escaped photons to the number of incident photons. Curve (a) illustrates the ratio attributable to the escape of the characteristic X-rays.(item 2) Photon escape occurs over the energy above the absorption edges of Cd and Te, resulting the crosstalk between the adjustment elements. The ratio is a constant over the above energy range and is about 0.3; this was obtained experimentally via ^{241}Am gamma-ray exposure. Curve (b) shows the ratio of photo-electric events in which the photoelectron escaped out from the element, compared to the total number of photoelectric events (item 3). Curve (b) was obtained by comparing the range of the photoelectron in CdTe and the distances between the event points and the surfaces. The value obtained was fairly small, 2.5 % at 100 keV. Curve (c) is the ratio of the Compton-scattering events to the absorption events. It was obtained by using the absorption coefficient and the scattering attenuation coefficient of CdTe. As can be seen in the figure, the dominant factors affecting deformation are the energy dependence of X-ray absorption and X-ray escape. Item 3) and 4) mentioned above can be considered to be vanishingly small. Thus, ignoring the two minor factors, the dominant factors only was taken into account and the spectral response function was calculated. Putting the incident X-ray spectrum as $f_0(E)$, the absorbed X-ray spectrum f(E) becomes:

$$f(E) = f_0(E)\{1-\exp(-\mu(E)d\} \quad (1)$$

where E is the photon energy, $\mu(E)$ is the absorption coefficient. and d is the thickness of the detector element. Now the output X-ray spectrum generated by the detector element g(E) can be written corresponding to the photon energy regions as

$$g_1(E) = f_0(E)\{1-\exp(-\mu(E)d\} \quad E<K \quad (2)$$

$$g_2(E) = (1-A)f_0(E)\{1-\exp(-\mu(E)d)\} \quad E\geqq K \quad (3)$$

$$g_3(E-Ek) = Af_0(E)\{1-\exp(-\mu(E)d\} \quad E\geqq K \quad (4)$$

where K is the K-shell absorption energy (keV), A is the ratio of the escape counts to the total counts and d is the detector thickness. Figure 3-3 shows a conceptual drawing of these equations. It may be noted that the spectral curve changes discontinuously at the K-shell absorption energy. The spectrum of the output count for E below K, as shown by (2), is governed by the element thickness. When E is larger than K, there are two possibilities: One is that the photoelectric absorption peak itself is being displayed and the other, that it represents the X-ray escape peak. The probability of the latter is A, whereas that of the former is (1-A).The output spectra are governed by the thickness multiplied by the above two probability.

Then the final output spectrum becomes

$$g_{fin}(E)=g_1(E)+g_2(E)+g_3(E) \quad (5)$$

The curve from equation (5) is also drawn in Figure 3-3. This method of calculation was applied to the CdTe detector array, and the calculated

result is shown in Figure 3-4. The incident X-ray spectrum used in the calculation was that measured by Birch et al.1) The value A was experimentally obtained using the method shown in Figure 3-2(B); the result was A=0.3 for the total escapes of the absorption edges for 26.7 keV (Cd) and 31.8 keV (Te). In the figure, the broken line is for the incident spectrum modified by the data obtained by Birch et al. The dotted line shows the absorbed spectrum by the detector of 0.3 mm thick; the solid line shows the output spectrum calculated by the equations, This spectrum, as observed by the equations, wholly shifts to the low energy side compared with the incident spectrum.

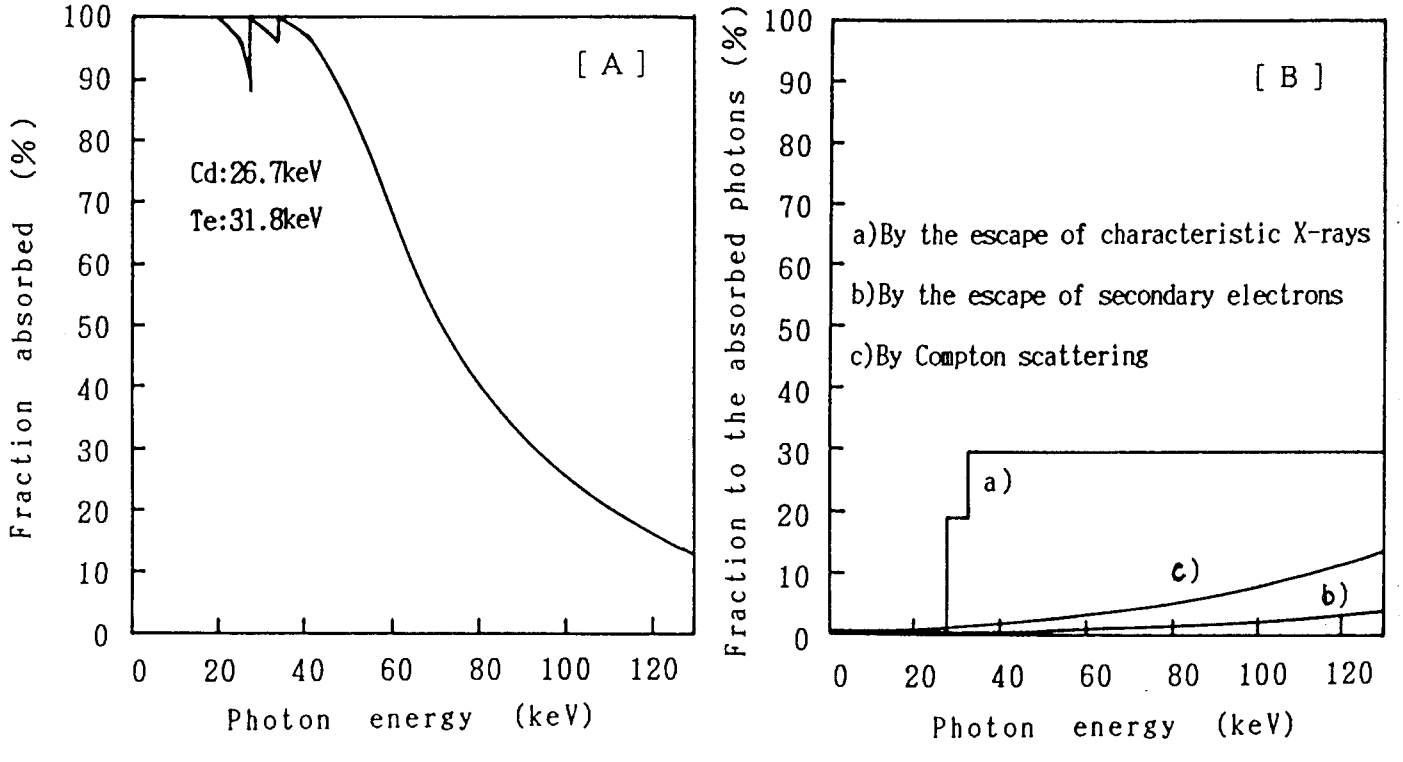

Fig.3-2 Deformation factors for the X-ray spectral response of the 0.3 mm thick CdTe detector; [A] fractions of the photo-electrically absorbed photons per incident photons; [B] curve (a) fractions of the absorbed but photo escaped photons per absorbed photons, curve (b) fractions of the absorbed photons of which the secondary electrons escaped out of the element. curve (c) ratio of the Compton scattered photons to the photo-electrically absorbed photons.

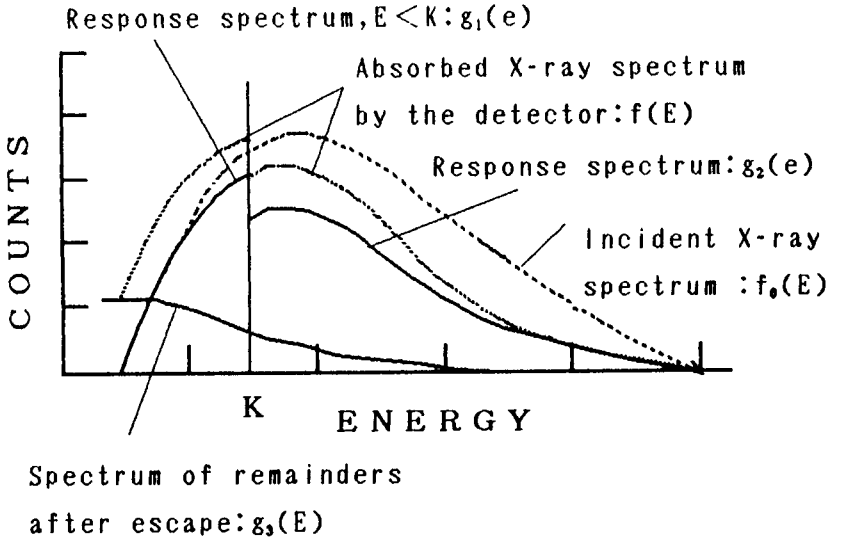

Fig.3-3 Conceptual drawing of the CdTe spectral response.

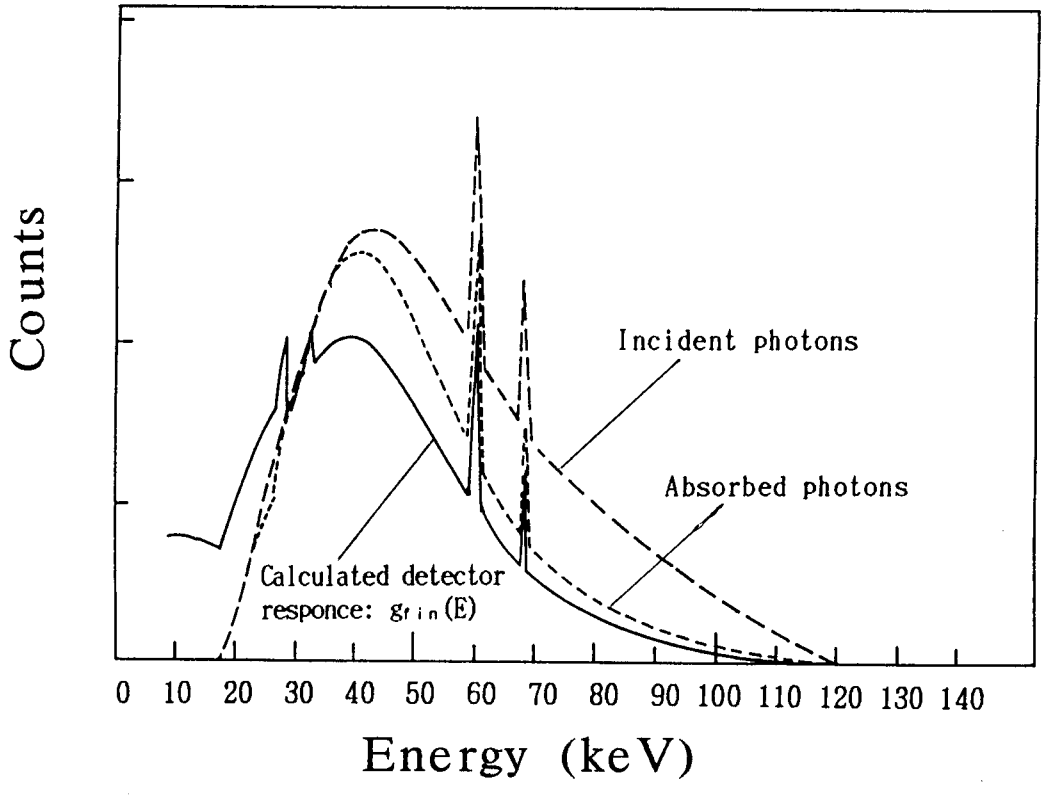

Fig.3-4 Calculated 0.3 mm CdTe detector response for X-rays from X-ray source: the source conditions are: applied constant voltage of 120 kV, target angle of 17° and with 2.5 mm Al filter (Bilch's conditions)

3-4. X-ray spectrum measurement

Figure 3-5 shows the experimental results of the X-ray output spectrum obtained by our CdTe detector array. The X-ray source used was a Simazu CIRCLEX P38D of rotating tungsten target type with a target angle of 12° and a total filtration of Al 2.5 mm. The operating parameters are shown in the figure. A collimator was used to form the X-ray into a fan-beam to minimize the scattering of X-rays from neighboring materials. The counting rate was 3×10^4 cps at the applied voltage of 120 kV and the current integration time of 8 sec. As shown in the figure, the experimental result coincides well the simulation result as a whole; Good coincidence is seen in the high energy region, whereas the output counts by the simulation are less than the experimental data in the low energy region. This minor difference in the low energy region may arise from the X-ray source geometry; the X-ray source described by Birch et al.and used in the simulation had a target angle 17° ,while the source used in the experiment was 12° . The reason is that; the target ungle becomes larger, the distribution of the X-ray generation points originated by Bremsstrahlung becomes near to the target surface and then lower energy X-rays generated in the target become easy to go out of the target. The fluence of the X-rays in the low energy region generated by the X-ray source having the target ungle of 17° becomes larger compared to those having the target ungle of 12° .

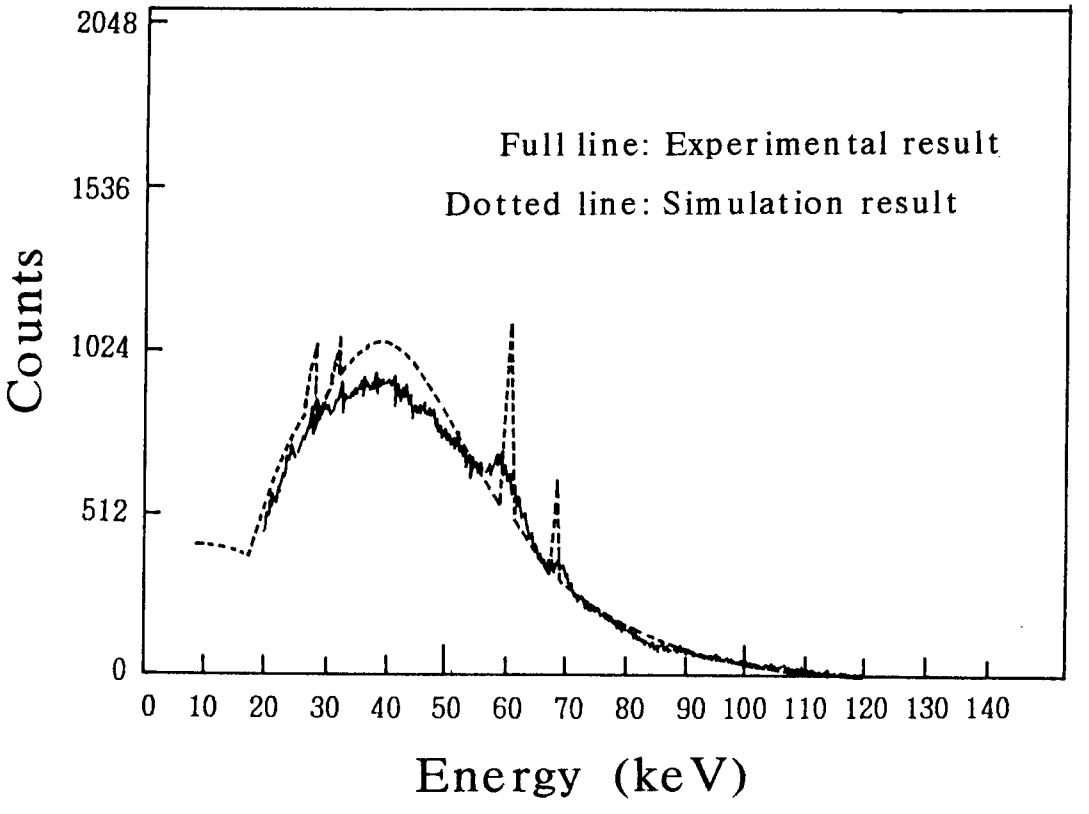

Fig.3-5 Output spectrum experimentally obtained by the CdTe detector for X-rays from X-ray source: applied constant voltage of 120 kV, target angle of 12° , distance between the detector and the focus of 100 cm air path and sampling time of 2 sec.

3-5. Discussion

The results here concern about continuous X-rays from an X-ray source for medical imaging. The necessary requirement of a detector element to be used for X-ray imaging is that the element size be small; it should be less than 0.25 mm in width, or more than four elements should be arrayed per millimeter to realize an image resolution of 2 lp/mm. In this experiment, the size of the element was designated as $0.25 \times 1 \times 0.3$ mm^3 to satisfy this requirement. We have investigated the characteristics of deformation generated by the CdTe detector. Four types of possible origins of the deformation were listed in the previous section and the evaluated results of these errors is shown in Figure 3-2 - Figure 3-4. The most dominant is the item 1) in chapter 3-3, the photoelectric absorption characteristics of the CdTe. The error caused by item 4), Compton scattering is below 2 % and can be neglected. Similarly, the error caused by condition 3), the escape of secondary electrons, is also small. The range of the electrons induced by photoelectric events are within 50 μ m and can be absorbed within the element. The deformation caused by photoelectrons indicates that the grid should be designed to prevent secondary electron crosstalk between adjacent elements. A grid width of about 50 μ m may be satisfactory, and the requirement for high element density in the array might be also satisfied. In the field of X-ray imaging, a rough energy separation method using a filter of high Z material is being studied, in which the image signals are separated into two energy zones, a high-energy zone and a low-energy zone. The difference signal between those of two zones can be used to form a new image that provides unique information. The detectors described in this report may give even more energy information, expanding the field of practical use of X-ray imaging.

3-6. Conclusion

A CdTe detector array designed for X-ray imaging was examined about its X-ray energy response. We were able to clarify two major sources of deformation in the spectral response of the detector; one was the energy dependence of the photoelectric absorption process, and the other was the characteristic photon escape from the element.

The results for their compensation which was experimentally applied to a CdTe detector array composed of very small elements were concluded to be practicable in the application of X-ray detection containing energy information. We expect that this technique can be applied to a new type of energy analysis of X-ray images.

References

[1] R.Birch, M.Marshal and G.M.Adran HPA, Scientific Report Series 30, London 1979 Catalogue of Spectral Data for Diagnostic X-rays

[2] H.I.Israel, D.W.Lier and E.Storm "Comparison of Detectors used in Measurement of 10 to 300 keV X-ray Spectra"
Nuclear Instruments and Methods 91 (1971) 141-157

[3] R.Birch and M.Marshal "Computation of Bremsstrahlung X-ray Spectra and Comparison with Spectra Measured with a Ge(Li) Detector"
Phys. Med. Biol., 1979, Vil.24, No.3, 505-517

[4] Y.Kodera, H.P.Chan and K.Doi "Effect of Collimators on the Measurement of Diagnostic X-ray Spectra"
Phi. Med. Biol., 1983, Vol. 28, No.7, 841-852

[5] L.C.Baird X-ray Spectra Vs. "Attenuation Data: A Theoretical Analysis"
Med. Phys., 8(3), May/June 1981

[6] E.Storn, H.I.Israel and D.W.Lier "Bremsstrahlung Emission Measurement from Thick Tungsten Targets in the Energy Range 12 to 300 kV (Sodium Iodide Scintillator, Germanium and Silicon Semiconductors), and Xenon Proportional Counter)" Los Alamos Scientific Laboratory Report LA-4624, UC-34, Physics, TID-450, 1971

[7] L.Kaufman, S.H.Williams et al "An Evaluation of Semiconductor Detectors for Position Tomography"
IEEE Trans Nucl Sci NS-26: 648, 1979

[8] D.Ortendahl, L.Kaufman et al " Operating Characteristics of Small Position-Sensitive Mercuric Iodide Detectors"
IEEE Trans Nucl Sci NS-29: 784, 1982

CHAPTER 4
Energy Separation System

4-1. Introduction

X-ray radiographic images from conventional electronic detectors like scintillators or image intensifiers, are generally constructed from analog signals of integrated information of X-ray strength. In recent years a dual energy subtraction method has been developed utilizing Computed Tomography (CT) scanner detectors, Computed Radiography (CR) phosphor plates and Digital Chest photodiode arrays.[1],[2] Because of the poor energy resolution of these detectors, numerous methods have been developed to provide X-rays in two energy bands. For CT scanners, alternate low and high energies are obtained by switching the X-ray tube voltage. For CR plates, a copper plate is placed between two phosphor plates to provide two energy regions, and for Digital Chest arrays, two detector elements, consisting of low and high atomic number phosphors are used.[3]-[6]

Output signals from semiconductor detectors described in preceding chapter are pulses induced by absorption of photons within the detector. Operation of these detectors in photon counting mode can provide a number of advantages over the systems described before. Firstly, high sensitivity and high signal to noise ratio can be obtained with these devices. Secondly, energy measurement of incident radiation is possible by using pulse height measurement techniques. A number of studies have been reported on the feasibility of constructing gamma cameras using HPGe, HgI_2 and CdTe semiconductor detectors, [7]-[12] and these works have been extended to include X-ray camera and X-ray array detectors.[13],[14] It also has been shown that a CdTe semiconductor detector array is capable of obtaining simultaneous

images of X-ray strength in association with images of X-ray energy spectrum. It is possible to derive information about the composition of an object by comparing the variations in the spectrum before and after penetration of the object.

In this chapter a linear array CdTe semiconductor X-ray imaging sensor is described. Descriptions of construction, counting circuit design and basic characteristics are included. In addition, the energy separation method is applied to experimental images and the advantages of this technique are highlighted.

4-2. Photon counting method

The most important problem in the application of pulse counting method to X-ray radiography is the requirement for the high counting rate requirements. Additional condition such as: (1) high impedance of the detector elements, (2) small output signal and (3) high speed response also make it difficult.

To obtain a suitable preamplifier for CdTe semiconductor detector, the following approaches were investigated: 1) current-voltage conversion and high impedance - low impedance conversion, 2) high-frequency amplification without gain decrease.

The solution was to use a negative feedback circuit to create a high-speed preamplifier. Figure 4-1 (a) shows an equivalent circuit. Ro, Rf, Co, Ci refer to detector resistance, negative feedback resistance, detector capacity and input floating capacity respectively. Figure 4-1 (b) shows a circuit which realizes the equivalent circuit described in (a). A FET was used for the first stage. The output voltage of Vo is described in the following equation

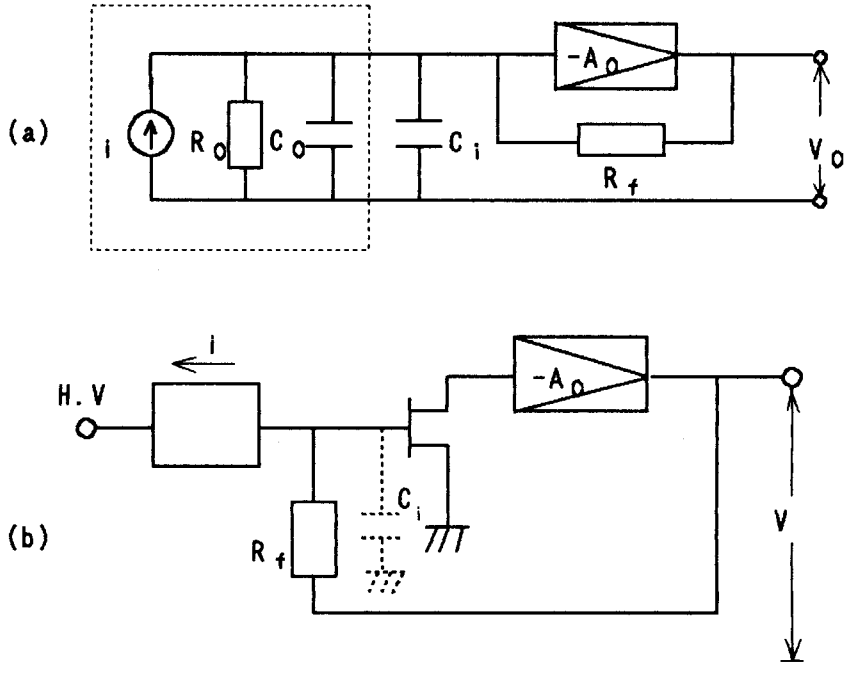

Fig.4-1 The negative feed-back circuit of the fast speed preamplifier, (a) shows the equivalent circuit of a sensor and an amplifier circuit and (b) shows a negative feed-back amplifier.

$$Vo = \frac{i}{\frac{1}{AoRo} + \frac{1}{Rf}(1 + \frac{1}{Ao}) + \frac{jw}{Ao}(Co + Ci)} \quad (1)$$

In this equation, Ao ≫ 1 and generally Rf ≪AoRo and, Vo is described as follows:

$$Vo = - \frac{Rfi}{1 + \frac{jw}{Ao}(Co + Ci)Rf} \quad (2)$$

$$|Vo| = \frac{Rfi}{1 + \frac{f}{fc}} \quad (3)$$

$$fc = \frac{Ao}{2(Co + Ci)Rf} \quad (4)$$

In equations (3) and (4), fc is the cut-off frequency. This circuit structure makes it possible to decrease the output impedance and to amplify the signal in the higher frequency region. An amplifier capable of operating up to 10 MHz was obtained with the circuit parameters: Co+Ci=5pF, Rf=10MΩ, Ao=250.

4-3.X-ray energy separation method

X-ray energies are separable using the circuit shown in Figure 4-2. This circuit has 2 sets of discriminator and counter for each detector element. Output pulses are amplified and separated into two groups by discriminators 1 and 2. Applying low and high voltage to discriminator 1 and 2 respectively, It is possible to perform simultaneous energy measurements. The discriminator 1 operates as a low level discriminator, and all pulses generated by X-rays are counted by counter 1. The discriminator 2 is for high level discrimination, and only X-rays of

sufficient energy are counted.

Figure 4-3 shows the irrustration of the X-ray energy separation method. D1 and D2 are the setting level of the discriminator 1 and the discriminator 2 respectively. Figure 4-4 (a) shows a measurement of the total energy region S(L+H) above the level D1 and Figure 4-4 (b) shows a measurement of the high energy region S(H) above the level D2. A measurement of the low energy region only, S(L) is obtained by subtraction S(L+H)-S(H).

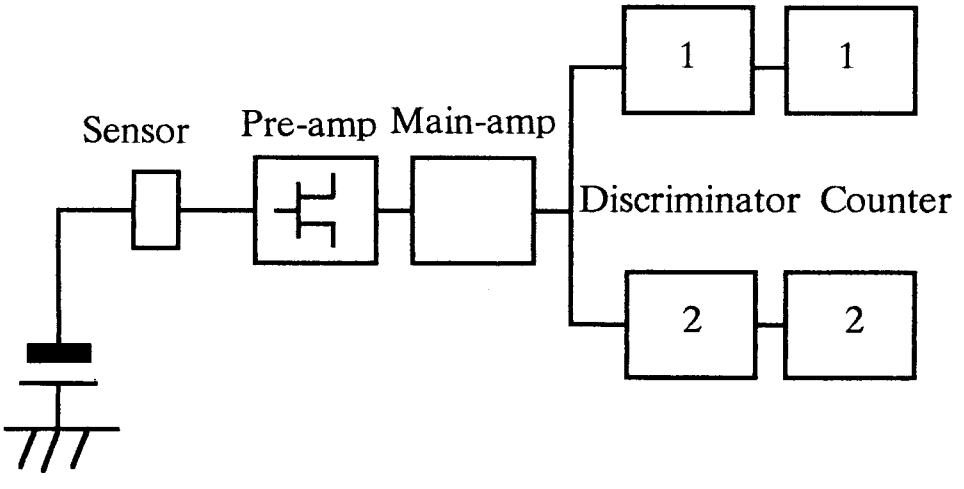

Fig. 4-2 Block diagram of X-ray energy separation circuit. Comparator-1 and counter-1 (the set 1) are able to count the whole energy range of X-ray photons over discrimination level D1 and the set 2 are able to count the energy range of photons over discrimination level D2.

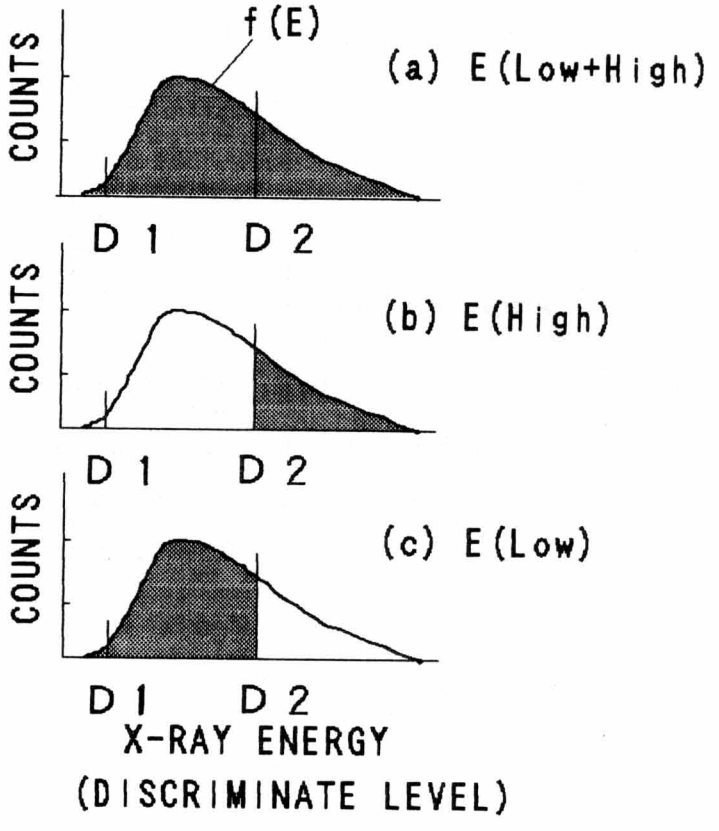

Fig. 4-3 Illustrations of energy separation process: total energy range (a), high energy range (b), low energy range (c) can be measured respectively.

4-4.X-ray spectrum

4-4-1.Measurement of X-ray spectrum

To obtain X-ray energy spectrum, photon pulses induced by X-rays were counted with different discriminator levels. The spectra were obtained by subtraction of pulse counts of each discriminator level. Data were obtained under the following conditions. The X-ray source was operated at 120 kV constant voltage and 0.1 mA constant current. Differential counts were calculated by increasing the discriminator level at 10 mV steps as in single channel analysis. Figure 4-4 shows the result of the X-ray spectrum measurement. In Figure 4-4, although tungsten characteristic X-ray peaks were not obtained in the spectrum because of the large discriminator voltage increments, the spectrum did show a good coincidence to an X-ray absorption spectrum for a CdTe detector element. This analysis confirmed that X-ray energy information can be obtained through the use of the different discriminator voltage levels.

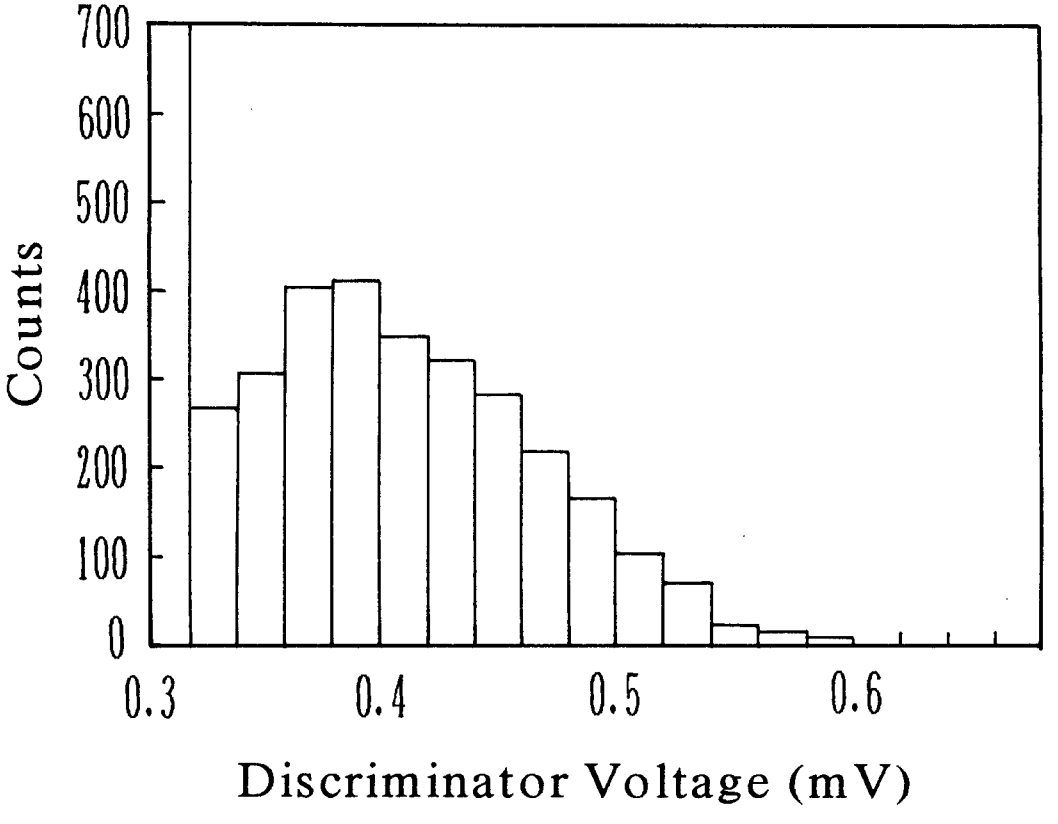

Fig.4-4 X-ray energy spectrum obtained with energy separation circuit. Discriminator voltage was varied at 10 mV step.

4-4-2 X-ray energy separation

Effective energies were measured using the separation method described above. Copper plates with different thickness were exposed to X-rays and transmitted X-rays were detected by the X-ray imaging sensor having several discrimination levels. X-ray effective energies for each discriminator level were corrected by calculating the first half value layers obtained from attenuation curves of copper.

Figure 4-5 shows attenuation curves of count number obtained with copper plate thickness varying from 0.1 mm to 2 mm (and 2 mm Al equivalent thickness to X-ray source). The low discriminator level was fixed at 0.36 V and the high discriminator level was varied from 0.41 V to 0.48 V. The thick line shows the attenuation curve at the discrimination level of 0.36 V and this line indicates total absorption. The thin lines show attenuation curves for discrimination levels between 0.41 V to 0.48 V. These lines indicate high energy levels. Dotted lines show attenuation curves for true low energy discriminator levels obtained by subtracting counts for high discriminator levels from those for low discriminator levels.

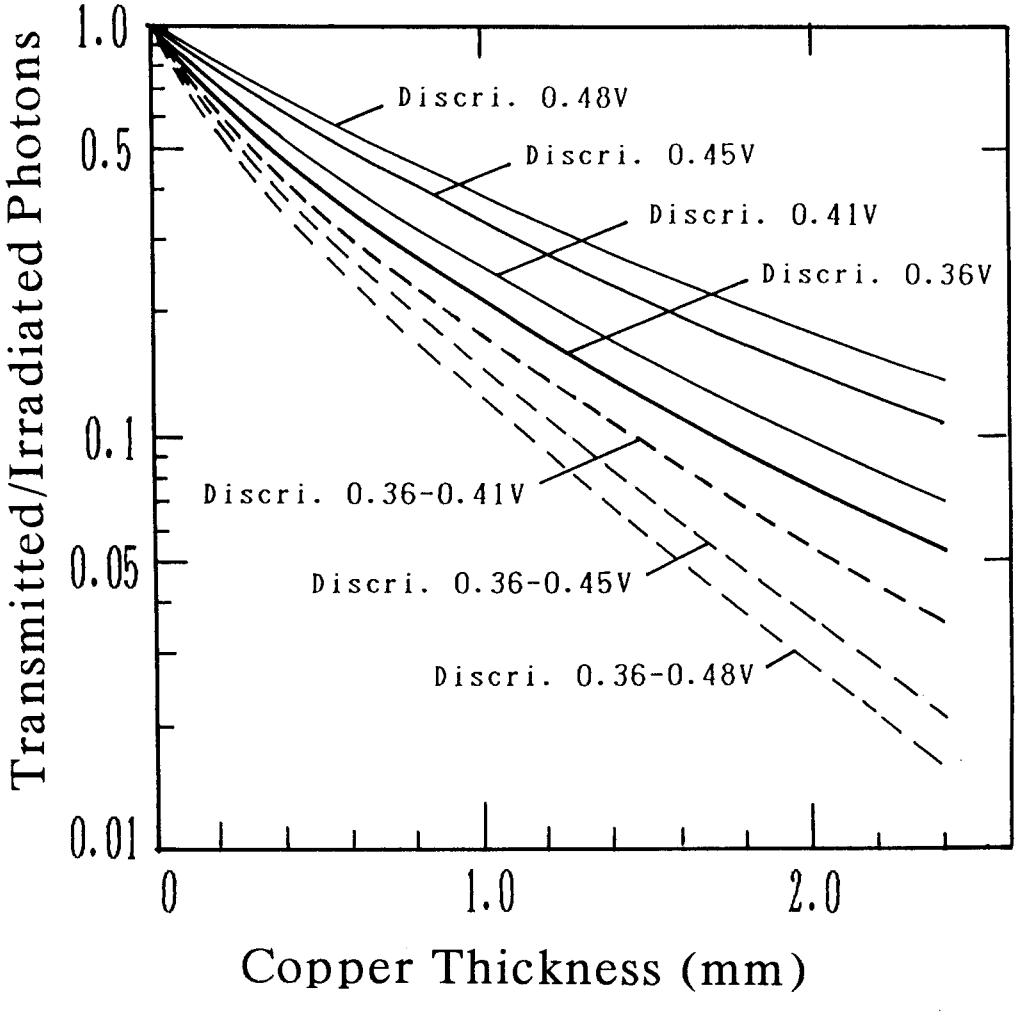

Fig.4-5 Attenuation curve of copper for various discriminator levels. D1 = 0.36 V and D2 = 0.41, 0.45, 0.48 V respectively. X-ray tube voltage was 120 kV.

Table 4-1 shows the effective energy values obtained from half value layers of copper for each attenuation curve. An effective energy was calculated using the half value layer. The transmission equation is described as follows.

$$I/I_0 = \exp\{-\mu(E)x\} \quad (5)$$

$$\mu(E) = \ln(I/I_0)/x \quad (6)$$

where I/I_0 means a transmissivity and $\mu(E)$ means a thickness for copper.From the figure 4-5, the value x=0.030 (cm) was obtained for I/I0=0.5 and then $\mu(E)$ was calculated as 22.9 (cm^{-1}). Using the conventional data showing the relations between photon energies and absorption coefficients for copper, effective photon energy E was obtained as 50.0 (keV) at $\mu(E)$=22.9 (cm^{-1}). Applying this method to the high discrimination level at 0.41 V, separated effective energies of 45.0 keV and 54.5 keV were obtained for the separated low and high energy levels respectively.Applying this method again, separated energies of 44.0 keV and 60.5 keV were obtained for the high discrimination level at 0.45 V, and those of 46.0 keV and 63.0 keV were obtained for the high discrimination level at 0.48 V, respectively.

TABLE 4-1

Effective energy calculated from First Half Value Layer (First HVL) using a copper filter

Discriminator level	Effective energy (cave)	
L = 0.36 V	E(low + high) = 50.0 keV	
H = 0.41 V	E(low) = 45.0 keV	E(high) = 54.5 keV
H = 0.45 V	E(low) = 44.0 keV	E(high) = 60.5 keV
H = 0.48 V	E(low) = 46.0 keV	E(high) = 63.0 keV

4-5. Radiographic measurement

Radiographic measurement was carried out in the case where a linear array detector was exposed to a fan beam of X-rays. Radiographic images were obtained by scanning the detector around the focus of the X-ray tube. The distance from the focus to the imaging sensor was 100 cm. Applied tube voltage was 100 keV and tube current was 4 mA. The scanning speed was 5 mm/sec and scanning pitch, 0.25 mm. A linear array detector of 256 elements (6.4 cm) were prepared and with 1024 scanned lines, it produced simultaneously low and high energy radiographs of 256×1024 pixels (6.4×25.6 cm).

Specific resolution can be obtained by measuring the contrast of X-rays transmitted through the X-ray chart (Micro chart R-1) along the scanning direction. The X-ray chart is consisted of tungsten thin film of 0.5 mm thick and has the slit patterns from 0.5 to 5 line pairs/mm. Figure 4-6 shows the output data of the X-ray chart contrast pattern of the X-ray chart along the scanning direction. The vertical axis shows the photon counts penetrated the X-ray chart and the horizontal axis shows the position of the scanning direction. A modulation transfer function curve (MTF) was obtained by plotting the contrast data shown in the figure 4-6. Figure 4-7 shows the MTF curve where the spatial resolution of 2.5 lp/mm is obtained for the response value of 0.3.

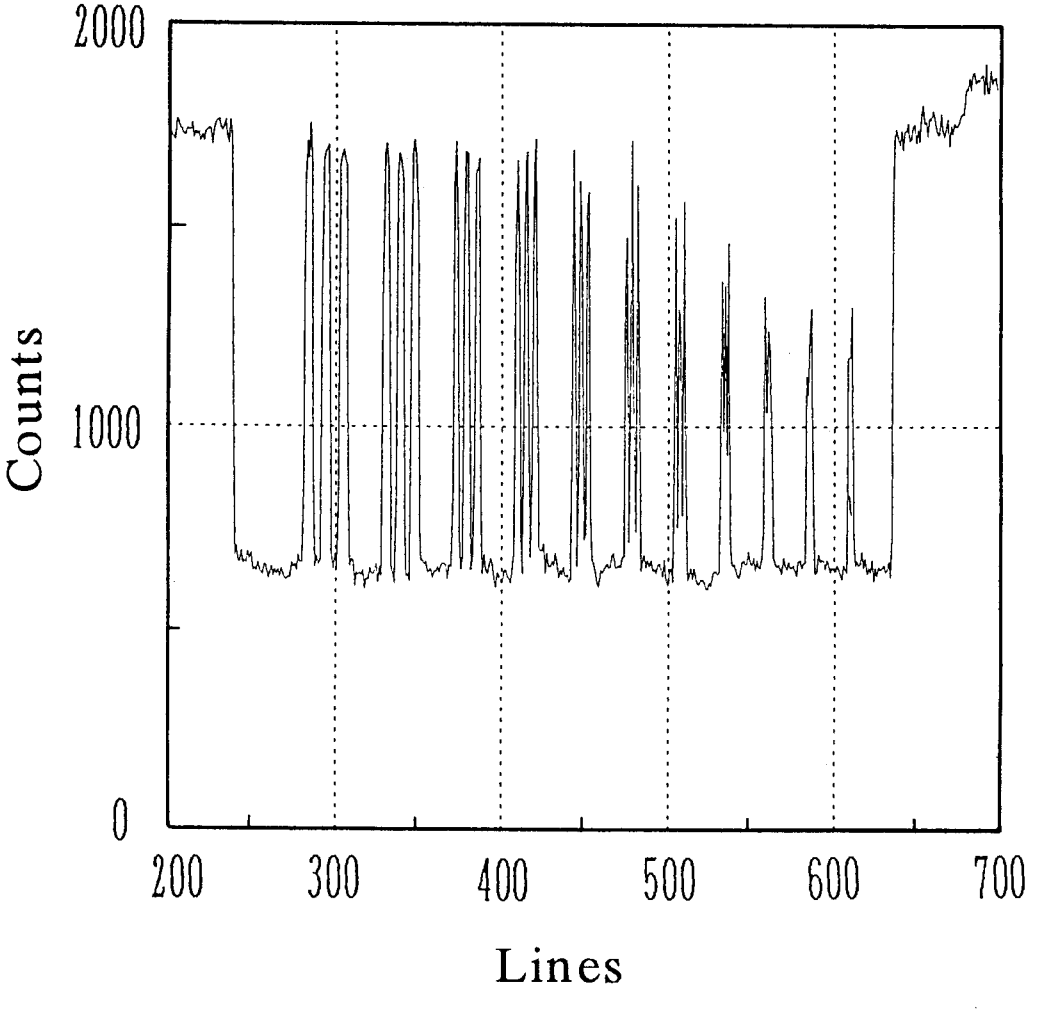

Fig.4-6 Output data of the contrast pattern of an X-ray chart along the scanning direction

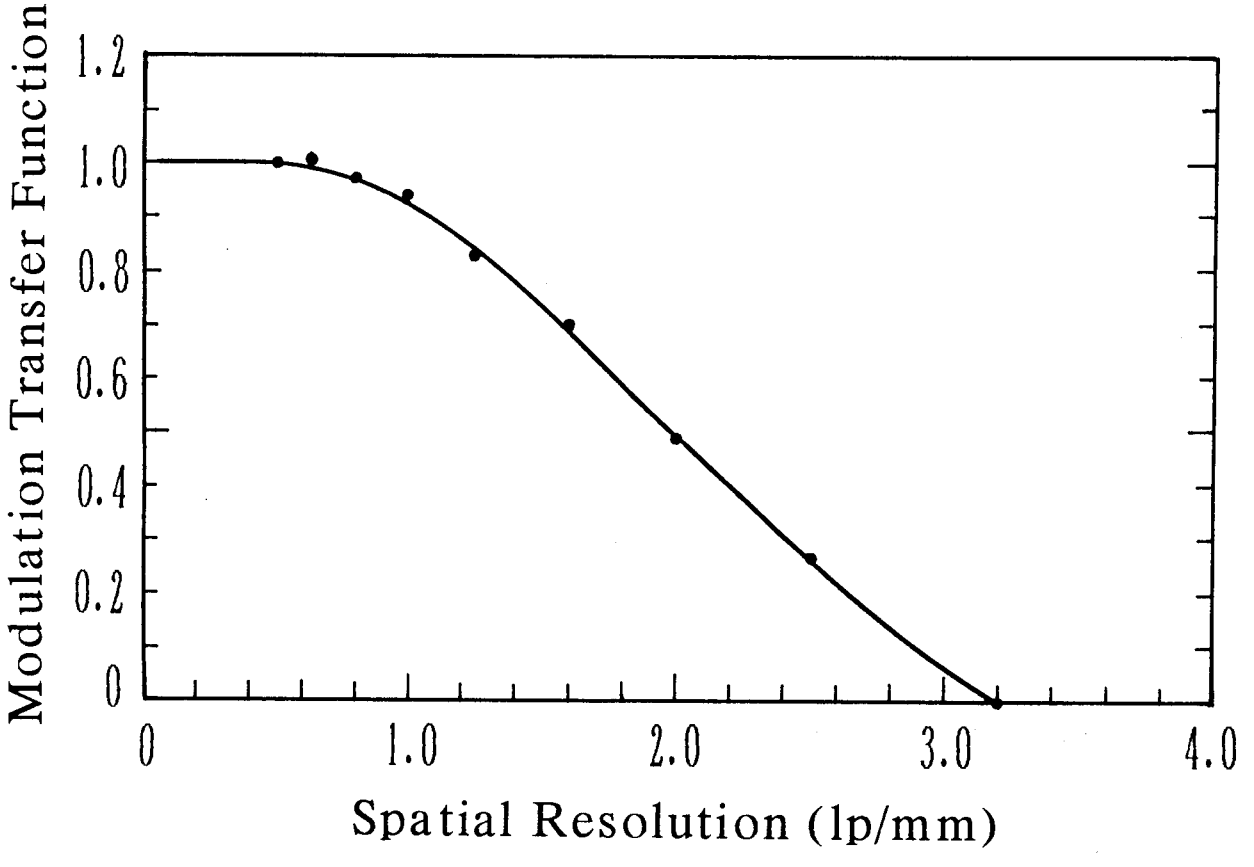

Fig. 4-7 MTF curve of the scanning direction at the scanning pitch of 0.25 mm

Figure 4-8 shows a radiographic image displayed on a CRT. Figure 4-8 (a) shows a low energy image of a hand phantom, and (b), the tissue image and (c), the bone image. Images of (b) and (c) were obtained by calculating different energy image data using the energy subtraction method.

4-6. Discussion and conclusion

A linear array imaging sensor was developed using a miniature CdTe radiation detector. The advantage of using this radiation detector is the possibility of measuring the energy information of incident X-rays applying the photon counting method. The CdTe radiation detector was able to detect photon counts over a small sensing area of 0.5×0.2 mm^2. To realize digital X-ray imaging, the sensor needs the fast counting rate of X-ray photons. By developing a negative feedback circuit amplifier, it was possible to obtain a counting circuit of 10 MHz frequency band. Energy separation procedure was established using 2 pairs of discriminator and counter for each channel. The detector was calibrated by measuring effective energies of separated X-rays. Results of spatial resolution test demonstrated the potential of using this setup as a diagnostic X-ray tool. Compared with conventional equipment, it has better response in low spatial frequency regions. This new type of X-ray imaging sensor using CdTe enables the simultaneous production of both photon counting images and energy information images. These results show that utilizing CdTe detector makes it possible to obtain new information on the composition of the object being examined.

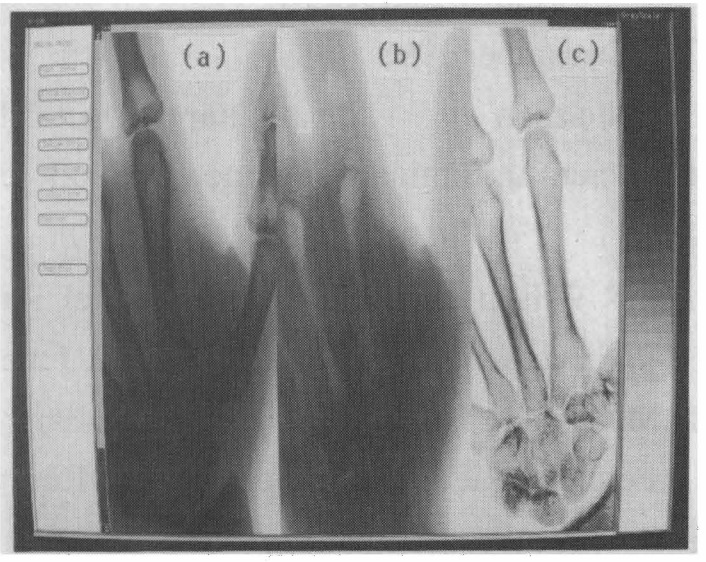

Fig.4-8 Radiographic images: (a) shows a low energy images of a hand phantom, (b) shows a tissue image and (c) shows a born image.

References

[1]R.G.Fraser,G.T.barnes, N.M.Hickey et al "Scanned Projection Digital Radiography of the Chest, A Review of Five Years Experience" The Alabama Journal of Medical Science, Vol.24, No. 3 258-266, 1987

[2]C.S.Mark, S.Frank et al "Metastatic Calcification of the Hart and Lungs in End Stage Renal Disease"
AJR 149: 881-887, November 1987

[3]S.E.Friedman, E.V.Dudovsky et al "Mineral Content of Bone: Measurement of Energy Subtraction Digital Chest Radiography"
AJR 149: 1199-1202, December 1987

[4]N.M.Hickey, L.T.Niclason et al Dual Energy Digital Radiographic Quantification of Calcium in Simulated Pulmonary Nodules AJR 148: 19-24, January 1987

[5]L.R.Goodman, C.R.Wilson and W.D.Foley Digital Radiography of the Chest: Promise and Problems AJR 150: 1241-1252, June 1988

[6]W.R.Brody, D.M.Cassel, F.G.Sommer, L.A.Lehman, A.Macouski R.E.Aluvarez, N.J.Pelc, S.J.Rieder, A.L.Hall "Dual-Energy Projection Radiography: Initial Clinical Experiment"
AJR:037 August 1981 p201-205

[7]G.Entine "Cadmium Telluraide Gamma Camera" IEEE Trans. Nucl. Sci. NS-26, No.1, 1979

[8]L.Kaufman, V.Loren et al "Two-detector, 512-element High Puarity Germanium Camera Prototype"
IEEE Trans. Nucl. Sci. NS-25, No.1, 189-195, 1978

[9]L.Kaufman, S.H.Williams et al "An Evaluation of Semiconductor Detectors for Positron Tomography"
IEEE Trans. Nucl. Sci. NS-26, No.1, 648-653, 1979

[10]J.Watts, K.Hosier et al "Computer-Controled Gamma Camera"
IEEE Trans. Nucl. Sci. NS-27, No.1, 535-536, 1980

[11].A.Ortendahl, L.Kaufman et al "High Resolution Emission Computed Tomography with a Small Germanium Camera"
IEEE Trans. Nucl. Sci. NS-27, No.1, 1459-462, 1980
[12]D.A.Ortendahl, L.Kaufman et al "Operating Characteristics of Small Position-Sensitive Mercuric Detectors"
IEEE Trans. Nucl. Sci. NS-29, No.1, 784-788, 1982
[13]B.E.Patt, A.D.Duca et al "Mercuric Iodide X-ray Camera"
IEEE Trans. Nucl. Sci. NS-33, No.1, 523-526, 1986
[14]J.S.Iwanczyk, W.K.Warbulton et al," Development of Mercuric Iodide Energy Dispersive X-ray Array Detectors"
IEEE Trans. Nucl. Sci. NS-35, No.1, 93-97, 1988

CHAPTER 5

X-ray Imaging and its Energy Measurement

5-1. Introduction

CdTe detectors, described above, are able to convert X-ray or γ-ray photons into electric current pulse signals. The following advantages are obtained by counting X-ray photons: 1)high sensitivity and a high S/N ratio, 2)energy information on incident X-ray photons. By measuring the X-ray strength and X-ray spectrum being both irradiated and transmitted to an object, one is able to obtain the information on the material composition of the sample.[1]-[6] Because absorption coefficients for radiation energy are specific for materials, by separating X-ray energy into two ranges, high and low, and by comparing the incident and penetrated X-ray strength in these high and low energy regions, it is possible to identify the composition of the sample.

In this chapter, an energy subtraction method is described; the former is how component materials of the object will be separated on the image using high and low energy information, and the latter is concerned with the material component will be identified by calculating the subtraction parameter of low and high energy information.

The CdTe X-ray imaging sensor is newly designed and improved to obtain the better spatial resolution to use an improved wide band amplifier for the pulse amplification. The characteristics of the new linear array CdTe X-ray imaging sensor and the feasibility study using high and low energy X-ray radiography are described in this chapter.

5-2. Energy subtraction method

5-2-1. The principle

The energy subtraction method is carried out using the energy information of two energy regions penetrating an object composed of two materials 1 and 2 having thicknesses of X1 and X2. The penetrating strength of X-rays I(E) for the two energy regions, E1 and E2, are described as follows.

$$I(E_1) = I_0(E_1) \exp\{-\mu_1(E_1)X_1 - \mu_2(E_1)X_2\} \quad (1)$$

$$I(E_2) = I_0(E_2) \exp\{-\mu_1(E_2)X_1 - \mu_2(E_2)X_2\} \quad (2)$$

where $I_0(E)$ is the irradiated X-ray photons and $\mu_1(E)$ and $\mu_2(E)$ denote linear absorption coefficients. Calculating the logarithm of equations (1) and (2),

$$\ln I_0(E_1) - \ln I(E_1) = \mu_1(E_1)X_1 + \mu_2(E_1)X_2 = S(E_1) \quad (3)$$

$$\ln I_0(E_2) - \ln I(E_2) = \mu_1(E_2)X_1 + \mu_2(E_2)X_2 = S(E_2) \quad (4)$$

where $S(E_1)$ and $S(E_2)$ are

$$S(E_1) = \ln I_0(E_1) - \ln I(E_1) \quad (5)$$

$$S(E_2) = \ln I_0(E_2) - \ln I(E_2) \quad (6)$$

Solving equations (3) and (4), X_1 and X_2 are obtained.

$$X_1 = \frac{\begin{vmatrix} S(E_1) & \mu_2(E_1) \\ S(E_2) & \mu_2(E_2) \end{vmatrix}}{\Delta} \quad (7)$$

$$X_2 = \frac{\begin{vmatrix} \mu_1(E_1) & S(E_1) \\ \mu_1(E_2) & S(E_2) \end{vmatrix}}{\Delta} \tag{8}$$

$$\Delta = \begin{vmatrix} \mu_1(E_1) & \mu_2(E_1) \\ \mu_1(E_2) & \mu_2(E_2) \end{vmatrix} \tag{9}$$

5-2-2. Material analysis

Equation (7) can be rewritten as follows,

$$X_1 = \frac{1}{\Delta}\{\mu_2(E_2)S(E_1) - \mu_2(E_1)S(E_2)\}$$

$$= \frac{\mu_2(E_2)}{\Delta}\left\{S(E_1) - \frac{\mu_2(E_1)}{\mu_2(E_2)}S(E_2)\right\}$$

$$= k_1\left\{S(E_1) - \frac{\mu_2(E_1)}{\mu_2(E_2)}S(E_2)\right\} \tag{10}$$

Equation (10) represents a processed image which contains only the information of the material 1. The information about the material 2 has been eliminated. This method which eliminates the information about a specific material from the obtained image, is called the energy subtraction method, since equation (10) has a form of subtraction of the high energy image from the low energy image.

In the case that the materials 1 and 2 are known, the value $\mu_1(E)$ and $\mu_2(E)$ can be previously determined. Even when the materials 1 and 2 are not known, the capability of material identification is preserved since the parameter, $\mu_2(E_1)/\mu_2(E_2)$, depends on the atomic number of the material 2.

5-3. Preparation of the CdTe linear array detector elements

The size of the detector element was chosen in order to obtain a specific resolution of over 2.5 line pairs/mm (the same specific resolution as that of a conventional X-ray screen/film system) and a linear array detector was developed with a element pitch of 0.2 mm. Figure 5-1 shows a schematic diagram of the linear array detector. A CdTe single crystal ingot was sliced into 0.3 mm thick wafers. Linear array detectors were cut out after depositing divided electrodes on one side and common electrodes on the other side using electroless platinum plating. This linear array detector of 1 mm x 6.4 mm x 0.3 mm^3 size has 32 channel electrodes of 0.2 mm pitch. Two detectors of this type are mounted on the ceramic plate to form a 64 channel detector unit.

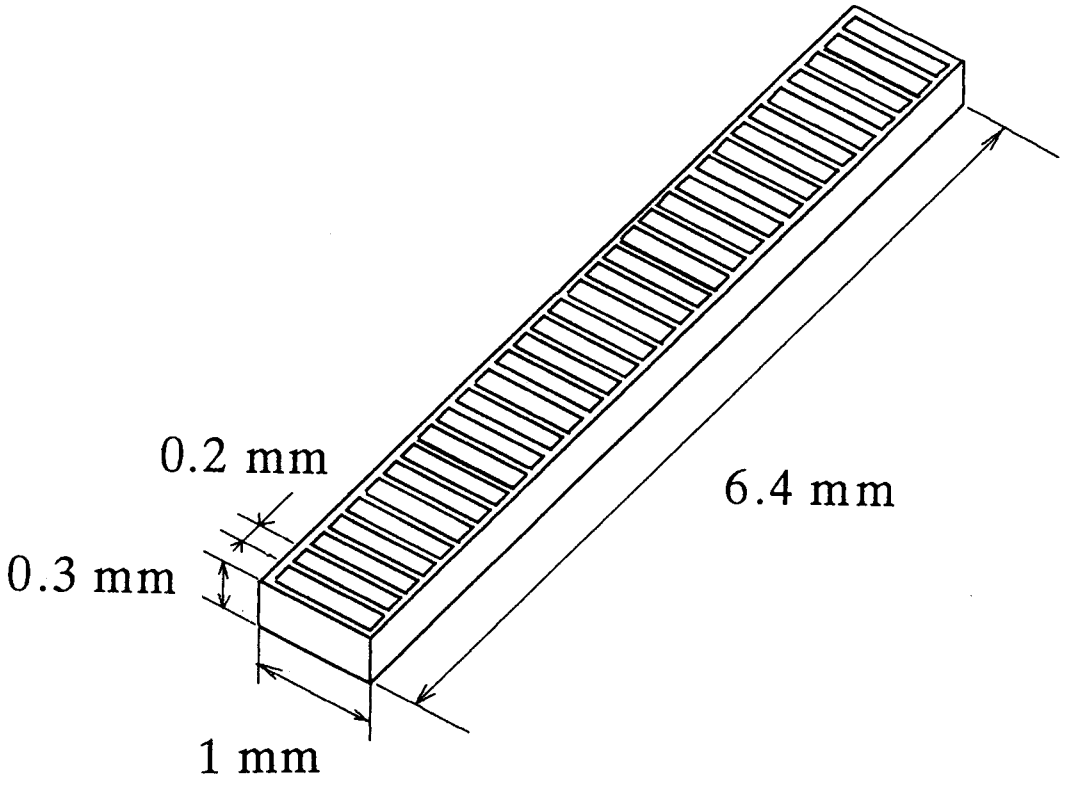

Fig.5-1 A schematic diagram of the CdTe array detector, which is 1 mm (width) × 6.4 mm (length) × 0.3 mm (thickness). The detector has 32 divided electrodes of 0.2 mm pitch.

5-4. Photon counting method

The main aim of the pulse counting method in X-ray radiography is to obtain a radiographic image in a short time. To design a suitable preamplifier circuit, the following points were specially attempted:

1) To attain C-V conversion and impedance conversion simultaneously.

2) To get the better high frequency response.

A wideband negative feedback pre-amplifier having a frequency range of up to 30 MHz was developed. FETs and feedback resisters, making up a head amplifier for impedance conversion, were put apart from the pre-amplifier circuits and mounted near the detector elements. Figure 5-2 shows a photograph of the CdTe detector array units and head amplifiers. (a) shows the 64 channel array unit composed of CdTe detector elements, head amplifiers (FETs and feedback resistors) and flexible leads, and (b) is a magnified photograph of the CdTe detector elements covered with resin. Figure 5-3 (a) shows the 64 channel unit covered with a radiation shielding grid. Figure 5-3 (b) shows a magnified photograph of the radiation shielding grid. The radiation shielding grid was newly designed, especially to make the aperture size larger, and placed over the detector elements at a distance of 1.6 mm to prevent crosstalk from adjacent elements. The radiation shielding grid consists of 0.5 mm thick tungsten with an aperture size of 0.5 mm (length) $\times$ 0.15 mm (width) for each channel.

(a)

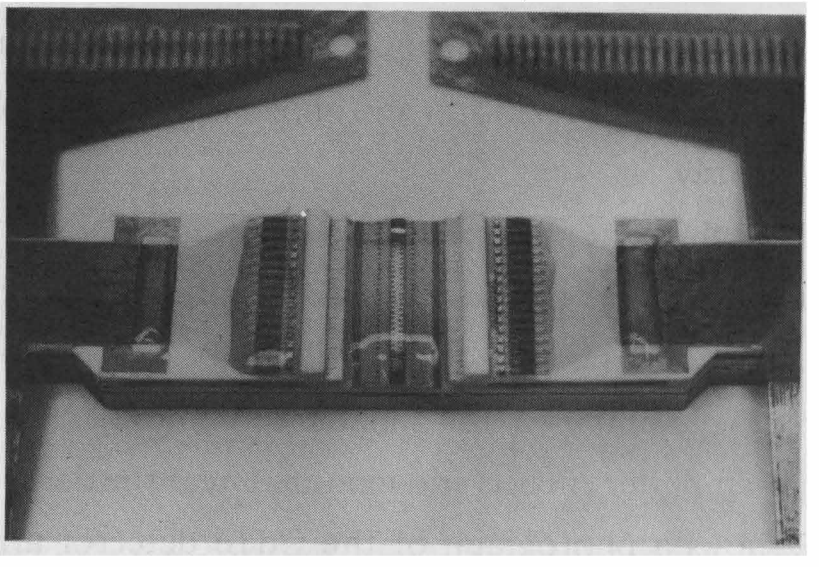

(b)

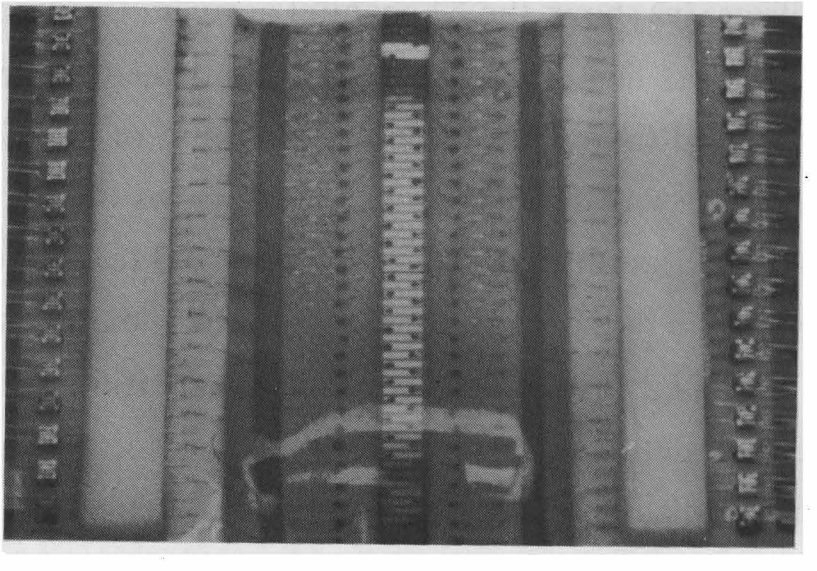

Fig. 5-2 A photograph of the 64 CdTe detector elements and head amplifiers composed of FET chips and feedback resisters.

(a)

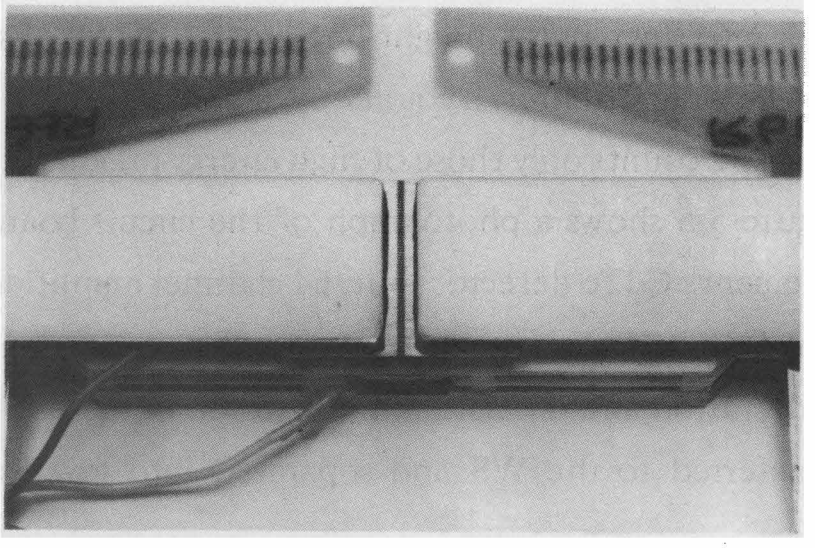

(b)

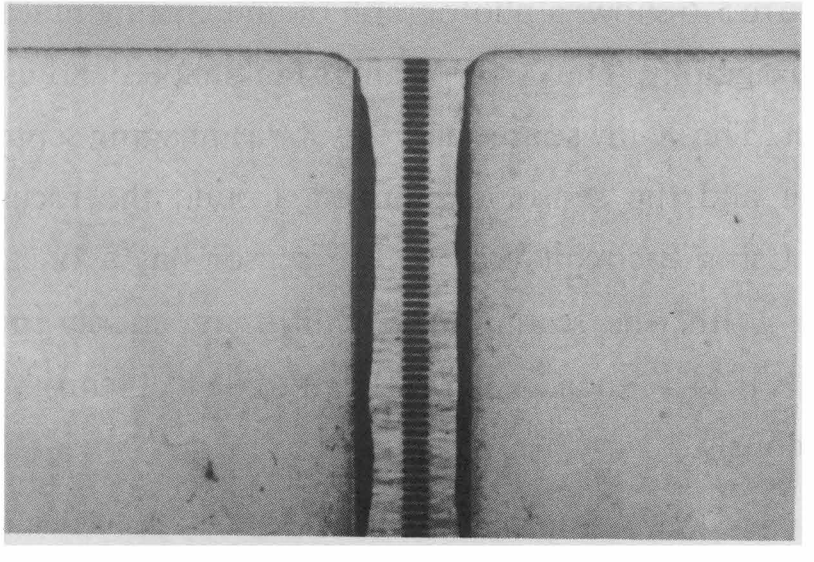

Fig 5-3 A photograph of the 64 array detectors covered with a radiation shielding grids.

5-5. Radiographic setup for X-ray energy separation

Figure 5-4 shows a block diagram of the apparatus consisting of the X-ray imaging sensor, the counting circuit and the controller. Output signal pulses from the CdTe detector element are amplified and separated into two pulse height regions with two discriminators as described before. Counter 1 counts pulses of all X-ray energy regions and Counter 2 counts only those of high energy regions.

Figure 5-5 shows a photograph of the circuit board consisting of the 64 elements CdTe detector unit, 64 channel amplifiers, 128 channel discriminators and gate arrays. These circuit boards are controlled by a SUN work station and data are initially stored in the buffer memory and then transferred to the WS and separated into low and high energy ranges.

Figure 5-6 shows a photograph of an experimental setup to obtain X-ray radiography. The X-ray beam is fan-shaped and used to irradiate the object. The X-ray source and the X-ray imaging sensor are made up into a set and the sensor is scanned around the focus of the X-ray source. Using 8 circuit boards, the sensor has a linear array of 512 elements. With one scanning, two different energy images from 512 channels×1024 lines (102.4 mm×204.8 mm) are obtained simultaneously.

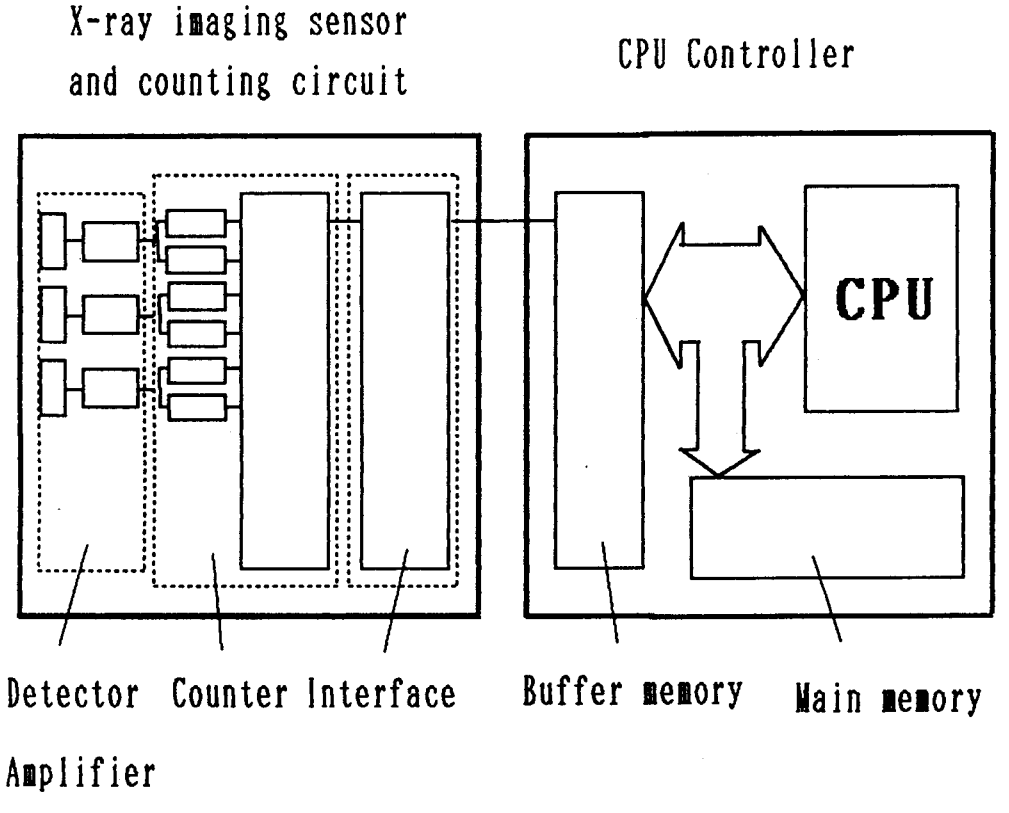

Fig 5-4 Block diagram of X-ray imaging sensor.

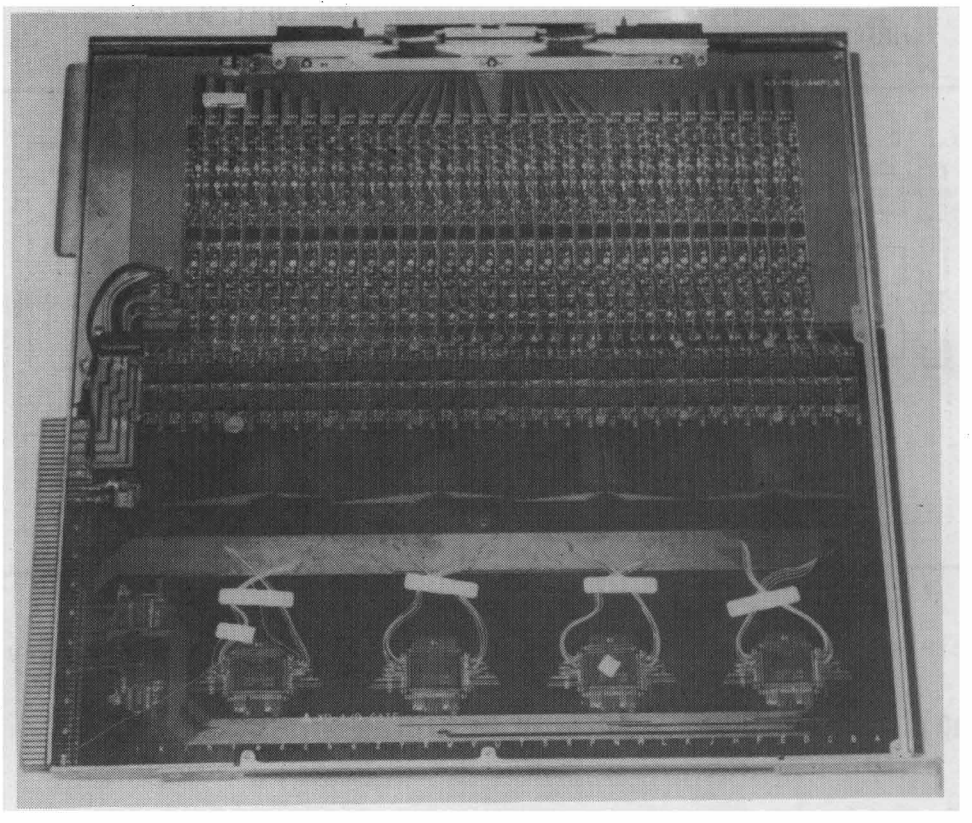

Fig. 5-5 A photograph of a circuit board consisting 64 elements CdTe detector unit, 64 channel amplifiers and 128 discriminators and gate arrays.

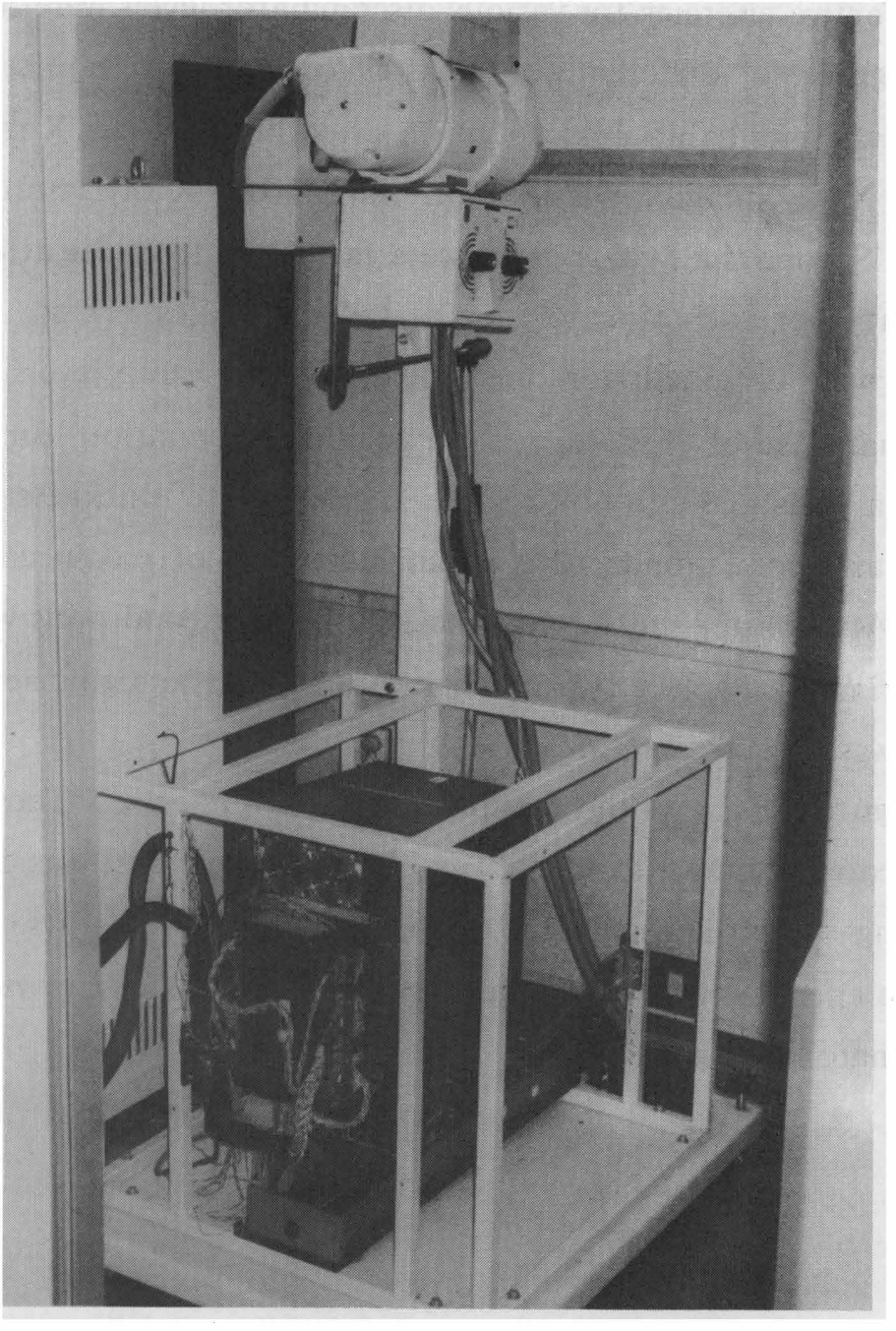

Fig. 5-6 A photograph of the radiographic measuring apparatus

5-6. Experiments

5-6-1. X-ray energy separation

Effective energies for various discriminator levels were measured using a group of different thickness of copper plates. First, copper plates of different thicknesses were inserted between the X-ray source and the X-ray imaging sensor, and transmitted X-ray photons were counted. Second, half value layers were calculated from the attenuation curve data for including copper plate thicknesses. Third, effective energies were obtained from measured first half value layers for each discriminator level. Figure 5-7 shows the attenuation curves. The horizontal axis corresponds to the copper plate thickness and the vertical axis corresponds to normalized values of measured photon counts. Attenuation curves were measured under conditions where the low discriminator voltage was fixed at 0.48 V and the high discriminator voltage was varied from 0.53 V to 0.83 V.

Figure 5-8 shows the calculated effective energies. The effective energy corresponding to the lowest discriminator level was 53.0 keV, indicating the effective energy of the total incident X-rays. Obtained effective energies were varied from 54.5 keV to 82.0 keV by varying the discriminator voltages.

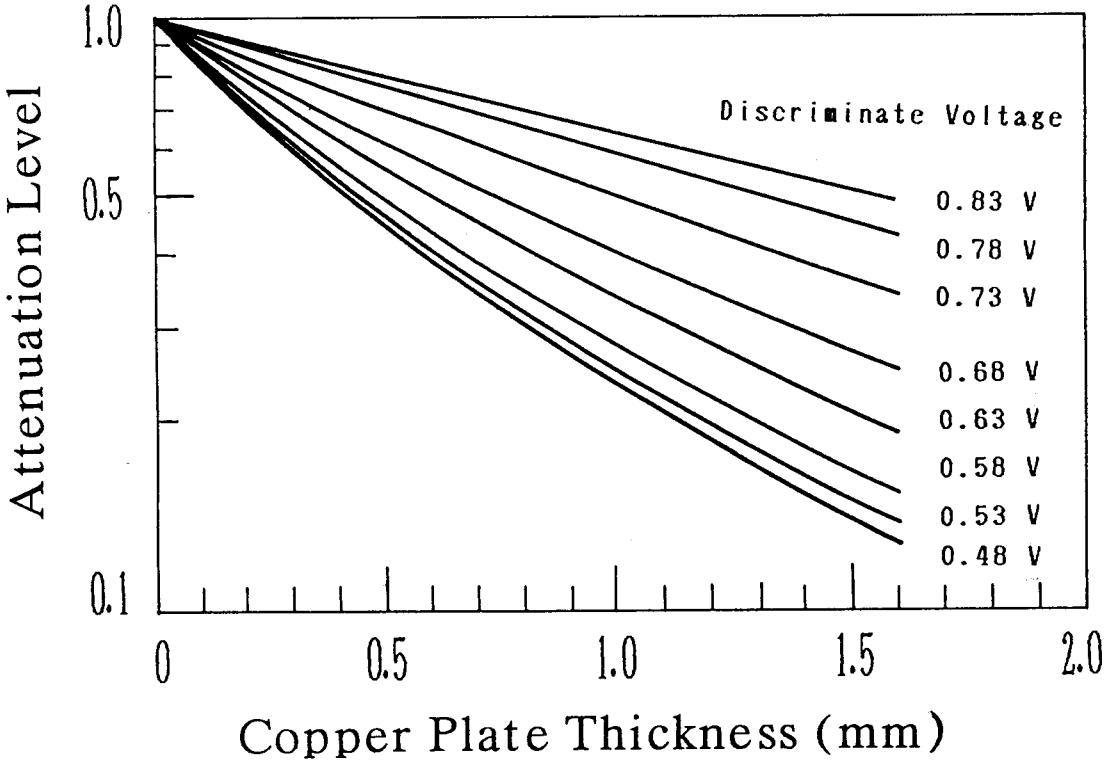

Fig. 5-7 The attenuation curve of penetrated X-ray photons for the range of copper thickness with the discriminator level as a parameter.

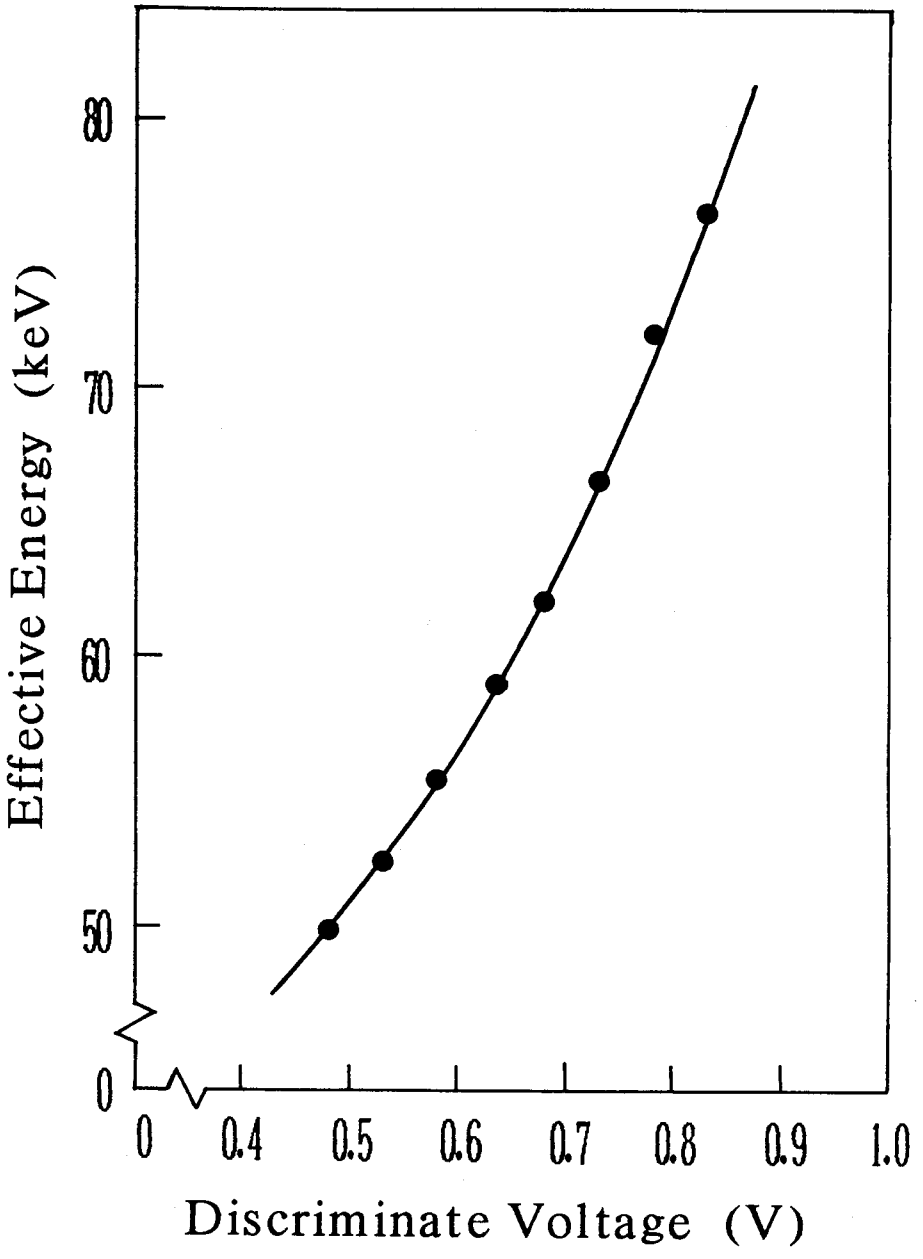

Fig. 5-8 The effective energy for various discriminator voltage.

5-6-2. Measurement of spatial resolution

The spatial resolution is obtained from the modulation transfer function (MTF) curve. The MTF curve was drawn by measuring the contrasts of an X-ray chart at a distance of 100 cm from the focus of the X-ray tube, the spot size of which was 0.6 mm. Figure 5-9 shows a photograph of the X-ray chart displayed on the CRT monitor. Figure 5-10 shows the MTF curves in the direction of arrays of the X-ray imaging sensor and in the direction of scanning. As previously described, the MTF curves are different between the array direction and the scanning direction, because the shape of the effective detection area of one element is rectangular (0.15×0.5 mm^2). The spatial resolutions obtained were over 2.5 line pairs/mm for the array direction and 1.6 line pairs/mm for the scanning direction with a scanning pitch of 0.2 mm.

There are two possibilities for the explanation of the differences of the specific resolutions between the array direction and that for the scanning direction. For the array direction, the resolution has larger value than that expected. The reason is that the Moire pattern effect is realized because of the digitally dispersed sampling. For the scanning direction, the resolution has smaller value than that expected, because the effective detection size of the detector element was longer than scanning pitch. When this X-ray imaging sensor is used, the MTF value in the low frequency region keeps at a high level compared with other conventional X-ray imaging systems, because the crosstalk of each element is smaller than those of the conventional X-ray imaging systems.

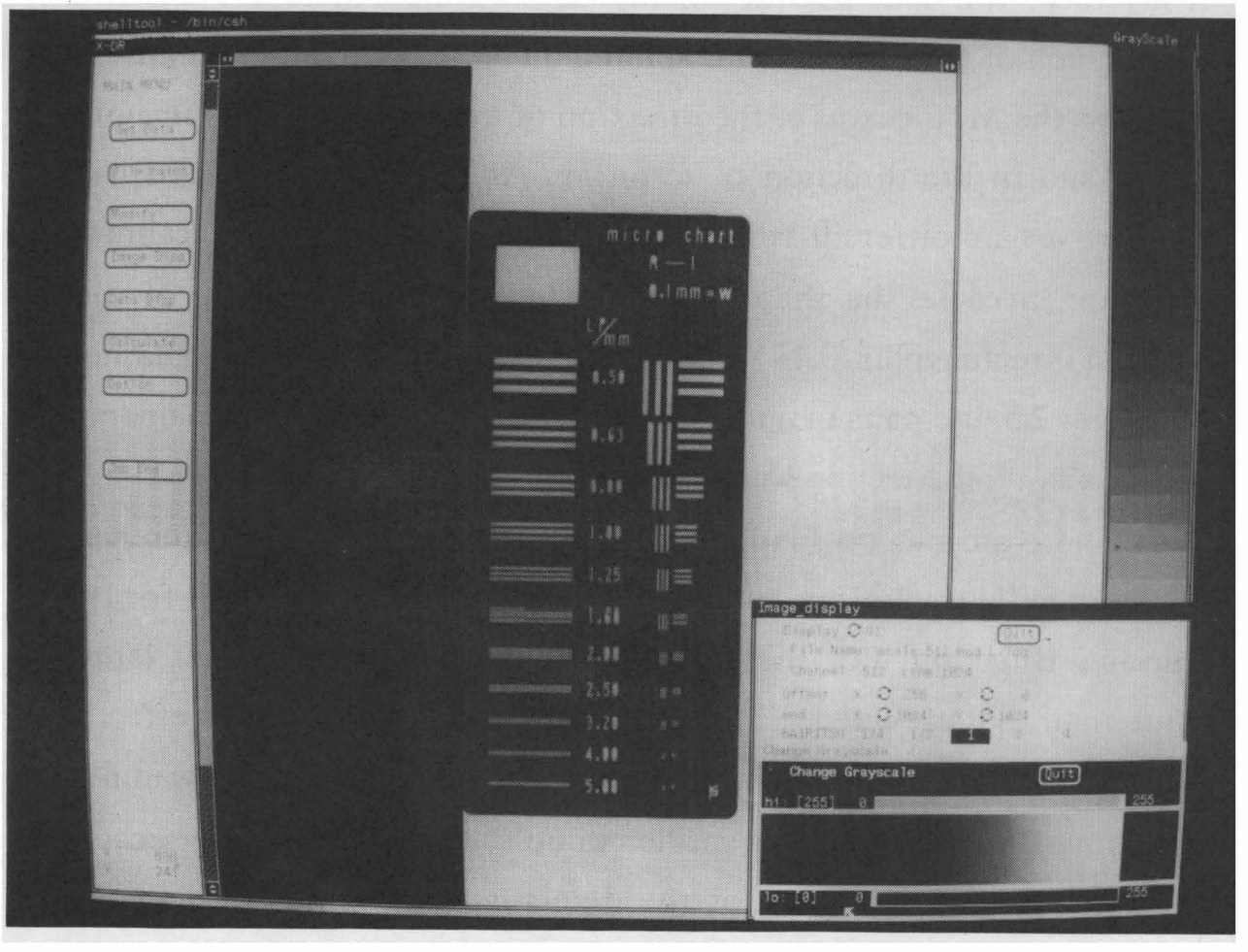

Fig. 5-9 A photograph of the X-ray chart.

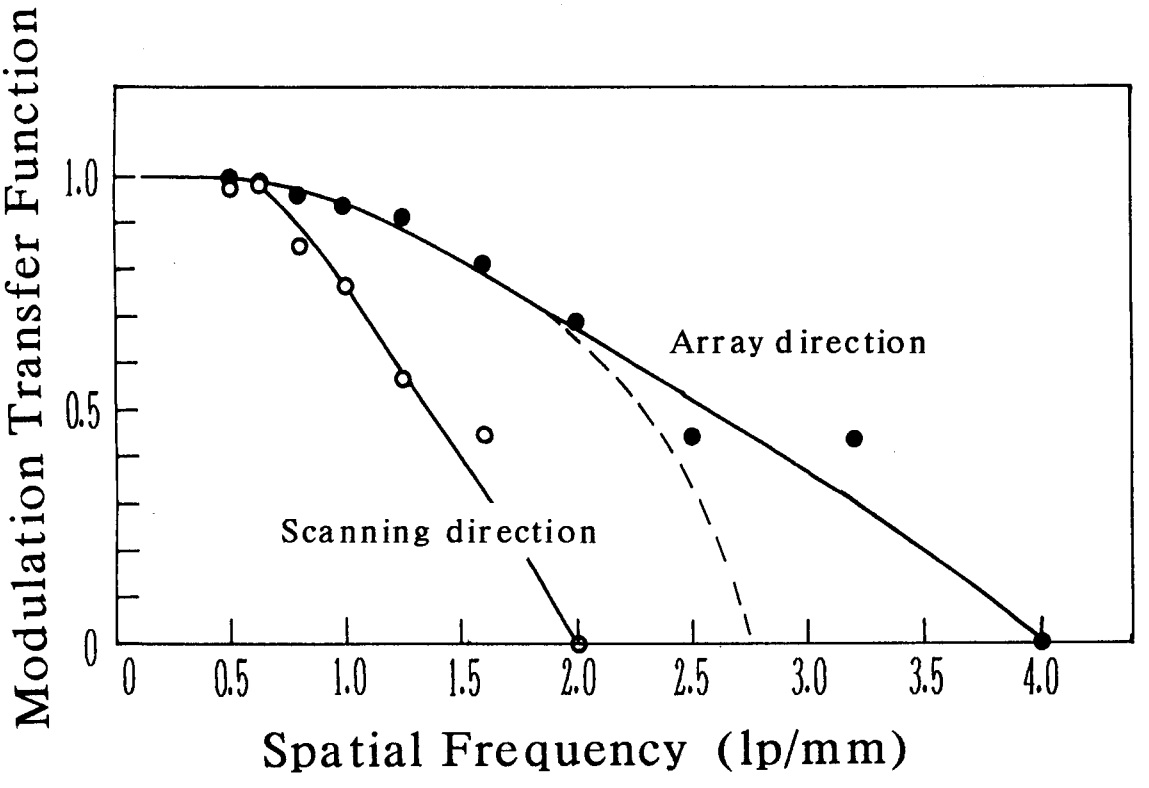

Fig. 5-10 The MTF curve for scanning direction and array direction

5-6-3.Radiographic measurement

Figure 5-11 shows radiographic images of an experimental phantom. The object phantom was a plastic toy air gun and covered with a thin metal plate. Radiographic data of 1024×1024 pixels was obtained by scanning twice with 512 elements. Figure 5-11 (a) shows the normal x-ray radiography with low X-ray energy, (b) shows the image with plastic parts subtracted and therefore that of only the metal components., The Figure (c) shows the image of the plastic parts and the shape of the gun is clearly obtained. Figure 5-12 shows radiographic images of another experimental phantom. The object phantom was composed of acrylic resin for the face, titanium for the ears and the hat and aluminum for the ears, nose and mouth. Figure 5-12 (a) shows the normal x-ray radiography of the object phantom, (b) shows the image with the titanium hat subtracted, (c) shows the image with the acrylic face image subtracted.

5-6-4.Material analysis

As previously described in chapter 5-2, the subtraction parameter $\mu_2(E_1)/\mu_2(E_2)$, which is expressed in equation (10), reflects specific material about the object: that is proportional to the atomic number or if the material is a compound, it is proportional to the effective atomic number. In the energy range of 20-120 keV, the absorption coefficients come from the photoelectric absorption and the Compton scattering, and the contribution of the photoelectric absorption becomes larger in proportion to the atomic number. Figure 5-13 shows the relation between the subtraction parameter $\mu_2(E_1)/\mu_2(E_2)$,and atomic numbers of materials. The horizontal axis shows the atomic number and the vertical axis shows the contrast ratios. The figure shows that the subtraction parameter for each material is proportional to that of the atomic number.

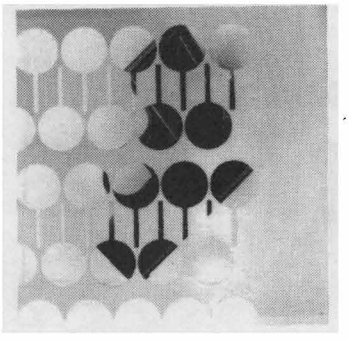

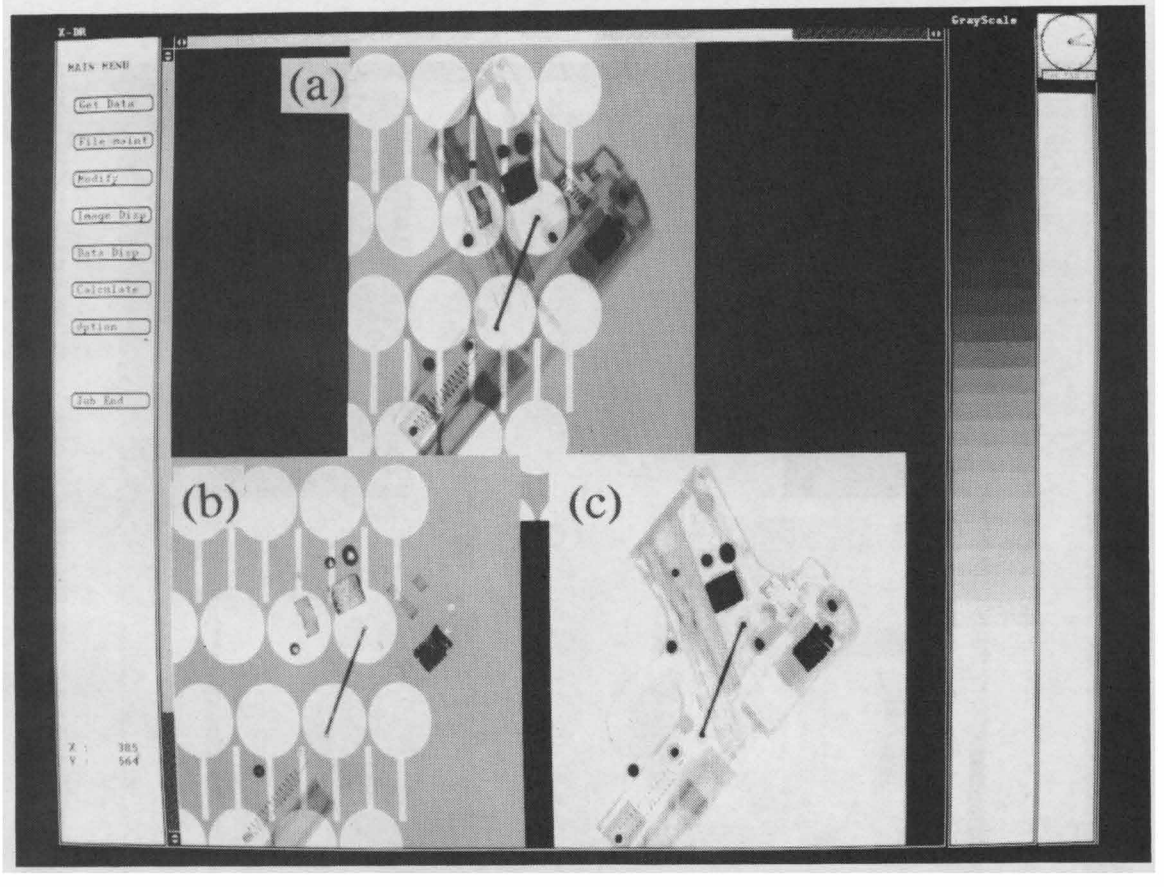

Fig. 5-11 The radiographic images of an experimental phantom composed of a plastic toy air gun covered with a thin metal plate.

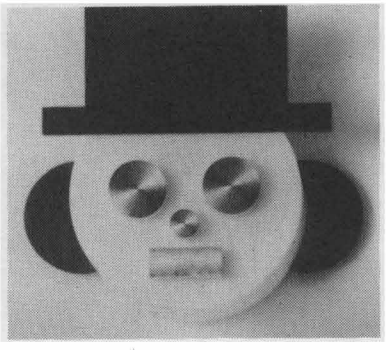

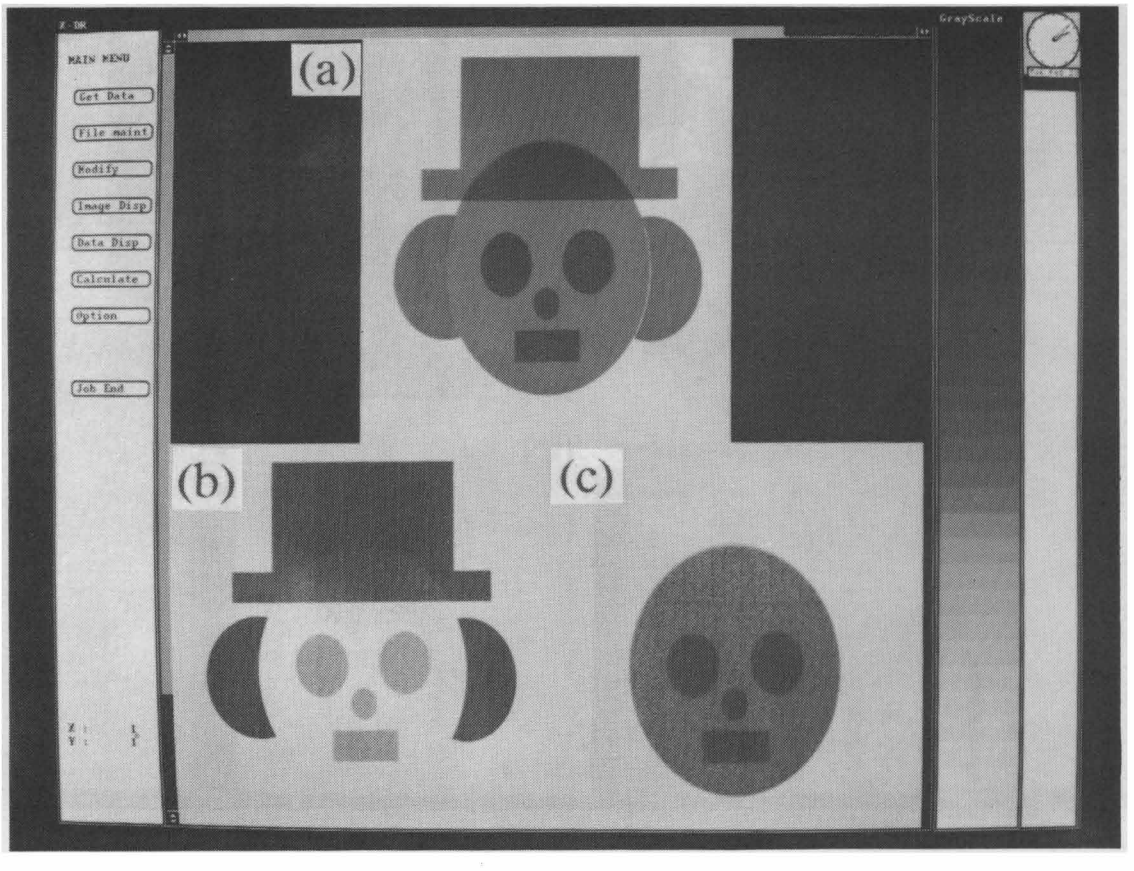

Fig. 5-12 The radiographic images of an experimental phantom composed of acrylic resin, aluminum and titanium.

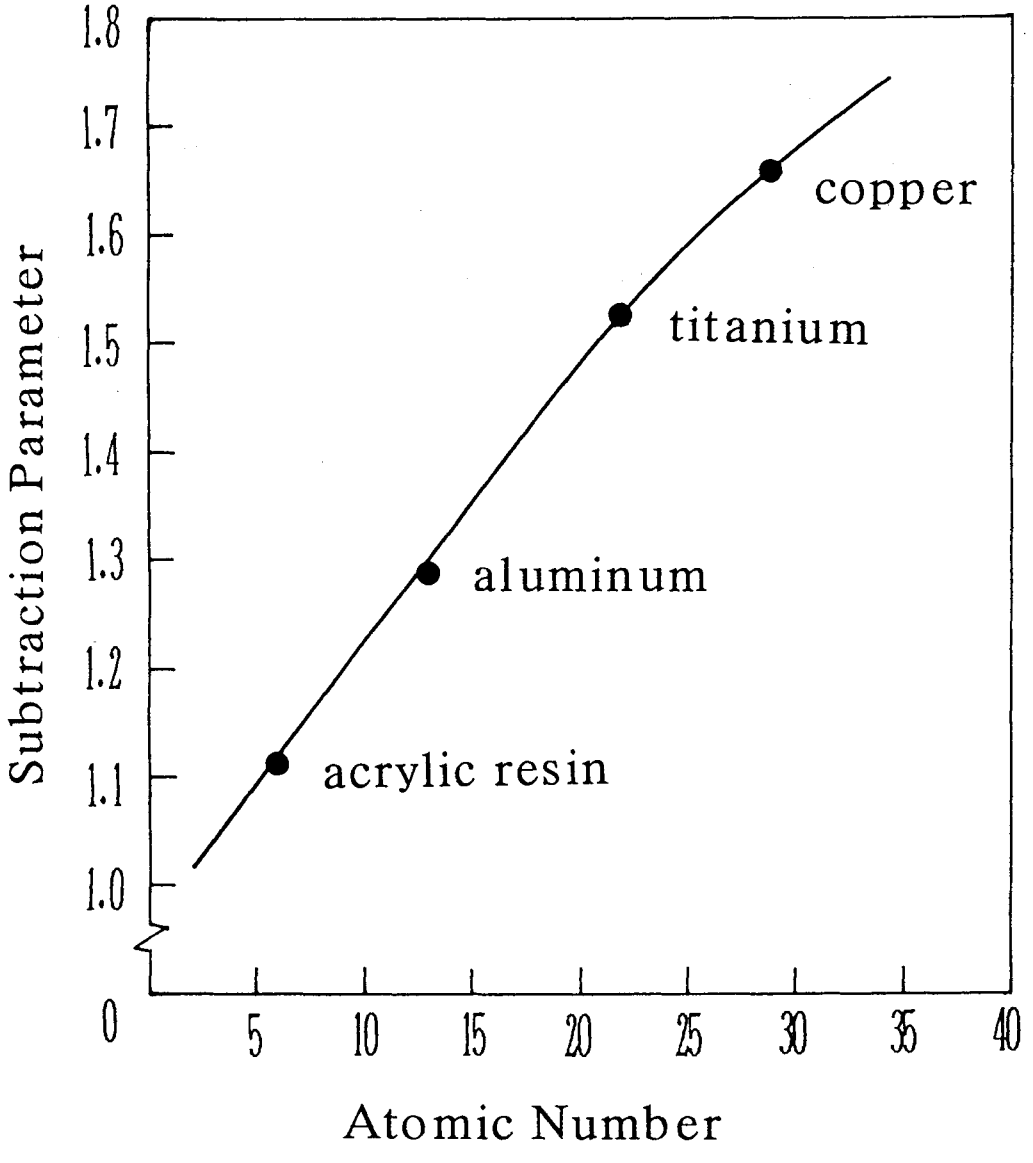

Fig. 5-13 Relation between contrast ratios and atomic numbers of materials.

5-7. Conclusion

Basic X-ray radiographical characteristics were examined using a newly developed X-ray imaging sensor composed of a CdTe compound radiation detector. This X-ray imaging sensor makes it possible to measure X-ray photons directly, and simultaneously obtain X-ray energy information. A feasibility study of the material identification was made using the energy subtraction method and found that the subtraction parameter $\mu_2(E_1) / \mu_2(E_2)$ was proportional to the atomic number or effective atomic number of materials constituting of the object.

References

[1] William R.Brody,Douglas M.Cassel,F.Graham Sommer,Leonard A.Lehman et al "Dual-Energy Projection Radiography: Initial Clinical Experience" AJR 137:201-205,August 1981

[2]H.Nishitani,Y.Umezu,K.Ogawa,H.Yuzuriha,H.Tanaka,K.Mtsuura "Dual-Energy Projection Radiography Using Condencer X-ray Generator and Digital Radiography Apparatus" Radiology 1986;161:535

[3]Colleen Sanders,Mark S.Frank,Gary T.Barnes et al. "Metastatic Calcification of the Heart and Lungs in End-Stage Renal Disease: Detection and Quantification by Dual-Energy Digital Chest Radiography" AJR 149:881-887,November 1987

[4]Samuel E.Friedman,Eva V.Dudovsky et al "Mineral Content of Bone:Measurement b Energy Subtraction Digital Chest Radiography" AJR 149:1199-1202, December 1987

[5]Nancy M.Hickey,Loren T.Niclason et al "Dual-Energy Digital Radiographic Quantification of Calcium in Simulated Pulmonary Nodules" AJR 148:19-24,January 1987

[6]Robert G.Fraser,Gary T.Barnes,Nancy M.Hickey et al "Scanned Projection Digital Radiography of the Chest, A Review of Five Years' Experience" The Alabama Journal of Medical science Vol.24, No.3, 258-266,1987

CHAPTER 6
Imaging quality of Digital Radiography

6-1.Introduction

X-ray images have usually been obtained using the X-ray film, the image intensifier and the imaging plate (IP). Recently, the techniques of the digitization and processing of X-ray signal have been developed, and it can be used to digitally treat the image and then observe the it on a CRT display. However, the signals obtained by the ordinary sensing systems are analog signals which must be digitized using an analog-digital converter.

In the field of nuclear science, RI images are measured using a scintillation camera and the photon counting method. In the early 1970's, V.Perez-Mendez and S.N.Kaplan developed the multiwire proportional chamber and studied RI or neutron images using photon counting.[1]-[5] Recently, L.Kaufman and D.A.Ortendahl studied the feasibility of producing RI images using a semiconductor detector [6]-[9]. But in the field of X-ray radiography, there have been no studies of imaging digitally using the photon counting method or estimating the contrast resolution of the image.[10]-[13]

A CdTe semiconductor radiation detector is very suitable to obtain digital signals with energy information and good spatial resolution because of the following reasons: 1) a high absorption coefficient, 2) operation at room temperature and 3) availability of small size element. Using the CdTe detector, the technology of all digital X-ray radiography containing X-ray energy spectrum information has been established and the following advantages are obtained.

1) X-ray photons are directly counted and a high signal to noise ratio is attained.

2) X-ray images having X-ray energy information are simultaneously acquired.

In discussing the image quality of the X-ray radiography, the threshold contrast is one of the most important factors. It is important especially in medical applications such as the early diagnosis or treatment of the cancer. The size of the lung cancer in the early stage is as small as 5 mm in diameter, which has not been detected by the conventional diagnostic X-ray imaging system because of the pile-up of many kinds of noises. The factors of the origin of noises are categorized as,

1) the fluctuation of the source X-ray photons,

2) the Compton scattered X-rays generated from the object, and

3) the noise of the electric circuit.

The problem is that the influence of the Compton scattered X-rays has not been evaluated quantitatively because the measurement include difficulties. The amount of the Compton scattered X-rays generated from the object increases in proportional to the increase of the object thickness and the amount of those X-rays depends on the atomic number of the object.

In this chapter, it will be shown that the Compton scattered X-ray and the noise from the electric circuit can be eliminated by using the linear array detector and the photon counting method, which will result in an image with fluctuation of the source X-rays only.

The evaluation testings to obtain threshold contrast were carried out in two ways; one is to observe the simulated contrast images using the Poisson random value displayed on a CRT, and another was to observe the contrast images obtained using a CdTe X-ray imaging sensor for the contrast phantom exposed to the X-rays. The evaluation results of the photon counting images and the contrast resolution are described. The relation between average counts of X-

ray photons detected by the detector element and contrast resolution was then estimated.

6-2. Simulation of threshold contrast

6-2-1. The method of simulation

Generally, the random event of the decay probability of a radioisotope or the generation probability of X-ray photons can be described by the Poisson process. In this manner, the timing fluctuation of the X-ray photons generated from the X-ray source are determined. The deviation noise contained in the image can be defined by adding the Poisson random number to the average counts of each pixel in the image.

The Poisson distribution is described as follows,

$$P(k) = \frac{e^{-\lambda}\ \lambda^{k}}{k!} \qquad (1)$$

where P(k) is the probability to produce a value k and λ is the mean value. For the Poisson distribution, the mean value and variance are equal to λ, and P(k) in equation (1) is described by only the λ parameter. When λ becomes larger, the P(k) distribution can be approximated by the normal distribution. The method to obtain the random numbers of a normal distribution id described as follows.

Suppose f(x) is a probability density function.

$$f(x) = \begin{cases} 1 & 0 \le x \le 1 \\ 0 & x<0,\ x>1 \end{cases} \qquad (2)$$

If the expected value of the random variable is E(x), then E(x) is able to describe as the continuous type.

$$E(x) = \int_{-\infty}^{\infty} xf(x)dx \tag{3}$$

The variance of the equation (4) is calculated.

$$\sigma^2 = E\left[\{x-E(x)\}^2\right] = E(x^2) - \{E(x)\}^2$$

$$= \frac{1}{12} \tag{4}$$

Using the central limit theorem, the sum of the independent random values asymptotically approaches a normal distribution $N(\mu, \sigma^2)$, and $\bar{x}$ given by equation (5) has the normal distribution $N(\mu, \sigma^2/n)$

$$\bar{x} = \frac{1}{n} \sum_{i=1}^{n} x_i \tag{5}$$

As the mean value and the variance of f(x) are 0.5, 1/12, respectively, x* is defined by equation (6). under the condition of mean value $\mu = 0$ and variance $\sigma^2 = 1$.

$$x^* = \sum_{i=1}^{12} x_i - 6 \tag{6}$$

The first term on the right side follows the normal distribution N(6,1). The distribution of x* then follows the standard normal distribution N(0,1).

A random number y of normal distribution $N(\lambda, \lambda)$ is described by equation (7),

$$y = \sqrt{\lambda}\, x^* + \lambda \qquad (7)$$

where x* is a random number of normal distribution N(0,1). Thus the random number y of the normal distribution $N(\lambda, \lambda)$ is obtained from the random number of normal distribution N(0,1). In the field of radiography where $\lambda \geqq 1000$, Poisson distributions are nearly equal to the normal distributions. Here, the random numbers of normal distribution $N(\lambda, \lambda)$ without periodicity were obtained by substituting random numbers for xi in equation (6) using basic IBM software.

6-2-2. Method of contrast simulation

The contrast data of the simulated images is described by equation (9).

$$X = \frac{a - \lambda}{\lambda} \times 100 \qquad (9)$$

where X denotes the contrast data (%), a means image pixel data (counts) and λ means background display average image data (counts). The value for each pixel is calculated when λ and X are defined. For example, a=1030 is obtained when λ =1000 and X=3 (%). These image data have the noise which follows these normal distributions of $N(\lambda, \lambda)$ and N(a,a).

Figure 6-1 shows the simulated contrast image displayed on a CRT having 1024×1024 pixels. It is designed to obtain 21 areas of these contrast images; 7 different sizes ranging from 1×1 mm^2 to 20×20 mm^2 and 3 different contrasts are selectable. The mean value λ was selected among three values, 10^3, 5×10^3 or 10^4. Contrast data were selected among five parameters of 0.3, 0.5, 1, 2 or 3 %. Estimation was

done using the following two points; 1) recognition of the square shape, and 2) recognition of the existence of the contrast.

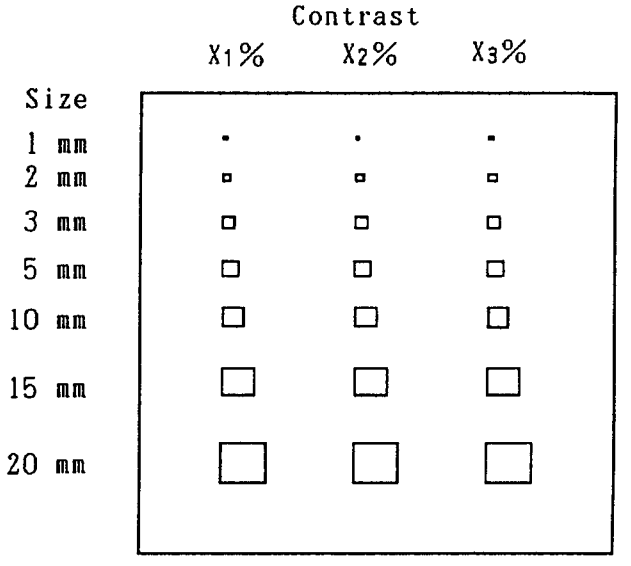

Fig. 6-1 The simulated contrast image displayed on a CRT having 1024 × 1024 pixels. 7 different sizes ranging from 1×1 mm^2 to 20×20 mm^2 and 3 different contrasts are selectable.

6-2-3.Evaluation of simulation quality

a) Confidence in the simulation data

Table 6-1 shows the comparison of the data of ideal standard deviation and simulated standard deviation for several mean values. Images were displayed with the contrast data of 1,2 and 3 % for $\lambda = 10^3$, 0.5,1 and 2% for $\lambda = 5 \times 10^3$, and 0.3, 0.5 and 1 % for $\lambda = 10^4$. Simulated values were estimated on the basis of the standard deviation of the simulated noise for one scanning line data of 1024 pixels from the average counts λ. Table 6-1 shows that the standard deviations of the ideal values and the simulated values are nearly equal to each other.

b) Analysis of the data using a plotter

The threshold contrast for the recognition was examined by plotting the data in the horizontal direction and the vertical direction using a plotter. Figure 6-2 shows the data in the horizontal direction for $\lambda = 5 \times 10^3$; a) shows the contrast pattern data for 20×20 mm^2 patch in the array direction and b) shows the data using a smoothing filter. Figure 6-3 shows the contrast pattern data in the vertical direction for $\lambda = 5 \times 10^3$; a) shows the 2 % contrast pattern data for each size in the vertical direction, and b) shows the data using a smoothing filter. It is difficult to extract the contrast pattern in such a noise without using a smoothing filter. Table 6-2 shows the mean values (counts) and the standard deviations being able to recognize the contrast pattern for the 20×20 mm^2 size.

TABLE 6-1

The standard deviations of the ideal and simulated values

Mean value	Standard deviation (ideal)	Standard deviation (simulated)
10^3	3.3%	2.9 - 3.2%
$5x10^3$	1.4%	1.3 - 1.4%
10^4	1.0%	0.9 - 1.0%

TABLE 6-2

The values which were able to recognize the contrast pattern for the size of 20×20 mm^2.

mean value	without filter	with filter
10^3	3%	2%
$5x10^3$	2%	1%
10^4	1%	0.5%

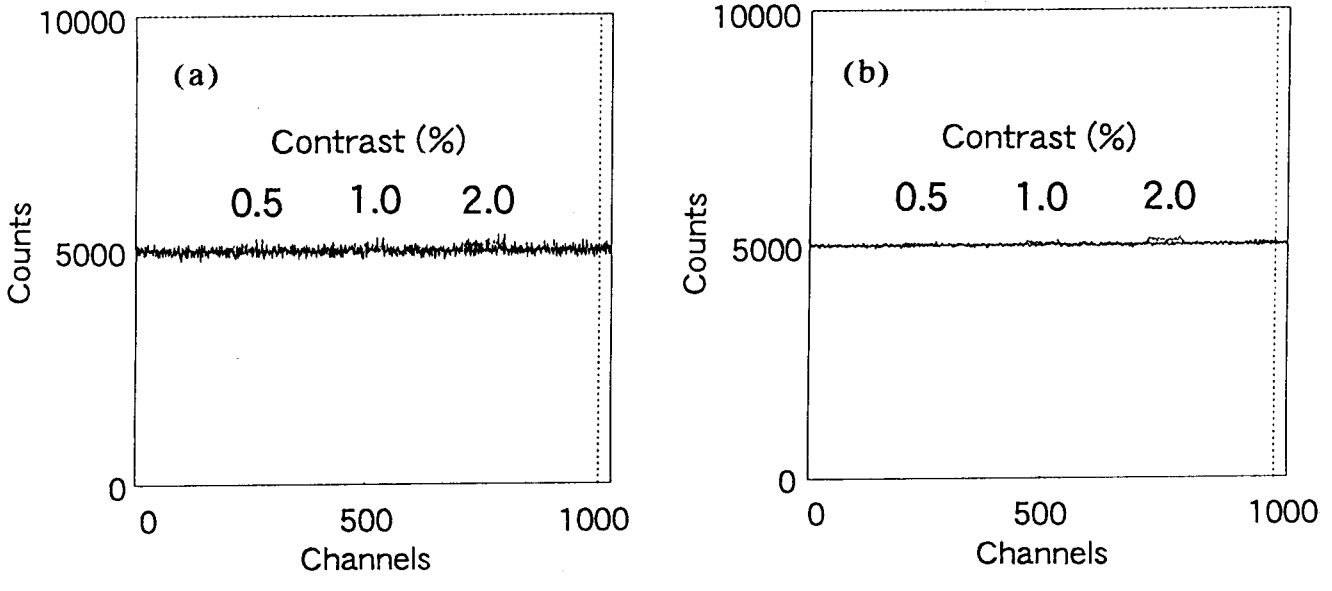

Fig. 6-2 The data in the array (horizontal) direction for $\lambda = 5 \times 10^3$.
a) shows the contrast pattern data for $20 \times 20\ mm^2$ patch and
b) shows the data with a smoothing filter.

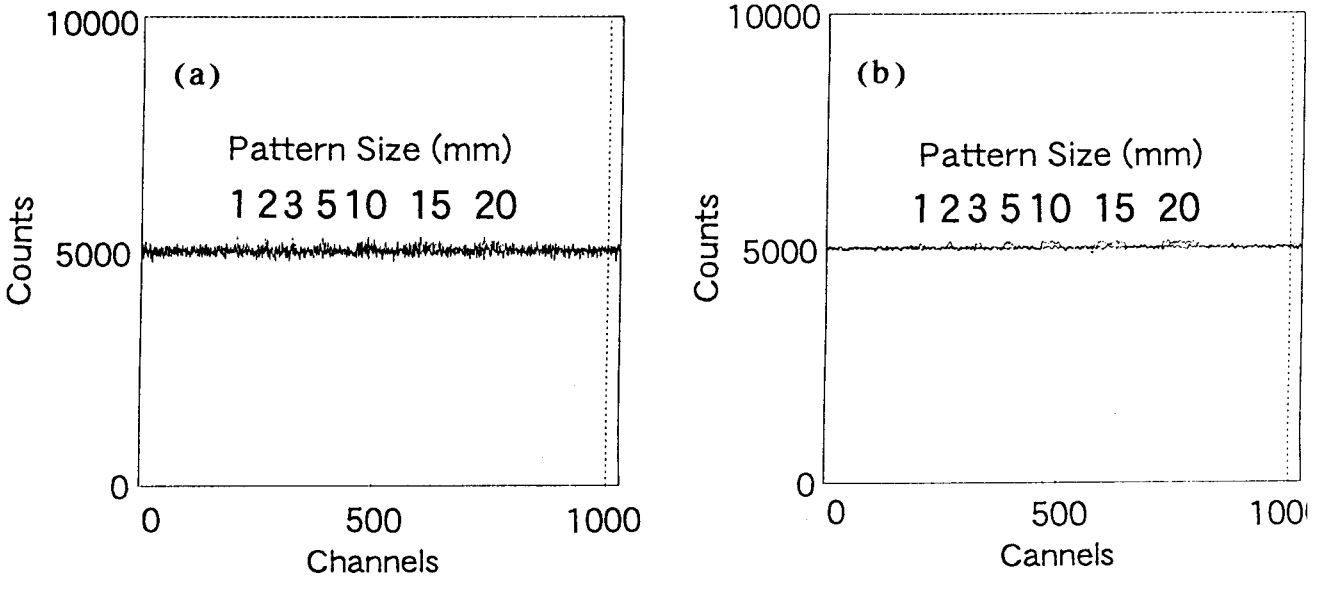

Fig. 6-3 The data in the scanning (vertical) direction for $\lambda = 5 \times 10^3$.
a) shows the 2 % contrast data for each pattern size and
b) shows the data with a smoothing filter.

c) Threshold contrast of the images displayed on a CRT

The images were displayed under the following conditions. The mean value λ was set at the center of the brightness of the CRT, while the maximum and the minimum values of the brightness of the CRT were varied from ± 5 % to ± 50 % different from the center value of the brightness. Figure 6-4 shows the photograph of the contrast image displayed on the CRT; a) shows the image displayed when the maximum and the minimum values of the brightness are varied ± 25 % from the center value, and b) shows the image when the maximum and the minimum values of the brightness are varied ± 5 % from the center value. Threshold contrast was measured using the contrast pattern recognition for each contrast image size.The measurement of the threshold contrast was performed by five persons.

Figure 6-5 shows the threshold contrast being able to recognize the shape of the pattern. Comparing the size for the case of the size 5 mm square, the contrast of 1 % for $\lambda = 10^4$, the contrast of 2 % for $\lambda = 5 \times 10^3$ and the contrast of 3 % for $\lambda = 10^3$ were recognized in each simulated noise level. These values agreed with the standard deviation of the mean value. This shows that the square contrast can be recognized in the case that the contrast value is larger than the value of the standard deviation of the fluctuation of the photon counts.

Figure 6-6 shows the threshold contrast at which the existence of the contrast pattern can be recognized. Comparing the threshold contrast for the size of 5 mm square, 0.3% for $\lambda = 10^4$, 0.5% for $\lambda = 5 \times 10^3$ and 1 % for $\lambda = 10^3$ were recognized. These threshold contrast data correspond to the value with one-third of the values of the standard deviation. The results shows that for photon count images, the contrast is one-third of the deviation of the photon counts.

(a)

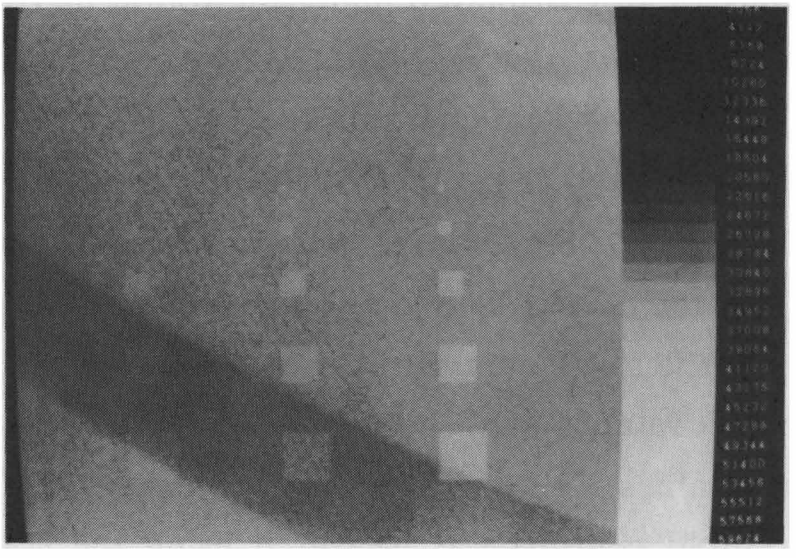

(b)

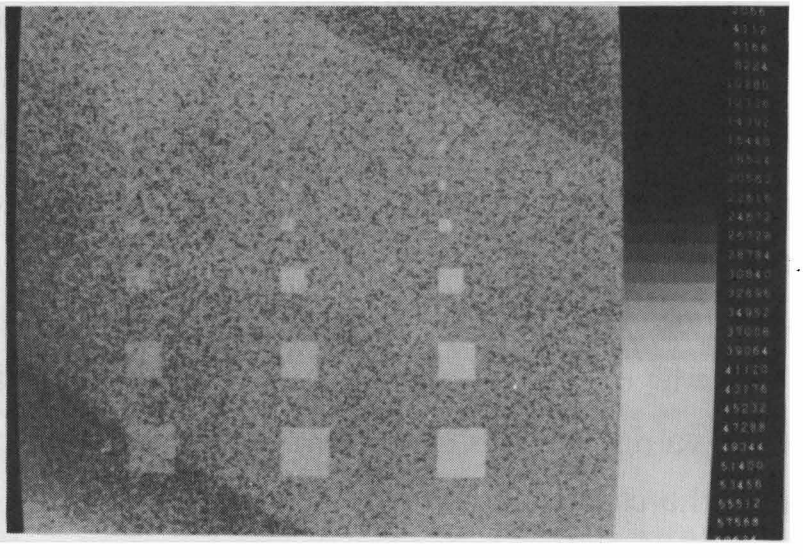

0.5 %　1%　2%

Fig.6-4 Photographs of the contrast image displayed on the CRT. a) shows the image displayed when the maximum and the minimum values of the brightness are varied ±25 % from the center value, and b) shows the image when the maximum and the minimum values of the brightness are varied±5 % from the center value.

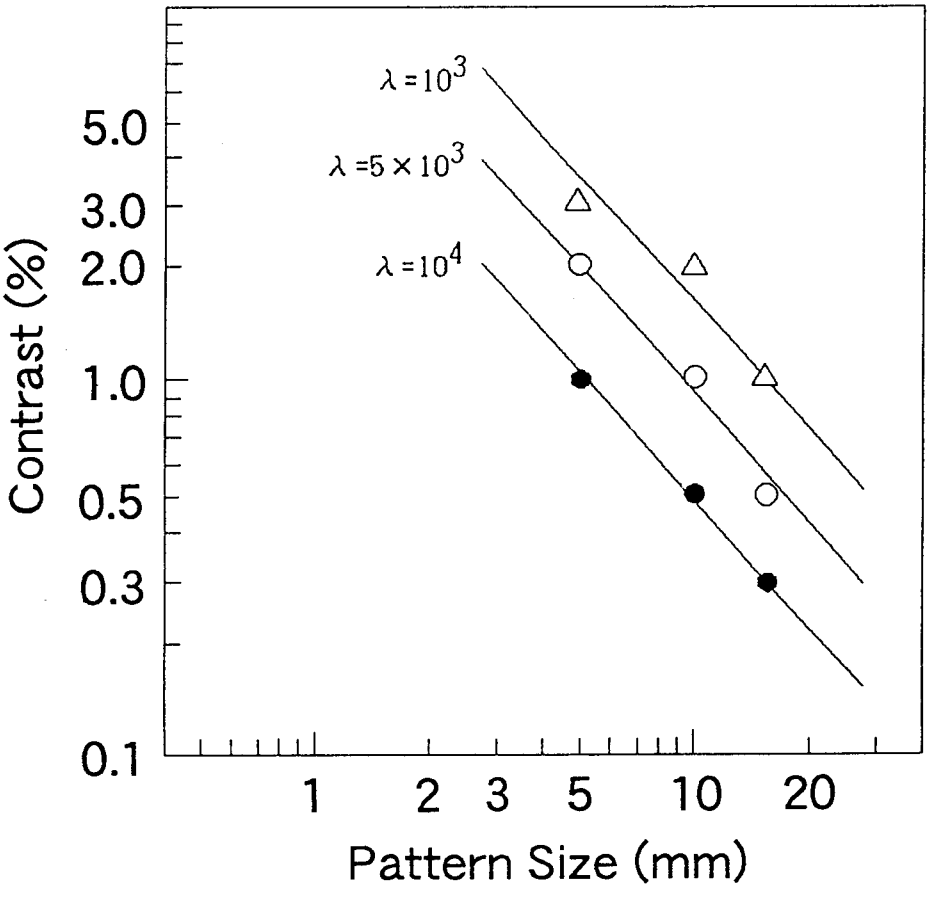

Fig. 6-5 The threshold contrast being able to recognize the pattern shape.

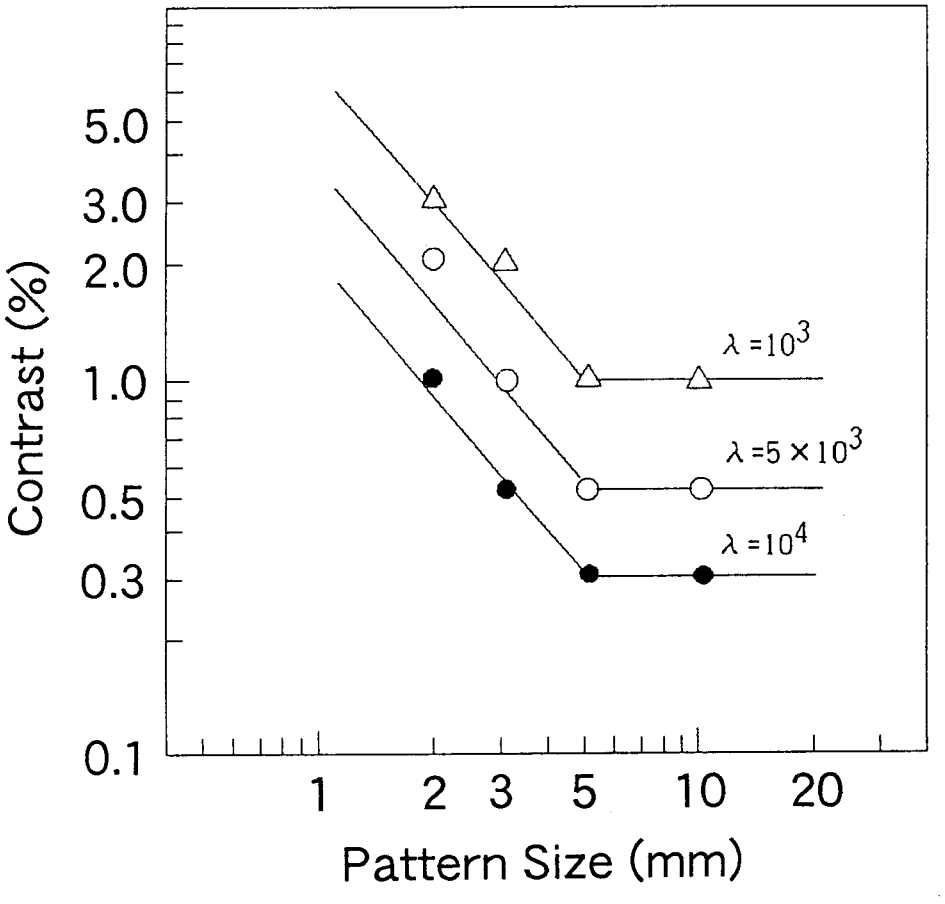

Fig. 6-6 The threshold contrast at which the existence of the contrast pattern can be recognized.

6-3. Experiment of contrast threshold

6-3-1. Preparation of the contrast phantom

Considering the simulation experiment data already described, contrast image sizes smaller than 10×10 mm^2 were necessary to measure the threshold contrast. The contrast phantom designed for the experiment has a combination of patterns having the area size ranging from 1×1 mm^2 to 10×10 mm^2 and the contrast ranging from 0.3% to 3 % as shown in figure 6-7. The thickness of the contrast pattern of the phantom was designed using the following equation (9).

$$I = I_0 \exp(-\mu d)$$

$$T = I / I_0 = \exp(-\mu d) \qquad (9)$$

In the equation, I_0 means the incident X-ray strength, I, the penetrated X-ray strength, μ, the linear absorption coefficient of the phantom material and d means the thickness of the contrast area of the phantom. d is obtained for the desired X-ray transmissivity T. The thickness d for each contrast area was obtained using the following parameters; voltage applied to the X-ray tube is 120 keV, effective energy of X-ray photons is 60 keV, and the absorption coefficient of the phantom material MIX-DP is 0.197 cm^{-1} for the effective energy of 60 keV. Table 6-3 shows the calculated results of d.

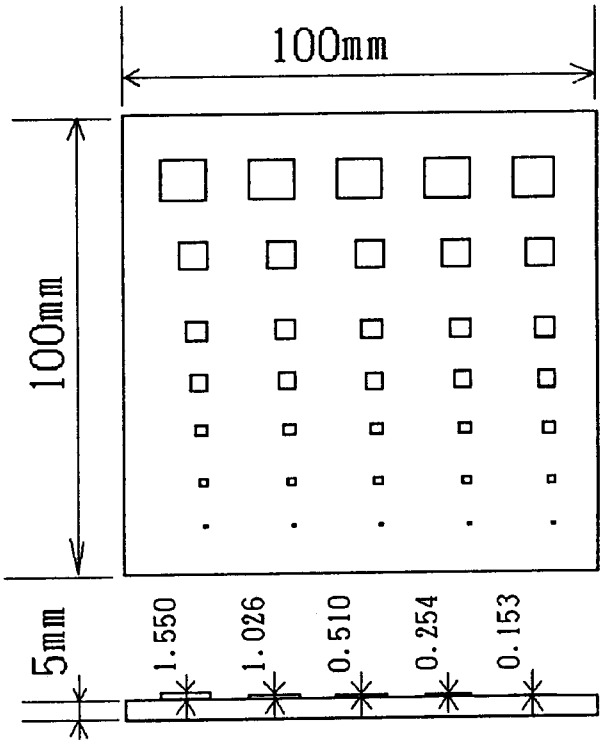

Fig. 6-7 The design of the contrast pattern

TABLE 6-3

The calculated value of the transmissivity of the contrast pattern

Contrast (%)	Transmissivity T	Phantom thickness d (mm)
0.3	0.997	0.153
0.5	0.995	0.254
1.0	0.990	0.510
2.0	0.980	1.026
3.0	0.970	1.550

6-3-2. Experimental procedure

The radiographic system used in this experiment was shown in figure 5-6. The X-ray source was operated in the direct current mode. The contrast phantom was exposed to and scanned by the X-ray beam which had a fan beam shape of the 3 mm width. The distance between the focus of the X-ray tube and the X-ray image sensor was 100 cm, and the distance between the image sensor and the contrast phantom was 5 cm. The radiographic images were obtained under the following conditions; applied voltage 120 keV, applied current 4 mA, sampling pixels 1024×1024 pixels, sampling area 204.8×204.8 mm, the sampling time of one scan 16 msec. The average X-ray photons counted by the X-ray image sensor was controlled by adjusting the background thickness of the phantom material to 5, 55 and 105 mm.

Threshold contrast is largely affected by the scattered X-rays generated from an object. Generally, when a two dimensional sensor like a film/screen system is used, the amount of the scattered X-rays increases in proportion to the thickness of the object, and the contrast becomes worse. The amount of the scattered X-rays was estimated from the comparison between contrasts: 1) with and without the fan-beamed X-rays, 2) with and without the X-ray grid.

Figure 6-9 shows the ratios of the scattered X-rays compared to the primary X-rays for the two combinations of the shape of X-ray beam and the existence of the grid. When the fan-beam X-rays and the X-ray grid were used, the detectable scattered X-rays was negligible small or nearly equal to zero and only the primary X-rays were detectable. (a) shows the data without using a fan beam of X-rays and the X-ray grid, and (b) shows the data without using the fan beam of X-rays and with the X-ray grid. The ratios of the scattered X-rays for the phantom of 10 cm thickness are about 25 % for (b) and about 83 % for (a) compared of the primary X-rays. These results show that by

using an X-ray fan beam and a linear X-ray imaging sensor with the X-ray grid, X-rays penetrating through an object are free from scattered X-rays. The number of penetrated X-ray photons is then able to be precisely controlled with changing the thickness of the phantom.

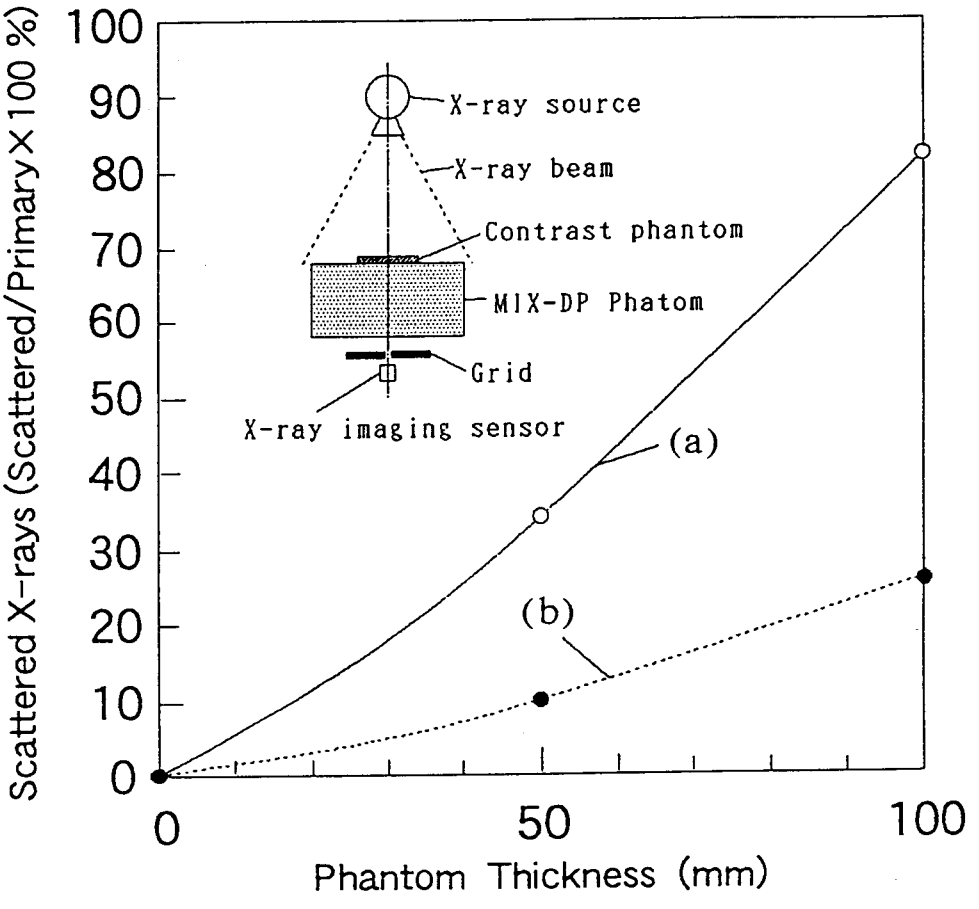

Fig. 6-9 The ratio of the scattered X-rays to the primary X-rays compared to the data using the X-ray fan beam and the X-ray grid. (a) shows the data without using the fan beam and the X-ray grid, (b) shows the data without using the fan beam X-ray grid.

6-3-3. Recognition of the contrast

Figure 6-10 shows an example of the contrast phantom image using the 5 mm thick phantom and having mean value of X-ray photon counts of 8,500. The images were displayed under the following conditions. The brightness corresponding to the mean value 8,500 was set at the center of the brightness of the CRT, while the maximum and the minimum values of the brightness were varied. Figure 6-10 (a) shows the image at the brightness corresponding between 5,000 and 12,000 counts for the minimum and the maximum value, and (b) shows the image between 7,500 counts and 9,000 counts for the minimum and the maximum value. Measurement of the threshold contrast was performed under the best conditions with the maximum and minimum counts adjusted.

Figure 6-11 shows the results of the measurements at three different photon counts. The photon counts were 8,500 for the 5 mm thick phantom, 4,500 for the 55 mm thick phantom and 900 for the 105 mm thick phantom. The following three remarks may be pointed out.

1)Threshold contrast was linear in the log-log scaling smaller than the size of 4×4 or 5×5 mm^2.

2)Threshold contrast was proportional to the X-ray photon counts but not proportional to the size larger than that of 4×4 or 5×5 mm^2.

3)For the size of 5×5 mm^2, the threshold contrast corresponds to one-third of the standard deviation of the background counts.

(a)

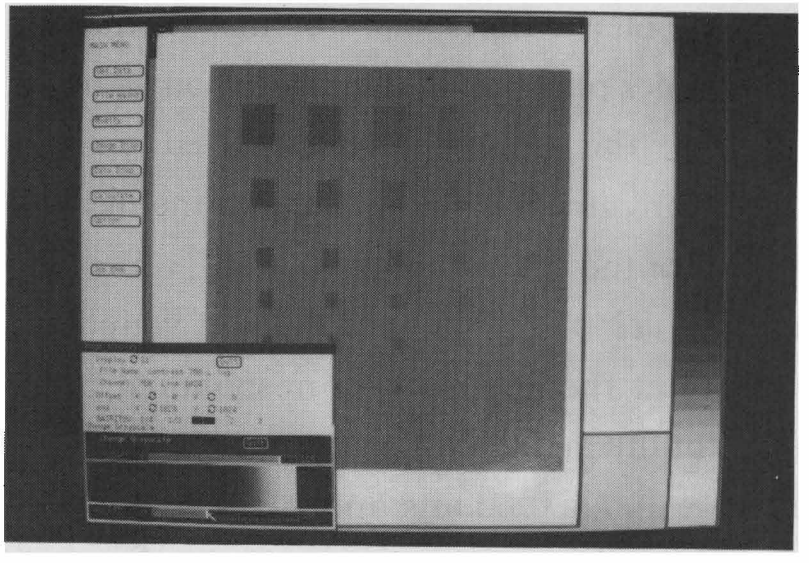

(b)

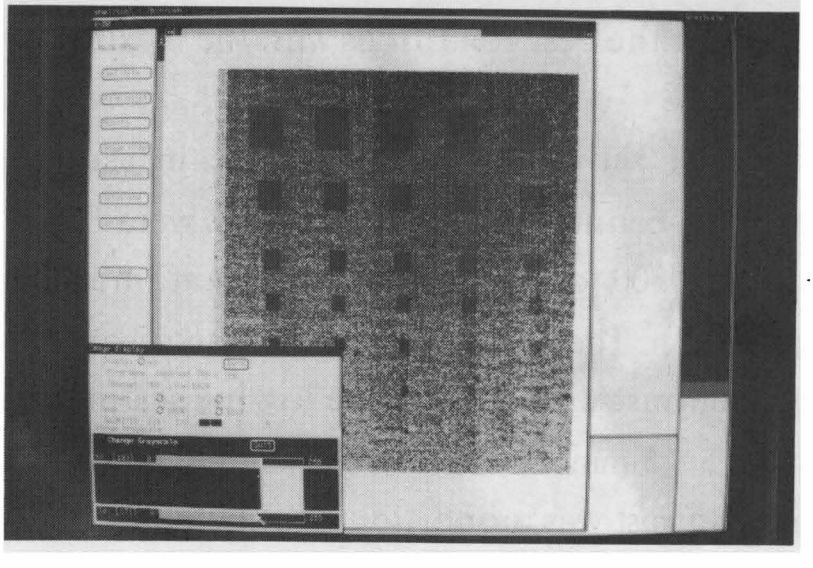

Fig. 6-10 An example of the contrast phantom image when the phantom of 5 mm thick and λ = 8,500 counts are used.

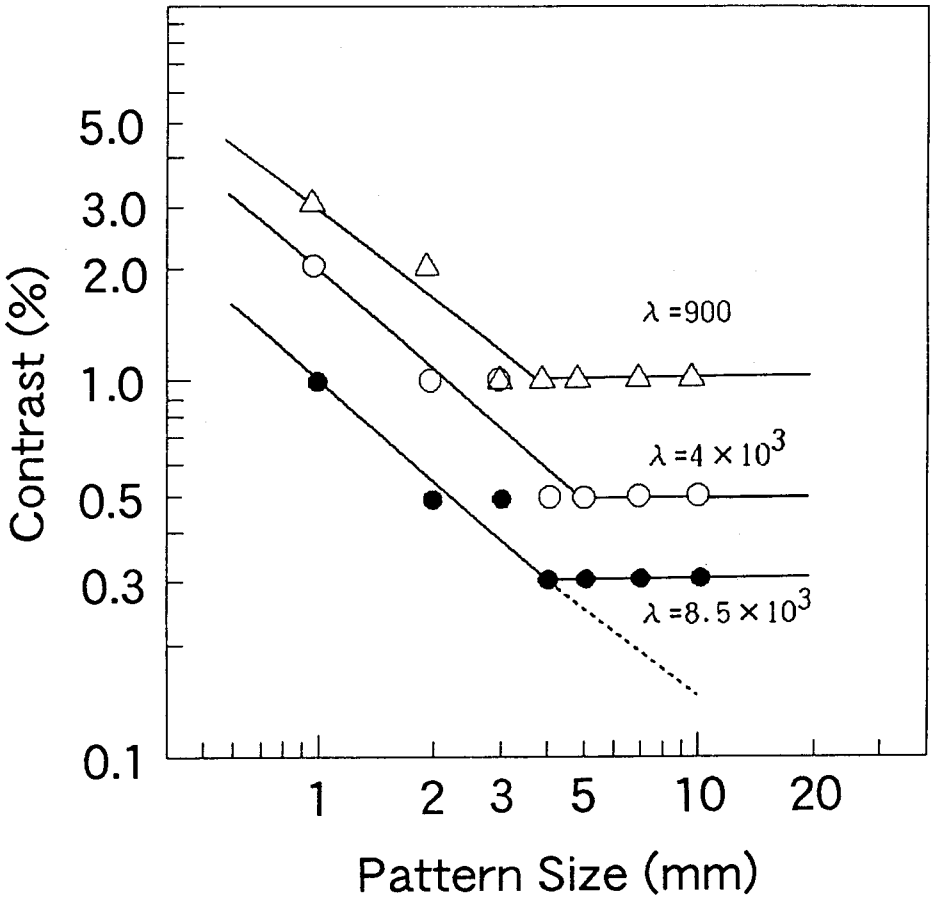

Fig. 6-11 Threshold contrast at three different photon counts

6-4.Conclusions

In this chapter, to evaluate the threshold contrast of the X-ray radiography using the X-ray photon counting method, the following two approaches were attempted. First, the threshold contrast of the simulated image using random count noise was evaluated on a CRT display. Second, threshold contrast of the radiographic images were evaluated using the CdTe semiconductor X-ray imaging sensor and the contrast phantom. Simulated data and measured data agreed each other very well in the following points: 1)the granularity or the radiographic mottle of the noise pattern of the background images, 2)statistical property of the noise, 3)the contrast for both image at the same level.

Generally speaking, the threshold contrast is equal to the standard deviation of the noise level from background counts. The results reported in this paper, however, show that the threshold contrast depends much on the size. When comparing the threshold contrasts for the 5×5 mm^2 pattern area size, threshold contrast are lower than one-third of the standard deviation for average photon counts. These results are some what different compared to the results generally reported. The reasons are described as follows;

1) With a fan beam X-ray and linear X-ray imaging sensor, the radiographic image was obtained free from the scattered X-rays generated from the object.

2) X-ray photons are counted directly free from analog noise in the measuring circuit.

By using the linear X-ray imaging sensor and X-ray photon counting method, it is also possible to quantitatively evaluate the radiographic image and measure low contrast radiographic images.

These experiments were carried out under conditions such that the locations of the contrast areas were fixed and the observer who

evaluated the image knew these locations. It will be necessary to carry out more correctly a recognition of contrast (ROC) study using random locations of the contrast area.

References

[1] L.Kaufman, V.Perez-Mendez, D.Shames and G.Stokar: "A Multiwire Proportional Chamber for Nuclear Medicine Applications."
IEEE Trans. Nucl. Sci. NS-19, No.1, 1972

[2] K.Valentine, S.Kaplan et.al.: "The Adaptation of Multi-Wire Proportional Chambers with Delay-Line Readouts for Neutron Radiographic Imaging"
IEEE Trans. Nucl. Sci. NS-19, No.1, 1972

[3] L.Kaufman, V.Perez-Nendez and G.Stoker: "Performance of a Pressurized Xenon-Field Multiwire Proportional Chamber",
IEEE Trans. Nucl. Sci. NS-20, No.1, 1973

[4] K.Varentine, S.Kaplan, V.Perez-Mendez and L.Kaufman: "A Multiwire Proportional Chamber for Imaging Thermal,Epicadmium, and Fast Neutrons", IEEE Trans. Nucl. Sci. NS-21, No.1, 1974

[5] R.S.Hattner, C.B.Lim, S.J.Swann, L.Kaufman,V.Perez-Mendez: Cerebral Imaging using 68Ga DTPA and the U.C.S.F. Multi-Wire Proportional Chamber Positron Camera",
IEEE Trans. Nucl. Sci. NS-23, No.1, 1976

[6] L.Kaufman, V.Lorenz: "Two-Detector, 512 Element High Puarity Gernium Camera Property", IEEE Trans. Nucl. Sci. NS-25, No.1, 1978.

[7] L.Kaufman, S.H.Williams: "An Evaluation of Semiconductor Detectors for Position Tomography",
IEEE Trans. Nucl. Sci. Vol.26, No.1, 1979.

[8] D.A.Ortendahl, L.Kaufman, W.Roman, R.Herfkens and D.C.Price "High Resolution Emission Computed Tomography with a Small Germanium Camera", IEEE Trans. Nucl. Sci. Vol.27, No.1, 1980.

[9] D.A.Ordendahl, L.Kaufman and K.Hosier: "Operating Characteristics of Small Position-Sensitive Mercuric Iodide Detector",
IEEE Trans. Nucl. Sci. Vol.29, No.1, 1982

[10] J.S.Iwanczyk, W.K.Warburton, A.J.Dabrowski, B.Hedman, K.O.Hodgson and B.E.Patt: "Development of Mercuric Iodide Energy Dispersive X-ray Array Detectors",
IEEE Trans. Nucl. Sci. Vol.35, No.1, 1988
[11] R.Bellazzini, A.Brez, A.D.Guerra, M.M.Massai and M.R.Torquati: "Digital Radiography using the Individual Photon Counting Technique", NATO ASI SERE Vol.119, pp197-224 1987
12)B.Collet: "Two-Dimensional Photon Counter for X-ray Imaging" Rev. Sci. Instrum. 59 (7) 1988
[13] R.A.Wick:"Quantum-limited Imaging using Microchannel Plate Technology", Applied Optics Vol.26, No.16 1987

CHAPTER 7
Summary and conclusions

The purpose of this study is to realize "X-ray radiography giving energy spectrum information". The conventional X-ray screen/film system, the X-ray TV using an image intensifier and the Computed radiography (CR) offer us only the information about the X-ray intensity that has penetrated through an object. To obtain the information about the energy spectrum is the situation similar to having a color picture. In the field of photography, changing a monochromatic image to a color image provides us with more information about the object. In the field of radiography, by incorporating the energy spectrum information, we are able to obtain not only the intensity information proportional to the thickness of the object but also the information about the composed materials. In other words, we are able to obtain both conventional radiographic images and material images simultaneously.

To obtain the energy spectrum information, CdTe semiconductor radiation detectors were used to separate the irradiated X-ray energy. For the design of the X-ray imaging sensor and its instrumentation, the following studies were needed:1) smaller detector elements to achieve the same spatial resolution as the X-ray film/screen system 2) the X-ray photon counting, the pulse height separation technology.

The research started on the CdTe semiconductor elements and its fablication of the X-ray imaging sensor, the radiographic apparatus, the X-ray energy separation method, and the image processing moreover including the energy subtraction method were developed. The image quality, spatial resolution and threshold

contrast of the photon counting X-ray radiography must be evaluated. The major contributions of this study are summarized as follows.

1. (Chapter 1)

The basic principle here for realizing "X-ray image giving energy spectrum information" and the physical basis for selecting the CdTe compound semiconductor detector as well as its characteristics are discussed here. It is concluded that the CdTe detector is suitable as an X-ray imaging sensor due to its high spatial resolution and sub-millimeter thickness.

2. (Chapter 2)

To realize the energy separation with high sensitivity and high spatial resolution, the proper size of a detector element and the 32 channel detector array are determined to be $0.25 \times 1.0 \times 0.3$ mm^3 and $8.0 \times 1.0 \times 0.3$ mm^3, respectively. When the response for single energy γ-rays is measured, the smaller the detector size is, the larger the X-ray escape peak counts are. By using a newly designed X-ray shielding grid, which is able to limit the sensitive area and avoid the escape X-rays from the adjacent elements, the response spectrum become better and resemble to a large single detector. An energy resolution of 12 % (FWHM) and an X-ray escape peak ratio of 30 % are obtained for ^{241}Am γ-rays (59.54 keV).

3. (Chapter 3)

Because of the small size of the detector element, the output X-ray energy spectrum is deformed from the irradiated X-ray energy spectrum. Using the response function for 59.54 keV γ-rays and the absorption coefficient for the CdTe detector thickness, the response to X-rays is calculated, and the response spectrum is found to closely

resemble to the measured X-ray spectrum using the CdTe detector elements.

4. (Chapter 4)

A pulse counting circuit and an energy separation circuit are both designed and prepared. The X-ray energy spectrum is obtained by changing the discriminator level step by step and differentiating each counts. The X-ray energy separation is realized and the effective energies are calculated using copper plates with different thicknesses and measured half-layer values.

5. (Chapter 5)

The X-ray imaging sensor and the counting circuit are developed and measurements are carried out.

Specific resolutions of 2.5 lp/mm in the array direction and 1.6 lp/mm in the scanning direction are obtained for the effective detection area of 0.5×0.15 mm^2, channel pitch of 0.2 mm and the scanning pitch of 0.2 mm.

By using the energy separation method, high and low energy images are obtained simultaneously. The image of the material composing the object is canceled from the image using the energy subtraction method.

A new evaluation method using the data of the "subtraction parameters" which means absorption coefficient ratio is applied to determine whether these parameters are proportional to the atomic number or the effective atomic number below a value of 30. This evaluation method demonstrates the ability to identify the material composing the object.

6.(Chapter 6)

The photon counts is used to evaluate the threshold contrast of the X-ray radiography on the basis of both simulation and experiment. In the simulation, random photon numbers having a Poisson distribution are used. The deviation from the average number is set to have the Poisson distribution. A contrast phantom is newly designed and the radiographic images are measured and evaluated.

The following two conclusions are obtained.

The fan beam X-ray and shielding grids eliminated the scattered component from the X-ray image.

The threshold contrast is recognized at 1/3 of the standard deviation of the average photon number λ for an area of 5×5 mm^2 square.

7.(Chapter 7)

In this chapter, the conclusion through this thesis is described. X-ray radiography is described covering through the selection of the detector material to the development of the radiographic imaging instrumentation. Because of the wide range of the counts, the individual analysis or the results of the experiments are not fully described. The main objective is to obtain "X-ray radiography giving energy spectrum information" as described. It is concluded that the combination of the X-ray imaging sensor, composed of the CdTe compound detector, and the imaging instrumentation incorporating the function of photon counting and energy separation provide us with the best solution. It is very happy for us that this thesis will give a view to the application of the CdTe radiation detector to the next generation of the X-ray radiography.

Acknowledgments

I would like to express my sincere gratitude to Professor Haruya Matsumoto and also express my sincere appreciation to my thesis advisors, Professor Takumi Minemoto and Professor Shinzo Kitamura of Kobe University for their expert guidance and constant support throughout this thesis.

I am also deeply grateful to Professor Tadaoki Yamashita of Kumamoto University for his many helpful discussion and collaboration.

The work presented in this thesis was, for most part, done at the Central Research Laboratory and the Device Process Research Laboratory, Matsushita Electric Industrial Co., Ltd. I would like to thank Dr. Sigeru Hayakawa, Dr. Tsuneharu Nitta, Dr. Kenji Kanai and Dr. Masanori Watanabe for their continuous encouragement. I also thank Mr. Seikoh Minamide and Mr. Taketoshi Yonezawa.

I am gratefully indebted to Mr. Osamu Yamamoto and Mr. Sueki Baba for their hearty guidance and continuous instructions from the beginning of this study.

I express my grateful thanks to Mr. Koichi Ohmori and Mr. Tetsuro Ohtsuchi, Mr. Sakae Noda Mr. Yoshitaka Sunagawa and Mr.Hiroshi Watanabe for their contributions in this study.

I also express my thanks to Mr. .Hideo Toyoda, Mr. Yasumi Miyakawa, Mr. Yoshinori Yamada, Mr. Hiromasa Funakoshi, Mr. Toshiyuki Kawara and Mr. Yoshiyuki Yoshizumi of the Central Research Laboratory in completing the circuits, the drivers and the system. This study depends largely on their contributions.

I am also grateful to Dr. Kenzo Hatada of the Semiconductor Research Center for his good support and advice.

I also thank Mr. Yoshitake Yasuno of Matsushita Industrial Equipment Co.,Ltd. for his discussion and advice.

List of Publications

Papers (for this thesis)

1) H.Tsutsui, T.Ohtsuchi, K.Ohmori, S.Baba
"Fabrication and Characteristics of a Submillimeter Detector Element formed on a Single Crystal CdTe Wafer as a Multichannel Detector Array applicable to a Diagnostic Imaging with Energy Information"
Jpn.J.Appl.Phys. Vol.32(1993), pp228-233

2) H.Tsutsui, T.Ohtsuchi, K.Ohmori, S.Baba
"Measurement of X-ray Spectrum using a small size CdTe Multichannel Detector"
IEEE Trans on NS. Vol.39, No.6, pp2282-2285, 1993

3) H.Tsutsui, T.Ohtsuchi, K.Ohmori, S.Baba
"X-ray Energy Separation Method using a CdTe Semiconductor X-ray Imaging Sensor and Photon Counting Method"
IEEE Trans. on NS. Vol.40, No.1, pp40-44, 1993

4) H.Tsutsui, T.Ohtsuchi, K.Ohmori, S.Baba
"CdTe Semiconductor X-ray Imaging Sensor and Energy Sub traction Method using X-ray Energy Information"
IEEE Trans. on NS. Vol.40, No.2 pp95-101, 1993

5) H.Tsutsui, T.Ohtsuchi, K.Ohmori, S.Baba, H.Matsumoto
"Evaluation of Contrast Resolution of Digital X-ray Radiography"
Being Contributed to IEEE.

Papers (radiation sensing)

1) Y.Yasuno, H.Tsutsui, O.Yamamoto, T.Yamashita
"Feasibility of Two dimensional Dosimetry or an X-ray Imasing Method using CaSO4 TL Film"
Radiation Protection Dosimetry Vol.6 No.1-4, pp341-343, 1983

2) Y.Yasuno, H.Tsutsui, O.Yamamoto, T.Yamashita
"Feasibility of an X-ray Imaging Method using CaSO4 Thermo luminescence Film"
Jpn.J.Appl.Phys. Vol.21, No.6, pp167, 1982

3) O.Yamamoto, Y.Yasuno, S.Minamide, S.Hasegawa, H.Tsutsui, M.Takenaga, T.Yamashita
"Construction of a Composite Thin-Element using an Optical

Heating Method"
Health Physics Vol.43, No.3, pp383-390, 1982

4) S.Baba, H.Tsutsui, K.Ohmori, T.Ohtsuchi, H.Toyoda, T.Kawara, F.Funakoshi,
"A High Speed Cadmium Telluride Radiation Detector"
IEEE Trans on NS. Vol.40, No.1, pp56-62, 1993

Symposium

1)T.Ohtsuchi, H.Tsutsui, K.Ohmori, S.Baba
"X-ray Imaging Sensor using CdTe Semiconductor"
Technical Digest of the 10th Sensor Symposium, pp97-100, 1991

2) T.Ohtsuchi, H.Tsutsui, K.Ohmori, S.Baba
"CdTe semiconductor Imaging Sensor for Dual Energy X-ray Bone Absorptiometry"
World Congress on Medical Physics and Biomedical Engineering 1991

3) H.Tsutsui, T.Ohtsuchi, K.Ohmori, S.Baba
"CdTe Multichannel X-ray Imaging Sensor and Measuring Method using X-ray Energy Information"
ICEMI pp 118-122 1992

4) 大森、大土、筒井、馬場
ＣｄＴｅ放射線検出器によるキャリア走行特性の影響
理工学における同位元素研究発表会

5) 筒井、大土、大森、馬場
X線エネルギー情報を用いた物質の判別方法及び画像化に関する研究
電気学会センサ技術研究会　ST-91-18 1992

Presentations

1) 筒井、渡、安野、山本
赤外線加熱による新型ＴＬＤ
日本保健物理学会第１３回研究発表会論文集, P3, (1978)2)

2) 筒井、大土、大森、馬場、渡辺
ＣｄＴｅ検出器によるX線スペクトルの測定
春期応用物理学会関係連合講演会予稿集1p-ZK-16 (1989)

3) 大土、大森、馬場、筒井、渡辺
ＣｄＴｅ放射線検出器のキャリア走行特性
春期応用物理学会関係連合講演会予稿集1p-ZK-9 (1989)

4) 筒井、大土、大森、馬場
ＣｄＴｅ検出器によるγ線スペクトルの解析
秋期応用物理学会学術講演会予稿集28-ZM-2
5) 大土、筒井、大森、馬場
ＣｄＴｅ検出器におけるＫ殻特性Ｘ線エスケープの解析
春期応用物理学会関係連合講演会予稿集31-A-3 (1990)
6) 大土、筒井、大森、馬場
高計数率ＣｄＴｅ検出器によるγ線スペクトルの計測
秋期応用物理学会学術講演会予稿集28p-MB-9 (1990)
7) 大森、筒井、大土、馬場
ＣｄＴｅ検出器によるＸ線エネルギー分離
秋期応用物理学会学術講演会予稿集28p-MB-10 (1990)
8) 筒井、大土、大森、馬場
ＣｄＴｅ半導体Ｘ線イメージセンサを用いた骨塩定量の試み
第３０回日本エム・イー学会大会講演集　(1991)

Another Field

Publications

1) M.Ikedo, H.Tsutsui, M.Watari, O.Yamamoto
"Infrared Fiber for CO2Laser"
National Technical Report Vol.28 No.6 pp60-68, 1982
2) 石渡、筒井
レーザの医学応用－特に炭酸ガスレーザメスを中心に－
製薬工場　Vol.3, No.8, 1983
3) 山田、山本、筒井、谷口（分割共著）
技術者が描くニューヘルスケアシステム
電子情報通信学会誌 Vol.71, No.1, pp16-22, 1988

Presentations

1) 筒井、渡、池戸
高パワー伝送用多結晶赤外光ファイバ
第３０回応用物理学関係連合講演会　1983
2) 筒井、渡、池戸
多結晶赤外光用ファイバの樹脂コーティング
第３０回応用物理学関係連合講演会　1983
3) 筒井、渡、池戸
多結晶赤外光ファイバの温度計測への応用
第４４回応用物理学会学術講演会　1983